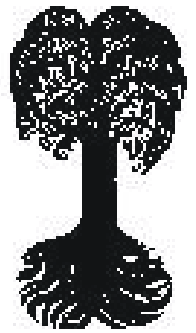




EBERHARD KARLS
UNIVERSITÄT
TÜBINGEN



Zentrum für Angewandte Geowissenschaften (ZAG)

TÜBINGER GEOWISSENSCHAFTLICHE ARBEITEN (TGA)

Reihe C: Hydro-, Ingenieur- und Umweltgeologie

Schriftleitung: P. Grathwohl, G. Teutsch

Carsten Leven

Effects of Heterogeneous Parameter Distributions on Hydraulic Tests - Analysis and Assessment

TGA, C65, 2002

Effects of Heterogeneous Parameter Distributions on Hydraulic Tests - Analysis and Assessment

Carsten Leven

2002

Zentrum für Angewandte Geowissenschaften
Angewandte Geologie
Sigwartstr. 10
72076 Tübingen
Germany

Herausgeber:

Institut und Museum für Geologie und Paläontologie
der Universität Tübingen
Sigwartstraße 10, D-72076 Tübingen

Schriftleitung der Reihe C:

Lehrstuhl für Angewandte Geologie
Prof. Dr. Peter Grathwohl & Prof. Dr. Georg Teutsch

Redaktion:

Dipl.-Geol. Björn Sack-Kühner

ISSN 0935-4948

ISSN 1610-4706 (Internet)

TGA	Reihe C	Nr. 65	88 S., 65 Abb., 7 Tab., 6 S. Anh.	Tübingen, Mai 2002
-----	---------	--------	-----------------------------------	--------------------

Effects of Heterogeneous Parameter Distributions on Hydraulic Tests - Analysis and Assessment

by Carsten Leven [§]

Abstract: Groundwater flow and transport processes are dominated by the heterogeneity and anisotropy of the subsurface. In the last few decades the importance of a detailed description, characterization, and quantification of aquifer heterogeneity and anisotropy became more and more evident. Since it was recognized that e.g. the spreading of contaminants in the subsurface greatly depends on spatial variations, i.e. on heterogeneity of the relevant hydrogeologic parameters aquifer characterization became of key interest of contemporary research in the field of hydrogeology. The present thesis is motivated by the requirement of an improved understanding and insight in the interrelationship of effects resulting from heterogeneity on particular measurements, and by the importance of a detailed characterization and quantification of aquifer heterogeneity for a reliable identification and prediction of flow and transport in heterogeneous aquifers. Two different approaches are applied in order to improve the understanding of effects that may arise from aquifer heterogeneity on hydraulic measurements: 1) In an experimental approach experimental measurements are conducted to a fractured sandstone block based on the concept of the aquifer analog. This approach allows the practical investigation of the system in terms of an examination of the effects arising from the strongly heterogeneous nature of the fractured sample. 2) A theoretical approach based on the analysis of sensitivity coefficients enabling the improvement of the theoretical comprehension of effects arising from aquifer heterogeneity. This approach allows the extension to more general considerations, i.e. regarding arbitrary parameter distributions. To provide a general statement, the approach is based on considerations of the hydraulic configuration of a conventional pumping test.

The experimental investigations provide an insight into the effects of the strongly heterogeneous fractured porous system on the employed measurements. In addition, an insight into the relevant processes for flow and pressure buildup in the heterogeneous media are given. The experimental series reveal the complexity of the system. The methods developed for the investigation of the strongly heterogeneous system of a fractured porous rock using practical measurements allow showing the effects arising from the heterogeneity of the investigated system. However, the comparison of the results from the experimental series exemplified the necessity of an improved understanding of the interrelation between an arbitrary parameter distribution and the response of a particular hydraulic measurement or measuring method, respectively. A promising concept to account for this interrelationship is the Sensitivity Coefficient Approach (SCA). The approach of sensitivity coefficients is applied to investigate the intrinsic characteristics of hydraulic tests giving a better understanding of the response of hydraulic test methods due to aquifer heterogeneity. As the approach allows the assessment of information from distinct time periods during a hydraulic test, e.g. data from definite sections of the time-drawdown curve of a pumping test, the assignment of estimated parameters to particular spatial information can succeed. Based on the SCA an alternative measuring concept is suggested for an improvement of the conventional approach of hydraulic investigations of heterogeneous aquifers. A proof of the suitability and applicability of the approach is given by numerical examples and field measurements.

[§] Dissertation an der Geowissenschaftlichen Fakultät der Universität Tübingen
Zentrum für Angewandte Geowissenschaften, Angewandte Geologie, Sigwartstr. 10, 72076 Tübingen, Germany

Acknowledgements

The work presented in this thesis was funded by the German Research Foundation (Deutsche Forschungsgemeinschaft, Sa 501/12-2, Di 833/1-4) and by grants from the German Academic Exchange Service (Deutscher Akademischer Austauschdienst D/01/049/14) and the U.S. Army Research Office (DAAH04-96-1-0318).

I would like to thank my advisor Prof. Dr. G. Teutsch for the valuable scientific, financial, and administrative support in the last three years.

Special thanks to Dr. P. Dietrich for his guidance, his amicable support and the many, many discussions. A lot of his ideas stimulated this thesis and his advises helped me keeping the thread throughout the time of my dissertation.

I appreciate the contributions of all the colleagues from the “Hilzingerbau”. Special thanks to Dr. P. Merkel for the review of the manuscript and the inspiring discussions.

For his help in the laboratory I thank Marco Licht.

For the technical help for the experimental work I like to thank K. Faiß, W. Kürner, and H. Kurz.

For the great time in Boise (Idaho, USA), the support and his kindness I would like to thank Dr. W. Barrash from the Center for Geophysical Investigation of the Shallow Subsurface (Boise State University). For the help in Boise and in the field I also would like to thank Ed Reboulet and Tim Johnson.

Finally I’m thanking Claudia for her continuing support. Without her help this thesis wouldn’t have been possible at all. To Sarah and Till also a big “thank you” for their mental support during the last weeks...

Index

INDEX	I
LIST OF FIGURES	III
LIST OF TABLES	VIII
LIST OF SYMBOLS	IX
1 INTRODUCTION	1
1.1 Motivation and objectives	1
1.2 Outline	2
2 AN EXPERIMENTAL STUDY BASED ON THE AQUIFER ANALOGUE APPROACH	4
2.1 Introduction	4
2.2 The Aquifer Analogue Approach	5
2.3 Description and preparation of the block sample	6
2.4 Experimental concept	8
2.5 Pneumatic steady-state flow test with constant injection pressure	11
2.6 Pneumatic diffusivity tests	15
2.7 Conclusions	19
3 THE APPROACH OF SENSITIVITY COEFFICIENTS	21
3.1 Introduction	21
3.2 Governing equations	21
3.3 The Sensitivity Coefficient Approach	23
3.4 Calculation of the parameter derivative $\partial u/\partial k$	23
3.5 Performance of the sensitivity coefficient approach	27
4 ANALYSIS OF SENSITIVITY COEFFICIENTS	32
4.1 Introduction	32
4.2 General considerations	32
4.3 Sensitivity with respect to hydraulic conductivity	33
4.4 Sensitivity with respect to storage	37
4.5 Sensitivity distribution for different hydraulic tests	38

5	APPLICATION OF THE SENSITIVITY APPROACH FOR THE ASSESSMENT OF HETEROGENEITY AND ANISOTROPY - THE STEADY-STATE CASE	44
5.1	Introduction.....	44
5.2	Numerical realization - An example under steady-state conditions.....	44
5.3	Consequences for the assessment of hydraulic tests and conclusions	53
6	A THEORETICAL INVESTIGATION BASED ON THE ANALYSIS AND APPLICATION OF THE SCA.....	56
6.1	Introduction.....	56
6.2	Numerical example	57
6.3	Modification of the pumping test configuration based on sensitivity coefficients	61
6.4	Single well pumping tests	65
6.5	Further considerations and conclusions	69
7	APPLICATION OF THE CONCEPT OF SENSITIVITY COEFFICIENTS - A FIELD EXAMPLE FROM THE “BOISE HYDROGEOPHYSICAL RESEARCH SITE”	72
7.1	Introduction.....	72
7.2	Description of the test site.....	72
7.3	Single well pumping tests	74
7.4	Final remarks.....	77
8	SUMMARY AND CONCLUSION.....	78
9	REFERENCES.....	81

APPENDIX

<i>Appendix A-1</i>	<i>Photographs and maps of the fractured sandstone block.....</i>	<i>Appendix - 2</i>
<i>Appendix A-2</i>	<i>The multi purpose measuring device</i>	<i>Appendix - 4</i>

List of Figures

Figure 2-1.	Photograph of the fractured sandstone block [from <i>McDermott</i> , 1999].	7
Figure 2-2.	Diagram of the fractured sandstone block ($0.9 \times 0.9 \times 0.8 \text{ m}^3$); “fracture 1” and “fracture 2” mark dominant fractures in the block sample.	8
Figure 2-3.	Lognormal distribution of fracture apertures of the sandstone block based on 370 measurements. The frequency distribution is calculated using shifted averages according to <i>Scott</i> [1992].	8
Figure 2-4.	a) Drilling core of the fractured sandstone block. The horizontal and angled lines indicate the positions of fissures, which are mostly oriented parallel the sediment structures. b) Illustration of a “port” connected to the block through the resin sealing.	9
Figure 2-5.	Illustration of two operating states of the LabVIEW [®] based multi-purpose measuring device, which allows a variety of distinct hydraulic measuring configurations. a) Flow experiments with constant injection pressure. b) Pressure buildup experiments with constant injection pressure. A detailed scheme of the multi-purpose measuring device is given in the appendix A-2.	10
Figure 2-6.	The steady- and transient-state case for constant injection rate (a) and constant injection pressure (b) for flow and pressure buildup experiments (opened external ports or boundaries in infinite distance).	11
Figure 2-7.	a) Bimodal distribution of detected flow rates at the ports on the block surface normalized to the radial distance from the central borehole. The curves illustrate two distinct lognormal Gaussian distributions, characteristic the porous matrix (left) and the fracture network (right). b) Relative fraction of the injected flow rate and number of involved ports (numbers in graph) against the percentage of injected flow rate detected at each single port.	12
Figure 2-8.	Relative frequency of the different types of port connections: ports connecting to fractures (“fracture”), to matrix (“matrix”), and ports connected to matrix in the direct vicinity of fractures (“matrix w/ fracture”).	13
Figure 2-9.	Sections parallel to the horizontally aligned ports from top to bottom illustrating distribution of the flow fractions within the block under steady-state conditions (Symbols: \triangle - matrix dominated connection, \blacktriangle - matrix connection in direct vicinity of fracture, \blacktriangle - direct fracture connection). The center of each plot matches the position of the vertical borehole (flow rate normalized to the radial distance from the central borehole in $[\text{m}^3/\text{s}] \times [\text{m}]$).	14
Figure 2-10.	Pressure buildup curves recorded at all external ports at the block surface normalized to the radial distance.	15
Figure 2-11.	Variance of pressure buildup curves for a linear scale of normalized time for selected normalized pressures.	16
Figure 2-12.	Pressure buildup curves recorded at the uppermost horizontal row of ports with constant injection pressure (a) and the absolute difference to the pressure buildup at the inlet of the wellbore (b); (P_{well} - pressure at the inlet of the borehole, P_{measure} - pressure at external port).	17
Figure 2-13.	Selected pressure buildup curves for a fracture (P_f) and a matrix dominated port (P_m). The difference between the fracture (ΔP_f) and matrix (ΔP_m) dominated observation with respect to the pressure at the wellbore are obvious.	17

Figure 2-14.	Pressure buildup recorded at the uppermost horizontal row of ports for four different times (a - d). The orientation of each plot in terms of the position and orientation is identical to Figure 2-9 (Symbols in (a) and (e) valid for all plots: \triangle - matrix dominated connection, \blacktriangle - matrix connection in direct vicinity of fracture, \blacktriangle - direct fracture connection). The absolute difference between the pressure distributions at the particular time steps illustrates the affected domain within the block (e - g). Note the different scales between the plots of normalized pressure values (top; a - d) and the change in pressure (bottom, e - g).	18
Figure 2-15.	Relationship between the hydraulic disturbance of the system and the change of flow with time. (a) Evolution of the well flow at constant injection pressure. (b) Comparison of the injected pressure with the observed pressure at the external ports. (c) Arrows indicate the pressure gradient as difference between the injected and observed pressure within the matrix for three particular time steps (A - C).	20
Figure 3-1.	Principle of reciprocity. a) Initial positioning: pumping (Q = pumping rate) at well A leads to the observation u at well B. b) Situation with interchanged well positions: pumping at well B leads to the observation v at well A. Due to reciprocity observation v equals the observation u from the initial configuration.	26
Figure 3-2.	Flow chart of the consecutive steps for the computation of the sensitivity coefficients. Boxes in gray indicate steps necessary for computations for transient-state conditions.	27
Figure 4-1.	Two-dimensional sensitivity distribution for the times $t = 10, 100, 1000$ seconds. The black dots indicate the position of the pumping and observation well ($k = 10^{-4}$ m/s, $S = 10^{-4}$, $Q = 300$ m ³ /d).	34
Figure 4-2.	Sections through the two-dimensional distribution of sensitivity coefficients a) at $y' = 0$ intersecting the pumping and observation well, and b) at $x' = 0$. The numbers indicate the corresponding timesteps. The section with gray background indicates positive values of sensitivity. Note that the axes of ordinate have different scaling in a) and b) and the sensitivity coefficients at $t = 10$ s are only plotted in a) since the absolute values are very small compared to those at later timesteps (cf. Figure 4-1 a).	35
Figure 4-3.	a) Evolution of sensitivity coefficients with respect to hydraulic conductivity at different spatial positions illustrated in (c). b) Time series of the relative change of sensitivity coefficients for the spatial positions given in (c).	35
Figure 4-4.	Logarithm of relative change in sensitivity between consecutive logarithmic time steps a) between $t = 10$ and 100 s, b) between $t = 100$ and 1000 s and c) between $t = 1000$ and 10,000 s.	37
Figure 4-5.	Two-dimensional distribution of sensitivity coefficients with respect to changes in storage for the three time steps. The black dots indicate the position of the pumping and observation well ($k = 10^{-4}$ m/s, $S = 10^{-4}$, $Q = 300$ m ³ /d).	38
Figure 4-6.	a) Section through the two-dimensional sensitivity distribution of Figure 4-5 at $y' = 0$ intersecting the wells. b) Evolution of sensitivity coefficients at different spatial positions that can be gathered from Figure 4-3 c.	39
Figure 4-7.	Two-dimensional sensitivity distribution at $t = 1000$ s for different hydraulic measuring configurations (left column) with respect to transmissivity (middle column) and with respect to storage (right column): a - c) Hydraulic dipole with one pumping ($-Q$) and one injection well ($+Q$), changes of the potential h are observed in the injection well. d - f) Two well pumping test with observation in one pumping well. g - i) Pumping test with two observation well at which the hydraulic gradient (Δh) is observed. j - l) Two well pumping test with arbitrarily located pumping well. m - o) Two well pumping test with observation well in between the pumping wells. p - r) Two well pumping test with an observation well located on the axis perpendicular the axis of the pumping locations. The black dots in the sensitivity plots mark the position of the wells.	41
Figure 4-8.	Sensitivity distribution for the hydraulic test configuration illustrated in Figure 4-7 g for three consecutive logarithmic time steps. a) and b) at $t = 10$ s, c) and d) at $t = 100$ s, e) and f) at $t = 1000$ s with respect to changes in hydraulic conductivity (left column) and with respect to storage (right column):	42

Figure 5-1.	a. Model domain. b. Distribution of sensitivity coefficients for a homogeneous parameter field ($k=10^{-4}$ m/s, $Q=300$ m ³ /d).....	45
Figure 5-2.	Section intersecting the wells, (a) perpendicular and (b) parallel the axis of the pumping test configuration as shown in Figure 5-1. In (a), the wells are located at (0.5/0) and (-0.5/0), respectively (dashed line: positive sensitivity: $\log_{10}(I \times r)$; solid line: negative sensitivity: $\log_{10}(-I \times r)$).....	46
Figure 5-3.	Isolines of drawdown for a pumping test in an aquifer with homogeneous parameter distribution (solid line) and with a discontinuity of increased conductivity (#1 - dashed line, #2 - dotted line).....	46
Figure 5-4.	Sensitivity distribution for a pumping test for a homogeneous aquifer with different anisotropic parameter distributions. The arrows indicate the principal axis of anisotropy, with $k_1/k_2 = 1/3$. The black dots show the position of the wells.....	48
Figure 5-5.	Sensitivity distribution for a pumping test in an anisotropic aquifer with (a) $k_1/k_2 = 1/2$, (b) $k_1/k_2 = 1/3$ and (c) $k_1/k_2 = 1/5$. The scaling of the sensitivity coefficients can be gathered from Figure 5-4. The black dots indicate the position of the pumping and observation well.....	48
Figure 5-6.	Sensitivity distribution for a pumping test in an aquifer with a large-scale heterogeneity with contrasts in hydraulic conductivity of (a) $k_1/k_2 = 1/e$, (b) $k_1/k_2 = 1/10$, (c) $k_1/k_2 = 1/100$, (d) $k_1/k_2 = e/1$, (e) $k_1/k_2 = 10/1$, (f) $k_1/k_2 = 100/1$ with $e =$ Euler's number. The dashed line indicates the limit of the heterogeneity with increased conductivity k_2 . The black dots indicate the position of the wells.....	50
Figure 5-7.	Sensitivity distribution for a pumping test in an aquifer with a large-scale heterogeneity with a contrast in hydraulic conductivity of $k_1/k_2 = 1/10$. The boundary of the heterogeneity (dashed line) is running outside the wells (a, c), and between the wells (b), respectively. The black dots indicate the position of the wells.....	51
Figure 5-8.	Illustration of the relationship between the spatial extent of the depression cone at steady-state conditions and the hydraulic conductivity. The absolute drawdown value for the case of k_1 is ten times smaller than for the case of low conductivity k_2	52
Figure 5-9.	Sensitivity distribution for a pumping test in an anisotropic, and heterogeneous aquifer with $k_1/k_2 = 1/10$. The conductivity perpendicular the PTA (x -direction) is three times higher than parallel to that axis (y -direction). The black dots indicate the position of the wells (P - domain of positive sensitivity, 0 - line of zero sensitivity, N - domain of negative sensitivity).....	54
Figure 5-10.	Sensitivity distribution and results of a simulated pumping test with a discrete discontinuity of lowered conductivity at three spatial positions. The sensitivity distribution given for the undisturbed case corresponds to that shown in Figure 5-9.....	55
Figure 6-1.	Schematic illustration of the model domain showing the configuration of the simulated pumping test. The distance between the pumping well PW and each observation wells (O1 - O10) is $r = 7.5$ scale units. The squared model domain exists of 182,329 elements, with a central equally spaced subdomain of 100×100 units. Only the central subdomain includes aquifer heterogeneity.....	58
Figure 6-2.	Time-drawdown curves for a pumping test in a heterogeneous aquifer. The observation wells O1- O10 are in a radial distance of $r = 7.5$ units from the pumping well (cf. Figure 6-1).....	58
Figure 6-3.	Time-drawdown curve observed at well O2 (symbols) and the corresponding Theis fitting curve (solid line) for early times (k_{est} - estimated conductivity, S_{est} - estimated storativity).....	59
Figure 6-4.	Illustration of the relation between response time of drawdown and hydraulic conductivity for the early time of a pumping test with constant storage.....	60
Figure 6-5.	Sensitivity distribution of a pumping test with observation in the pumping well at $t = 10, 100, 1000,$ and $10,000$ seconds after start pumping. The values of the hydraulic parameters are the same as for the distribution shown in Figure 4-1.....	62
Figure 6-6.	One-dimensional sensitivity distribution for a single well pumping test for different time steps ($t = 1, 10, 100, 1000$ s). Note that the illustrated sensitivity coefficients are negative ($\log_{10}(I \times r)$).....	63

Figure 6-7.	Distribution of relative changes of sensitivity for three intervals between (a) 10 and 100, (b) 100 and 1000, and (c) 1000 and 10,000 seconds.....	64
Figure 6-8.	Time-sensitivity curves series at different radial distances from the well (a) and the relative change of sensitivity (b) for a single well test. The numbers indicate the radial distance; the interval between two curves is one meter.	64
Figure 6-9.	Time-drawdown curve for consecutive single well pumping tests at the wells <i>PW</i> , <i>O1 - O10</i> (cf. Figure 6-1).....	66
Figure 6-10.	Time drawdown curve recorded for the single well pumping test performed at well <i>O3</i> . A-B: Early drawdown phase with well bore storage, B-C: Evaluated section of drawdown curve based on the analysis of sensitivity coefficients. Increasing effects of the heterogeneous distribution of hydraulic conductivity influence the following time drawdown behavior.	66
Figure 6-11.	Distributions of coefficients of the relative change within the time interval for which the hydraulic parameters were fitted (a) for well <i>O3</i> , (b) for well <i>O10</i>	67
Figure 6-12.	Distribution of hydraulic conductivity based on the estimated parameters from the single well pumping tests in connection with the sensitivity coefficient approach. The circles around the well positions illustrate the portion of the aquifer from which no additional information can be gained for further time steps.	68
Figure 6-13.	Distribution of hydraulic conductivity of the model domain.....	69
Figure 6-14.	a) Section of wells perpendicular the main structure of heterogeneity and b) the time-drawdown curves for single well pumping tests.....	70
Figure 6-15.	Profiles of hydraulic conductivity based on the estimated parameters for three different time intervals. For early and intermediate times the estimated hydraulic conductivities are close to the model parameters. The late time curve includes bars indicating the radius of that portion from that no further information can be gained with ongoing time.....	71
Figure 7-1.	Photomap of the Boise Hydrogeophysical Site (BHRS) showing locations of 13 wells in the central portion of the site and 5 wells for information on hydraulic boundary conditions [from <i>Barrash et al.</i> 1999].	72
Figure 7-2.	Quarry exposure of analogue coarse, braided-stream deposits showing disconnected sand lenses (S) and a variety of cobble-dominated facies ranging from poorly sorted massive units (Gm), to moderately sorted horizontally-bedded units (Gh) and trough cross-bedded units (Gt). Heavy lines identify bounding surfaces between depositional sequences. For scale, quarry face is approx. 12 m high. Photograph and interpretation from <i>Barrash and Knoll</i> [1998]......	73
Figure 7-3.	Section of stratigraphic units at the BHRS based on porosity logs perpendicular to the main depositional direction [from <i>Barrash and Clemo</i> , 2000].	74
Figure 7-4.	Spatial distribution of Unit 5 (channel sand) thickening towards southwest (thickness in meters).	74
Figure 7-5.	Chair image from the 200 MHz GPR data showing time slices at 134 ns (~6.8 m depth), and vertical sections along the 5.6 m line and the 24.0 m station line [from: <i>Peretti et al.</i> , 1999]. Note the reflector interpreted as part of unit 5 (arrow).	75
Figure 7-6.	Time-drawdown curves from single well pumping tests employed to the wells in the central area of the BHRS.	76
Figure 7-7.	a) Time drawdown curve (dots) recorded at an observation well during a conventional short time pumping test with a best fit of the solution after <i>Neuman</i> [1974] indicating unconfined conditions with delayed yield. b) Calculated drawdown curve (symbols) after <i>Neuman</i> [1974] and a fitting curve (solid line) after <i>Theis</i> [1935] for late time data.....	76
Figure 7-8.	Distributions of coefficients of change in sensitivity for the single well pumping test at the central well <i>A1</i> of the BHRS for the interval between 100 and 1000 s.....	77
Figure 7-9.	Distribution of hydraulic conductivity utilizing the connection of coefficients of relative change in sensitivity and parameter estimates using the method of <i>Cooper and Jacob</i> [1946]. An agreement with the distribution of the sand channel (Figure 7-4) is evident.....	77

Appendix:

Figure A-1:	Photograph of the fractured sandstone block.....	Appendix - 2
Figure A-2.	Surface profiles and port locations of the fractured sandstone block.	Appendix - 3
Figure A-3.	The fractured sandstone block with resin coating and ports.	Appendix - 4
Figure A-4.	Setup of the multipurpose measuring device and illustration of the LabVIEW® based user interface.....	Appendix - 5
Figure A-5.	Technical realization of the multi purpose measuring device.....	Appendix - 6
Figure A-6.	Detailed diagram of the multi purpose measuring device.....	Appendix - 6

List of Tables

Table 2-1.	Parameters of the upper “Stubensandstein”- formation (“km4os3”).....	7
Table 2-2.	Properties of the fractured sandstone block (¹ AccuPyc 1330, ² GeoPyc 1360, ³ Gas permeameter with variable output pressure).....	8
Table 3-1.	Analogies to groundwater flow, after <i>Wang and Anderson</i> [1982].	21
Table 6-1.	Parameter estimates for a pumping test in a heterogeneous aquifer (<i>k</i> - hydraulic conductivity in length per time unit, <i>S</i> - storativity [-], <i>min</i> - minimum, <i>max</i> - maximum, <i>mean</i> - arithmetic mean, <i>std</i> - standard deviation, <i>geo</i> - geometric mean, read 5.5 e-4 as 5.5×10^{-4}).	59
Table 6-2	Estimates of the hydraulic parameters of the single well pumping tests.....	67
Table 6-3.	Comparison of model input parameters (K_{model}) and parameters estimated for the single well pumping test (K_{sw}) and conventional pumping test (K_{pt}).....	68
Table 7-1.	Hydraulic conductivities derived from single well pumping tests at the BHRS.	76

List of Symbols

a	[L]	Apertures
b	[L]	Aquifer thickness
e	[-]	Euler's number (2.71828182...)
h	[L]	Potential
h_0	[L]	Initial potential
h_D	[L]	Potential for boundaries of the first type (Dirichlet)
h_N	[L ³ /T]	Source term for boundaries of the second type (Neumann)
I	[1/L]	Sensitivity coefficient
k	[L/T]	Hydraulic conductivity
K_f	[L/T]	Hydraulic conductivity
k_i	[L ²]	Intrinsic permeability
m	[-]	Number of subdomains
n	[-]	Number of dimensions
P	[M/T ² L]	Pressure
P_0	[M/T ² L]	Initial pressure
q	[L ³ /T]	Source term
Q	[L ³ /T]	Pumping rate
q_N	[L ³ /T]	Source term of the second type of boundary condition (Neuman)
r	[L]	Distance
r_w	[L]	Well radius
S	[-]	Storage
s	[L]	Drawdown
S_y	[-]	Specific yield
t	[T]	Time
T	[L/T ²]	Transmissivity
u	[L]	Potential
v	[L]	Potential
x, y	[L]	Position vectors
x^i	[L]	Position vector to the point i
Ω	[L ²]	Domain
ω	[L ²]	Element of Ω
Γ	[L]	Limits of Ω
T	[T]	Time

Δ		Difference or change of a variable
ϑ	[°]	Angle
∇		Gradient
τ	[T]	Time step
σ		Standard deviation
η	[-]	Porosity
Γ_N	[L]	Part of the limit on Ω
ρ_s	[M/L ³]	Specific gravity

Indices:

f	Fracture
geo	Geometric mean
k	With respect to hydraulic conductivity
m	Matrix
$mean$	Arithmetic mean
OW	With respect to the observation well
p	Primary
PW	With respect to the pumping well
s	Secondary
S	With respect to storage
T	With respect to transmissivity

1 Introduction

1.1 Motivation and objectives

Groundwater flow and transport processes are dominated by the heterogeneity and anisotropy of the subsurface. In the past, flow and transport modeling and quantification of the relevant hydraulic parameters assumed mostly approaches, which are solely accepted for homogeneous and isotropic conditions. However, in the last few decades the importance of a more detailed description, characterization, and quantification of aquifer heterogeneity and anisotropy became more and more evident. Since it was recognized that e.g. the spreading of contaminants in the subsurface greatly depends on spatial variations, i.e. on heterogeneity of the relevant hydrogeologic parameters [*Dagan, 1989; Tompson and Gelhar, 1990; Miralles-Wilhelm and Gelhar, 1996*] aquifer characterization became of key interest of contemporary research in the field of hydrogeology. In this context hydraulic conductivity was identified as one of the ruling parameters [e.g. *Sudicky and Huyakorn, 1991; Butler et al., 1999*].

It was *Freeze and Cherry [1979]* who gave a comprehensive classification of heterogeneity, termed as trending, layered, and discontinuous heterogeneity. Trending heterogeneity is referred to a progressively increasing or decreasing change in hydraulic conductivity, e.g. caused by major depositional regimes. Layered heterogeneity is related to a stratigraphic framework made up of several beds of differing hydraulic conductivity, where the conductivity variations within the beds are assumed to be smaller

than the contrast between the beds. Discontinuous heterogeneity is referred to sharp contrasts in hydraulic conductivity over limited distances. Discontinuous heterogeneities are caused by preferential pathways as well as confining structures such as fissures and openings in fractured and karstified aquifers, or sand channels and clay lenses in porous media, respectively. Discontinuous heterogeneity can be identified as the most relevant structural element in the field of contaminant hydrogeology, as for example the efficiency of contaminant site remediation greatly depends on the spatial variability of the relevant hydraulic parameters.

Furthermore, the assessment of remediation concepts like in-situ remediation or natural attenuation requires a detailed knowledge of the spatial variation of aquifer parameters. Actually, strongly heterogeneous aquifers, like fractured media, show an increased hazard potential due to high flow velocities in the highly conductive zones, e.g. fractures, which allow an enhanced spreading of contaminants.

Most methods to characterize subsurface aquifers are based on simplified assumptions, which can lead to considerable problems when applied in heterogeneous environments. Therefore, the success of a reliable description, characterization and quantification of aquifer heterogeneity strongly depends on the utilized examination concepts, i.e. on the knowledge of the particular effects of heterogeneity on the employed investigation methods. Improving the fundamental understanding how definite heterogeneities affect hydrogeologic measurements, e.g. pumping tests, leads to a bet-

ter understanding of the governing processes of flow and transport in the subsurface at a particular site.

The work for this thesis was part of research efforts in the joint research project “Hard Rock Aquifer Analogue: Experiments and Modeling” (Festgesteins-Aquiferanalog: Experimente und Modellierung) founded by the German Research Foundation (Deutsche Forschungsgemeinschaft, Sa 501/12-2, Di 833/1-4). Detailed experimental and model investigations of flow and transport in fractured porous systems within the joint project revealed the necessity of an improved understanding of effects resulting from heterogeneity on a particular measurement. For example, difficulty and uncertainty exist in the understanding of the interrelation between an arbitrary spatially varying parameter distribution and the response or reaction of a particular hydraulic measurement, such as flow experiments.

Therefore, the present thesis is motivated by the requirement of an improved understanding and insight in the interrelationship of effects resulting from heterogeneity on particular measurements, and by the importance of a detailed characterization and quantification of aquifer heterogeneity for a reliable identification and prediction of flow and transport in heterogeneous aquifers. Consequently, the general objective of this thesis is to improve the understanding of effects that may arise from aquifer heterogeneity on hydraulic measurements. Thereby two approaches are applied:

1. **Experimental approach:** In this approach experimental measurements on laboratory scale based on the concept of the aquifer analog were conducted to a fractured sandstone block allowing the practical in-

vestigation of the system in terms of an examination of the effects arising from the strongly heterogeneous nature of the fractured sample. In particular, the specific objective of this experimental study is to illustrate those effects arising from heterogeneity as well as to give an understanding of flow processes that can be expected within such strongly heterogeneous systems like fractured porous aquifers.

2. **Theoretical approach:** This approach based on the analysis of sensitivity coefficients is chosen as it enables the improvement of the theoretical comprehension of effects arising from aquifer heterogeneity. This approach allows the extension to more general considerations, i.e. regarding arbitrary parameter distributions. To provide a general statement, the approach will be based on considerations of the hydraulic configuration of a conventional pumping test. Further objectives of this approach are the illustration of consequences that result from the analysis of sensitivity coefficients and their application for practical tasks. Additionally, an alternative approach is suggested for an improvement of the conventional approach of hydraulic investigations of heterogeneous aquifers. A proof of the suitability and applicability of the approach will be given by field measurements.

1.2 Outline

The following Chapter 2 contains experimental series based on the Aquifer Analogue Approach introducing two different hydraulic test methods conducted to a fractured sandstone block of 1 m³. The purpose of the experiments was the investigation of effects arising from the intense heterogeneity. In addition, an insight is given into processes

occurring during flow and pressure buildup in fractured porous media.

In Chapter 3 the theory of the Sensitivity Coefficient Approach (SCA) is introduced, which allows the analysis and evaluation of potential measurements, incorporating the influence of heterogeneities on the observation during hydraulic tests.

Based on the derivations of sensitivity coefficients, an analysis of sensitivity coefficients for homogenous parameter distributions is given in Chapter 4.

In Chapter 5 effects resulting from heterogeneity and anisotropy on hydraulic tests are evaluated based on the SCA. In this chapter a numerical implementation of the SCA under steady-state conditions is used in order to give an assessment of how discrete parameter disturbances affect hydraulic tests in homogeneous, anisotropic, and heterogeneous aquifers.

In Chapter 6 consequences for the evaluation and interpretation of hydraulic tests are discussed that result from the intrinsic characteristics of sensitivity coefficients and their development with time. In this chapter, an analytical solution is utilized for the derivation of sensitivity coefficients. The SCA is applied to results from a numerical modeling experiment of different pumping tests. With respect to the results from the previous chapters an example is given for the optimization of conventional pumping tests based on the SCA and to show the effects of the optimized configuration compared to standard pumping tests.

In Chapter 7 a field example from the Boise Hydrogeophysical Research Site (Idaho, USA) is given, for which the proposed configuration was used. The evidence of the suitability of the SCA and the configuration suggested in chapter 6 is given.

A summary and final conclusions will be presented in Chapter 8.

2 An Experimental Study based on the Aquifer Analogue Approach

2.1 Introduction

The fundamental understanding of the response of an investigated system to particular measurements is an essential prerequisite especially for the characterization of highly heterogeneous systems, such as fractured porous aquifers. This understanding is fundamental for the identification of the governing flow and transport processes as well as for the calculation and prediction of flow and transport in such systems.

Commonly employed hydrogeologic testing methods, e.g. conventional pumping tests, usually lead to effective parameter estimates. In fractured porous aquifers these parameters are averaged over the combined matrix-fracture-system with unknown relative contribution of the fractures and the matrix over a domain of uncertain spatial extent. Reasons for this can be found in the contrast of hydraulic properties between the highly permeable fractures and the much less permeable rock matrix, which induces very complex flow path pattern within the fractured rock [Karasaki *et al.*, 2000; McDermott *et al.*, 1998]. Although these facts are well known, detailed research with a focus on the investigation of fractured aquifers was only initiated during the last few decades, when considerable progress in the characterization of fractured porous systems has been made within the context of the investigation for potential nuclear waste re-

positories [e.g. Karasaki *et al.*, 2000 (Raymond field site, USA); Bodvarsson *et al.*, 1999 (Yucca Mountain, USA); Kickmaier and McKinley, 1997 or Savage, 1995 (rock laboratories in Europe: Grimsel (Switzerland), Äspö (Sweden), Fanay Augères (France), and many others)]. The geological formations, which are likely to host such repositories, are mostly fractured igneous rocks. Therefore, the results of investigations in these formations cannot directly be applied, if fractured systems with a significantly porous matrix are considered. In addition, the complexity of the flow and transport processes increases considerably for non-igneous systems, especially as a result of matrix heterogeneities, e.g. due to different sedimentologic structures, and the increased conductivity and storage of the matrix.

In addition, the extent of required knowledge on properties of fractured aquifers differs from the level at which such aquifers can actually be investigated with field methods. Most investigation techniques have limitations with respect to the spatial resolution needed to characterize such systems that is typically an inaccessible saturated aquifer. In this chapter flow and pressure buildup experiments are presented, which are based on the application of the aquifer analogue approach, in order to obtain high resolving data sets enabling a detailed investigation of the considered system. The introduced experiments allow the

analysis of the effects arising from heterogeneity as well as the characterization of the heterogeneous nature of the investigated system. In addition, the understanding of processes that can be expected within such strongly heterogeneous systems occurring during flow and pressure buildup can be improved.

2.2 The Aquifer Analogue Approach

Generally, traditional investigation methods are limited to measurements in boreholes, which only represent point information of the heterogeneous system. In the classical concept of the aquifer analogue, which was established in the petroleum industry [cf. *Flint and Bryant, 1993*], the potential reservoir rocks are investigated and characterized by detailed sedimentological studies in outcrops. The properties of the investigated system, i.e. geometry and petrography of the sedimentologic elements in the outcrop are considered as directly transferable to actual reservoir rocks.

In the field of fractured rock hydrogeology, this approach has very rarely been applied. *Billaux et al.* [1989] used data from the Fanay-Augères mine for the generation of a stochastic fracture network. Due to the lack of information caused by missing high resolution investigation and measuring methods, the properties of the fracture network such as its interconnectivity could not be quantified properly so that the modeling of the experimental results failed. In addition, their investigation revealed the problem of three-dimensional modeling based on one- or two-dimensional information.

In the application of the aquifer analogue approach presented in this chapter, accessible outcrops of the unsaturated fractured porous aquifer are examined. This concept allows the investigation of sections of an aquifer by field and laboratory techniques at several scales.

Employing appropriate investigation methods at each scale, high resolution and precise data sets can be obtained, e.g. detailed geometrical information of the fracture network and detailed information on the hydraulic characteristics of porous matrix. The results of the investigations and the revealed processes are then assumed to be transferable and applicable to the inaccessible section of the saturated aquifer.

Although this approach provides considerable advantages, some essential assumptions have to be made:

1. Because the aquifers under consideration are normally fully or partially saturated, experimental techniques have to be designed from which the natural hydraulic properties of the saturated system can be inferred. Due to the problems of obtaining fully water saturated conditions and problems arising from incomplete saturation (e.g. incomplete saturation leading to multi-phase flow, underestimation of the hydraulic conductivity due to incomplete saturation [*Lovelock, 1977*]), gas flow techniques were utilized with compressed air as the analogue fluid to water. Gas techniques allow relatively rapid measurements compared to experiments under fully saturated conditions with a high degree of accuracy. Resulting pneumatic parameters can easily be converted to hydraulic parameters [*Sampath and Keighom, 1982; Rasmussen et al., 1993; Bloomfield and William, 1995; Jaritz, 1998*].

2. The choice of a particular outcrop for the analogue investigation is critical, because the samples chosen determine the representativeness of the results for the fractured aquifer system. Attention is also directed to possible experimental artefacts, e.g. widening of the fracture apertures due to formation unloading. In this application of the approach, the focus of investigation is on fractured aquifers of the shallow subsurface so that such alterations in aperture are regarded to be of minor importance. In this part of the investigation the main focus is on basic experimental techniques for the determination of effects of the heterogeneous system on the employed measurements and on the identification of the governing processes, i.e. possible deviations from natural systems are of minor importance at this stage.

3. The investigations that are based on the analogue concept usually covering small volumes of the aquifer or the aquifer analogue (ranging from centimeters up to tens of meters) so that possible scale dependency effects of the hydraulic properties need to be taken into account. Hydraulic conductivity for example increases with the scale of measurement over several orders of magnitude until an upper bound is reached beyond which the conductivity remains constant [e.g. *Clauser, 1992; Sauter, 1992; Schulze-Makuch and Cherkauer, 1997*]. In fractured and conduit flow media, the hydraulic conductivity increases by about one order of magnitude with each order of magnitude increase in the scale of measurement [*Schulze-Makuch et al., 1999*]. The focus of the presented experimental series is directed at the meso-scale (about 1 m^3); the adaptation of resulting parameters in terms of up-scaling is still subject of ongoing research.

With the above assumptions, the aquifer analogue approach can be utilized in experimental and modeling investigations to characterize inaccessible fractured porous aquifers. For the presented experimental series, the concept of aquifer analogue is applied choosing a fractured sandstone block on laboratory scale. Experimental methods are developed, which allow controlled integral investigations of the combined system of the fracture network and the porous matrix system, including discrete geometrical information.

2.3 Description and preparation of the block sample

For the experiments a fractured sandstone block (Figure 2-1) was recovered from the upper Triassic “Stubensandstein”-formation, which is quarried in the southern part of Germany. The formation, which is also a regional aquifer, represents an intra-continental alluvial depositional system [*Hornung and Aigner, 1999*]. The recovered block was situated in a bed load channel dominated facies. Details on the properties of the arkose sandstone [*Heling, 1963*] of the “Stubensandstein”-formation are summarized in Table 2-1.

As it can be seen from Figure 2-1, the edges of the experimental block are somewhat irregular. In order to avoid disintegration of the sample during preparation due to the numerous fractures, it was only possible to cut the block to lengths of approximately $0.9 \times 0.9 \times 0.8 \text{ m}^3$.

Table 2-1. Parameters of the upper “Stubensandstein”- formation (“km4os3”).

Specific gravity	2.66 g/cm ³	1	
Porosity	19.5 %	1	
	7 - 23 %	2	
	10 - 25 %	3	
Hydraulic conductivity	$5 \times 10^{-8} - 1.5 \times 10^{-5}$ m/s	2	
	$10^{-6} - 10^{-5}$ m/s	3	
CaCO ₃ content	7.20 %	1	
C _{org} content	0.412 %	1	
Maximum saturation from humid air	12 %	1	
Dominant grain sizes	clay	1 - 5 μm	1
	quartz	100- 500 μm	1
Dominant pore size	0.1 - 1μm	1	
Percentage of			
Macro pores (> 1μm)	19.5 %	1	
Cement of matrix	kaolinit	3	

¹Mauch [1993], ²Bengelsdorf [1997], ³Heling [1963]

By common laboratory experiments (helium pycnometer and gas permeameter), the grain density and the porosity were determined. Values are summarized in Table 2-2.

For the description of the fracture network, the fissures at the block surface were recorded by tracing them on transparent polyethylene foil. The fracture apertures were also gauged using a caliper square and the type of filling was recorded (open, sand, clay filled). The fracture network of the block is dominated by a main fissure, which intersects sides I and III at a right angle and has apertures up to 4 mm (in Figure 2-2 marked with “fracture 1”).

For the description of the fracture network, the fissures at the block surface were recorded by tracing them on transparent polyethylene foil. The fracture apertures were also gauged using a caliper square and the type of filling was recorded (open, sand, clay filled).



Figure 2-1. Photograph of the fractured sandstone block [from McDermott, 1999].

The fracture network of the block is dominated by a main fissure, which intersects sides I and III at a right angle and has apertures up to 4 mm (in Figure 2-2 marked with “fracture 1”). Another dominant fracture lies nearly horizontal (in Figure 2-2 marked as “fracture 2”). The position of further vertical and horizontal fractures is also apparent from Figure 2-2. The fracture network has an arithmetic mean aperture of 0.6 mm (Table 2-2). Additional photographs and results from the mapping of the block surface are given in Appendix A-1.

The fracture apertures are distributed lognormally (Figure 2-3) with a large variability (Table 2-2). The flow velocity is typically higher in fractures with larger apertures. However, in regions of low apertures the flow velocity is reduced, so that the fractures with smaller apertures play an important role in reducing the effective conductivity of the fracture network [Keller *et al.*, 1999]. The geometric mean of the apertures, which represents a lower bound of conductivity of the fracture network, is also given in Table 2-2.

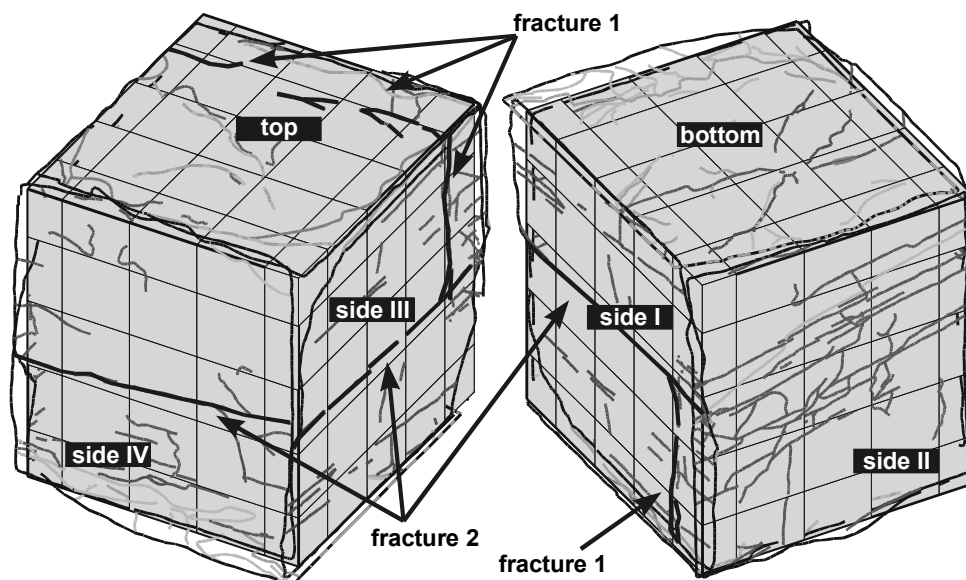


Figure 2-2. Diagram of the fractured sandstone block ($0.9 \times 0.9 \times 0.8 \text{ m}^3$); “fracture 1” and “fracture 2” mark dominant fractures in the block sample.

Table 2-2. Properties of the fractured sandstone block (¹ AccuPyc 1330, ² GeoPyc 1360, ³ Gas permeameter with variable output pressure).

General properties		
Size		approx. $0.9 \times 0.9 \times 0.8 \text{ m}^3$
Weight		approx. 1500 kg
Moisture content		approx. 1 %
Matrix properties		
Specific gravity	ρ_s	2.65 g/cm^3 ¹
Total porosity	η	approx. 15 % ²
Average intrinsic permeability	k_i	$4.4 \times 10^{-14} \text{ m}^2$ ³
Hydraulic conductivity	K_f	$4.3 \times 10^{-8} \text{ m/s}$
Fracture Network		
Fracture apertures	a	< 0.05 - 4 mm
Arithmetic mean	a_m	0.6 mm
Standard deviation	σ_m	0.67 mm
Geometric mean	a_g	0.38 mm

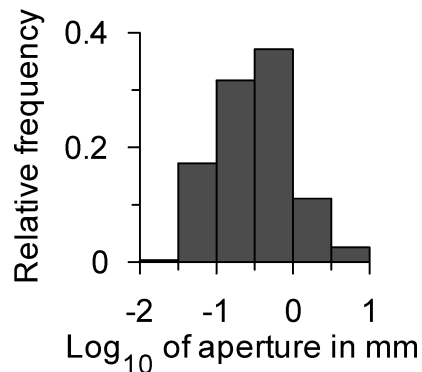


Figure 2-3. Lognormal distribution of fracture apertures of the sandstone block based on 370 measurements. The frequency distribution is calculated using shifted averages according to Scott [1992].

2.4 Experimental concept

Generally, hydraulic information is usually obtained from borehole experiments, i.e. in a radial flow field. In order to be able to com-

pare the experimental findings, a similar experimental setup using a borehole was created. The experimental series comprise two different test methods (boundary conditions) conducted in the fractured sandstone block. Firstly, a steady-state flow field with constant injection pressure and consequently constant flow rates was applied to the fractured sandstone block via a vertical borehole. The discharge of the injected gas was measured at the block surface. Secondly, a constant pressure was injected over the borehole and the transient pressure buildup was recorded at the block surface.

These methods allow the investigation of effects of fractured porous systems on hydraulic measurements, as well as the identification and understanding of the governing processes. In addition, the presented methods are suitable for the characterization of the heterogeneity of the fractured porous system and provide high-resolution data sets, which serve as reliable basis for the comprehension of the fractured porous system and the validation of different modeling approaches.

Based on a tomographical experimental setup for the investigation of fractured laboratory samples [McDermott, 1999], the block sample was prepared for the performance of pneumatic tests in radial flow fields under fully controlled boundary conditions. In addition, the development of a specific multi-purpose measuring device was needed to account for the specific task of simultaneously monitoring high resolution flow and pressure measurements at a large number of locations.

In order to obtain fully controllable boundary conditions, the surface of the block sample was sealed with an epoxy resin coating of approximately 5 mm thickness. Access to the rock material was achieved via a vertical borehole of 3 cm diameter drilled

through the center of the block. The obtained core is illustrated in Figure 2-4a. In addition, on each block face 16 holes with a diameter of 3 cm were drilled in a regular 4 × 4 grid through the resin cover and sealed by gas tight plastic plugs (“ports”), which allow the contact to clearly defined and specified areas on the block surface (Figure 2-4b). Further details of the recovery and preparation of the block can be found in McDermott [1999].

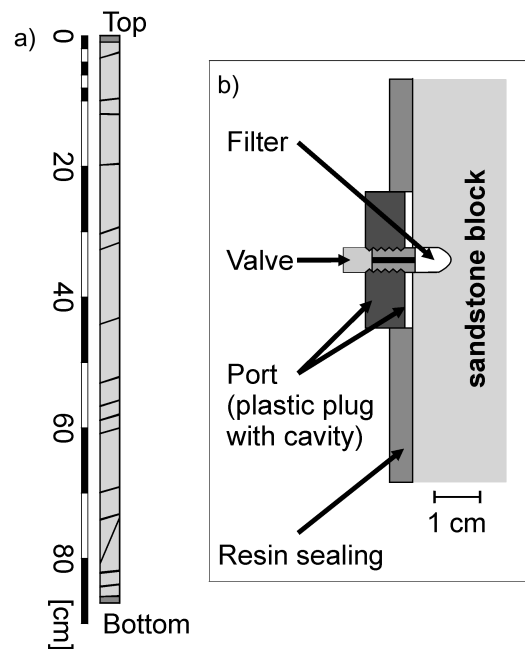


Figure 2-4. a) Drilling core of the fractured sandstone block. The horizontal and angled lines indicate the positions of fissures, which are mostly oriented parallel the sediment structures. b) Illustration of a “port” connected to the block through the resin sealing.

For the pneumatic investigation of the fractured sandstone block, i.e. the monitoring of flow and pressure buildup at multiple locations a fully automated multi-purpose-measuring device was developed using the measurement and automation software LabVIEW®. This device enables a fully automatic measurement and online data acquisition at rates of 1 Hz for flow rate measurements and rates of 0.3 kHz for pressure re-

cordings. The flexible design of the apparatus allows for variable input pressures and flow rates with a variety of different measuring configurations. In addition, it is possible to measure flow rates and pressures at any point in the measuring circuit. Figure 2-5 illustrates two possible measuring configurations for a radial flow field, each depending on the type of the input signal (constant pressure injection or constant injection rate) and on the type of external boundaries (ports are opened or closed). A detailed scheme and further details of the multi-purpose measuring device are given in Appendix A-2.

Measuring configurations with open ports can be implemented as steady- or transient-state tests. The performance of pneumatic tests with closed external ports is only pos-

sible under transient-state conditions. Figure 2-6 schematically shows the pressure and flow characteristics, which can be expected at any point in an open system (opened external ports), controlled by a constant flow rate or constant injection pressure.

Pressure buildup and flow at ports, which are dominated by the fracture network, will approach the steady-state conditions after a short time, while regions with lower conductivity only gradually approach the final value.

In the following section, the two different experimental series are sketched and the results are discussed in detail. For both series, the described multi-purpose measuring device was utilized with the experimental setups shown in Figure 2-5 applied.

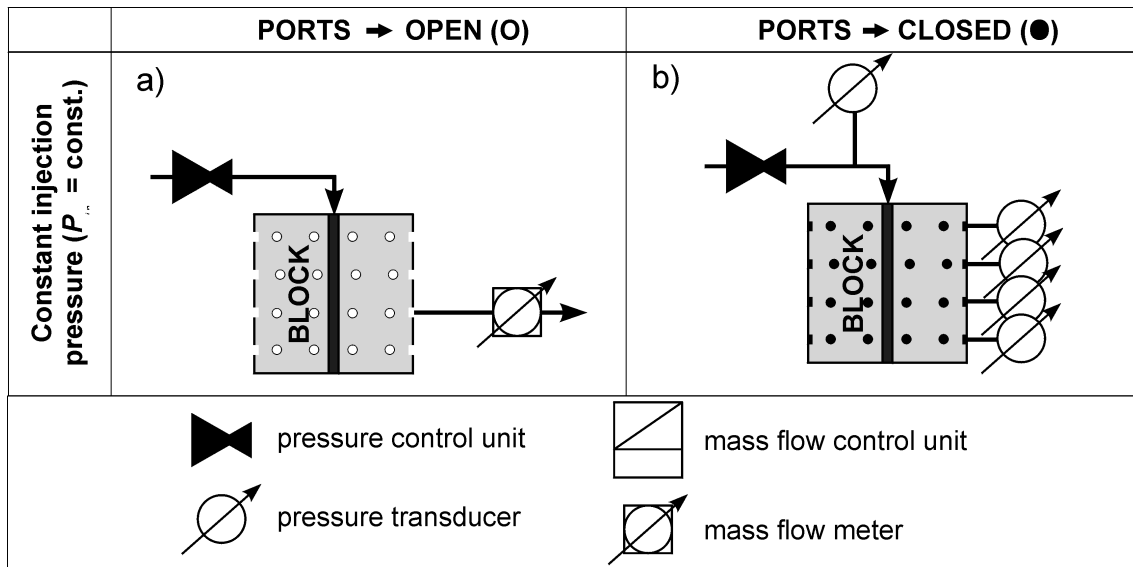


Figure 2-5. Illustration of two operating states of the LabVIEW[®] based multi-purpose measuring device, which allows a variety of distinct hydraulic measuring configurations. a) Flow experiments with constant injection pressure. b) Pressure buildup experiments with constant injection pressure. A detailed scheme of the multi-purpose measuring device is given in Appendix A-2.

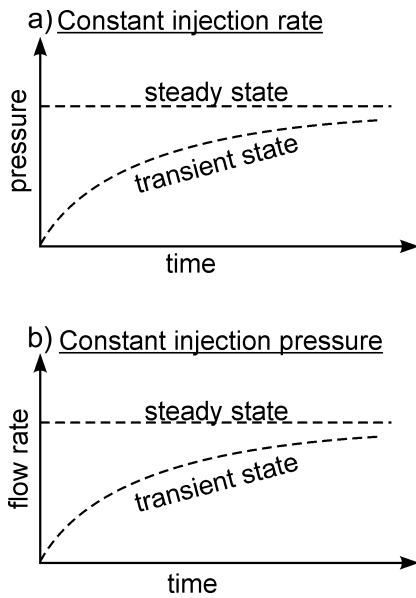


Figure 2-6. The steady- and transient-state case for constant injection rate (a) and constant injection pressure (b) for flow and pressure buildup experiments (opened external ports or boundaries in infinite distance).

2.5 Pneumatic steady-state flow test with constant injection pressure

For this configuration, compressed air is injected through the central borehole at a constant pressure, as shown in Figure 2-5a. All ports on the block surface with exception of those at top and bottom faces were opened, i.e. allowing the release of the injected gas through the external ports. Hence, a divergent radial flow field pattern is imposed. During the experiment the injection pressure and the injected flow rate remain constant (Figure 2-6b).

Figure 2-7a illustrates a frequency distribution of detected flow rates normalized to the radial distance of the corresponding

port from the central borehole. The data are distributed bimodal, consisting of two distinct lognormal distributions. The lognormal distribution with smaller normalized flow rates (left Gaussian curve in Figure 2-7 a) is characteristic for the response of the porous matrix of the block. A lognormal distribution of hydraulic conductivity in porous media is commonly accepted.

According to *Streltsova* [1988], the flow through a rock, containing an intersecting set of fractures, is proportional to the fracture porosity and to the cube of the fracture width. Latter relationship is described by the cubic law, which relates the fracture aperture to the cube of the flow rate through it [*Romm*, 1966]. Considering the even distribution of the fracture apertures of the block (Figure 2-3), the expected lognormal distribution for the detected flow rates was found in the lognormal distribution for higher normalized flow rates (right Gaussian curve in Figure 2-7 a).

With the specific task of an integral controlled investigation, the graph shown in Figure 2-7 b allows a detailed analysis of the resulting flow field, since also discrete information on the fracture porous system is available. The spatial discrete information is obtainable from the mapping of the block surfaces and from the core sample. Thus, it was possible to compare the flow rates with the corresponding type of port connection (direct fracture connection, matrix dominated, or connections to matrix with a fracture trace in direct vicinity), which allows the distinction of the fraction of flow from the matrix and from that of the fracture network.

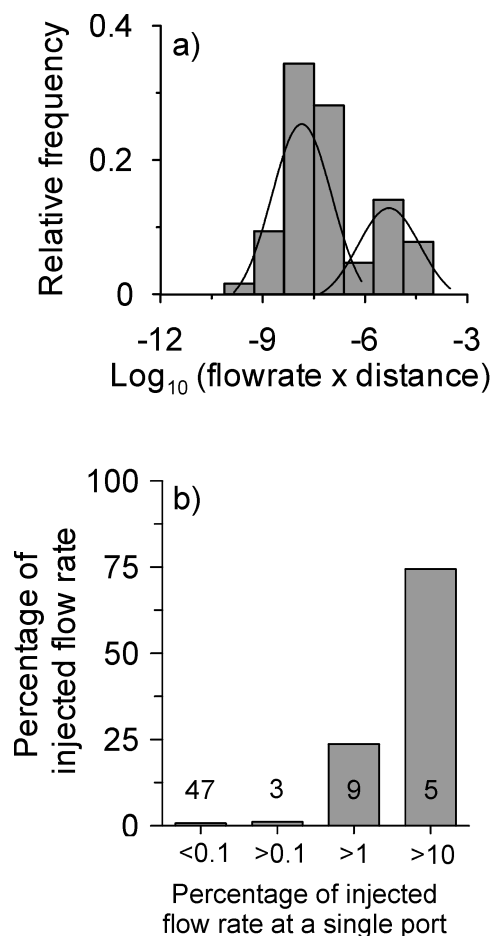


Figure 2-7. a) Bimodal distribution of detected flow rates at the ports on the block surface normalized to the radial distance from the central borehole. The curves illustrate two distinct lognormal Gaussian distributions, characterizing the porous matrix (left) and the fracture network (right). b) Relative fraction of the injected flow rate and number of involved ports (numbers in graph) against the percentage of injected flow rate detected at each single port.

It is obvious from Figure 2-7 b that about 75 % of the injected gas rate (left axis) is released through only five ports (numbers in plot), accounting for approximately 8 % of the available outflow area. More than 10 % of the total inflow is discharged at each of these five ports (bottom axis). In addition, if all ports are included that release more than 1 % of the injected air (both right columns),

approx. 97 % of the injection rate is released through approximately 20 % of the available surface (14 ports). In other words, less than 1 % of the total inflow is discharged at 47 ports (about 75 % of total available surface area), while each of these ports discharges less than 0.1 % of the injected rate (left column).

Figure 2-8 shows the frequency distribution of the types of connections. The comparison with the experimental results reveals that all ports connected directly to the fracture network (10 %) allow the discharge of 80 % of the inflow. This relationship is also apparent from the plots in Figure 2-9, where horizontal sections of the steady-state flow field are illustrated. The heterogeneous nature due to preferential flow paths within the fracture network becomes evident.

These results coincide with findings of *Baraka-Lokmane* [1999], who found by experimental and model investigations that for fractures with apertures larger than 0.03 - 0.04 mm connected to flow measurements the largest fraction of flow (50 - 80 %) occurs through the fracture network. For the case where fractures are not directly connected to the flow measurements, i.e. injection or discharge occurs through the matrix, no considerable influence on the flow distribution and no correlation to aperture were found.

All four plots in Figure 2-9 very clearly show the effect of the fracture network on the induced flow field by increased flow rates. The main component of the fracture network is a fissure with large apertures running from side I to III on the right parallel to side II. Other peaks in the flow field pattern, e.g. higher flow rates at the two

outer ports on side IV in row 3, indicate regions where the flow is also influenced by the presence and orientation of other individual fractures (cf. ports number 409 and 412 illustrated in Appendix A-1).

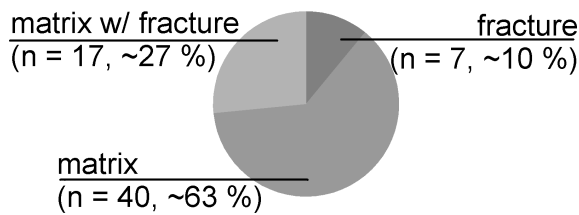


Figure 2-8. Relative frequency of the different types of port connections: ports connecting to fractures (“fracture”), to matrix (“matrix”), and ports connected to matrix in the direct vicinity of fractures (“matrix w/ fracture”).

These findings are in accordance with *Guglielmi and Mudry* [2001] who found that the flow in the fracture network in a “double-permeability” reservoir is concentrated in a few very conductive fractures.

However, in some cases the results of the flow experiment are somewhat unexpected if the results of the discrete fracture network mapping are considered. Two extreme situations were observed, where ports are directly connected to fractures but discharge a lower proportion of the injected flow rate as compared to ports connected solely to the rock matrix. Different interpretations can be given for this observation:

a. Distance from fractures

For connections to the matrix an increased influence of the fracture system can only be

found if a fracture is in the immediate vicinity (in this case less than 20 mm) to the connected port (e.g. port 110; cf. appendix A-1).

b. Fracture lengths

Connected fractures that discharge a decreased portion of the total inflow can be assumed to be of limited fracture length. Since the probability of fracture intersections decreases with decreasing fracture length [*Long and Witherspoon*, 1985], the influence of the considered proportion of the fracture system on the resulting flow will also decrease (e.g. port 215; cf. Appendix A-1).

c. Connectivity

A similar relationship applies to fissures that are not directly connected to other fractures, thus the flow field will show a reduced influence of the fracture system. This could be due to their limited length, as mentioned above, or due to directional limitation, e.g. parallel fractures along sedimentary planes, which will not intersect with each other (e.g. port 113; cf. Appendix A-1).

Generally, interpretations b) and c) are in accordance with *Streltsova* [1988], who stated, “it is fracture continuity and interconnectivity, however, not the characteristics of individual fractures that are responsible for the particulars of a fractured reservoir”. In addition as stated by *Guglielmi and Mudry* [2001], the precise characterization of the fracture network geometry is a prerequisite “for the determination of the particulars of behavior”.

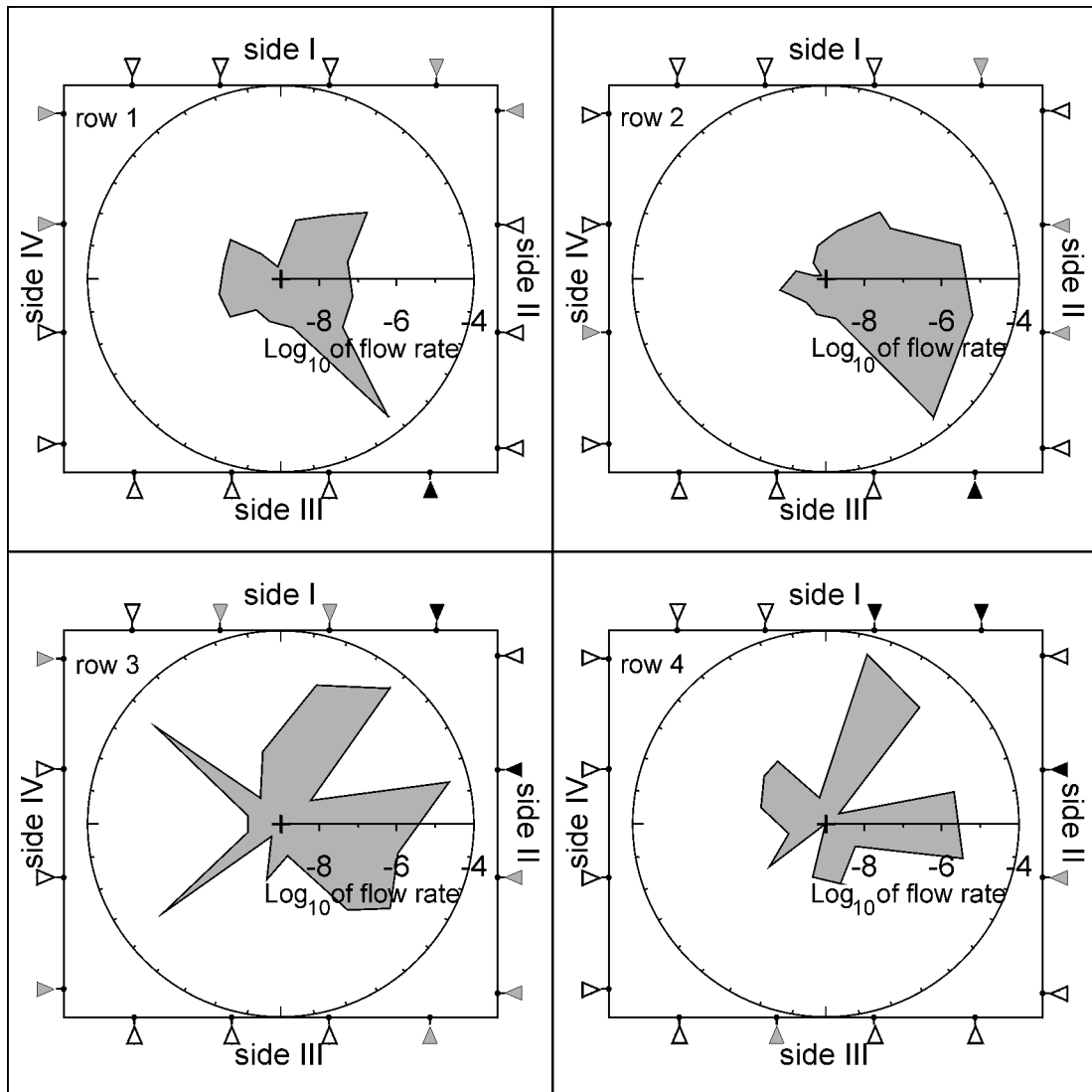


Figure 2-9. Sections parallel to the horizontally aligned ports from top to bottom illustrating distribution of the flow fractions within the block under steady-state conditions (Symbols: \triangle - matrix dominated connection, \blacktriangle - matrix connection in direct vicinity of fracture, \blacktriangle - direct fracture connection). The center of each plot matches the position of the vertical borehole (flow rate normalized to the radial distance from the central borehole in $[\text{m}^3/\text{s}] \times [\text{m}]$).

The above-described experimental series provides information on the distribution of hydraulic conductivity; an insight into the effects of heterogeneity in terms of preferential flow paths within the fractured sample can be given. No insight is gained on the effect of the variability of storage. In the following an experimental series is de-

scribed, which is additionally suitable to investigate the heterogeneity of the combined system of fracture network and porous system in a greater detail.

This series allows the examination of effects on the hydraulic measurement as a result of varying conductivity and storage

capacity, since the tests, so-called diffusivity tests, are conducted under transient-states. Wang and Dusseault [1991] gave the physical meaning of diffusivity, where the “pressure diffusion” depends on permeability, fluid viscosity and is a function of porosity and fluid compressibility. Therefore and according to Streltsova [1988], the generalized parameter of diffusivity is the quotient of hydraulic conductivity to storage and is a quantitative measure for the response of a formation on hydraulic stimulation. Such tests are therefore suitable for the characterization of differences in the flow and migration paths because they accentuate the contrast between the fracture and matrix dominated system. Fractures usually have larger values of diffusivity due to their higher conductivity and the lower ability of storage consequently leading to shorter response times to hydraulic stimulation.

2.6 Pneumatic diffusivity tests

In this experimental setup, a constant injection pressure is applied over the central borehole, while all ports on the block surface are closed. The pressure buildup is recorded with a high sampling frequency simultaneously at the single ports (Figure 2-5 b). As this experimental series are by nature to be performed at transient-state, storage has to be taken into account. In order to reduce the effects caused by wellbore storage an inliner is placed in the center of the borehole to minimize the borehole volume. Thus, a maximum space of 1 mm is available around the inliner for the pressure injection. Further storage effects are given by the storing capacity of the supply pipe, which cannot be reduced, since the flow rate would be restricted by a pipe with a smaller cross sectional area as well. A reduction of storage capacity within the wellbore can be achieved by an increase in the absolute air pressure as a result of lowered air compressibility [Ves-

selinov and Neuman, 2001]. Because of the limited strength of the block sealing an increase in the absolute air pressure in the system would lead to failure. However, as borehole storage influences the pressure buildup during early times of hydraulic or pneumatic tests and make it difficult to obtain reliable assessments of the hydraulic parameters [Vesselinov and Neuman, 2001], it gets a considerable influence on diffusivity tests in strongly heterogeneous media. For that reason, the necessity of the reduction of “artificial” storage effects (e.g. wellbore storage), which are not intrinsic properties of the investigated system, is of prime importance, since the response to any hydraulic stimulation would be inaccurately represented, i.e. delayed.

The temporal pressure buildup curves recorded at the ports on the block surface are shown in Figure 2-10. It is obvious that the curves cluster at early and more extensively at late times. In general, the curves are distributed in wide range where the first arrival of the pressure signal at the external ports can vary over orders of magnitude of normalized time.

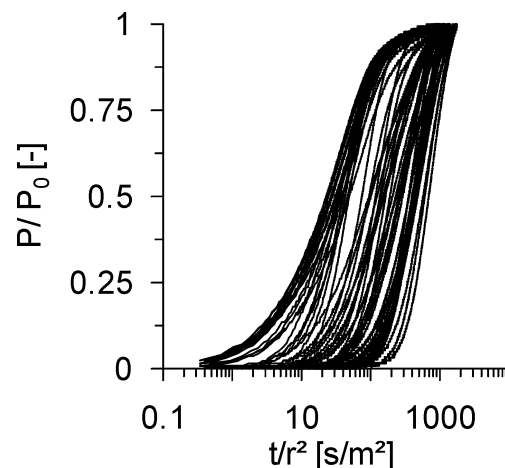


Figure 2-10. Pressure buildup curves recorded at all external ports at the block surface normalized to the square of the radial distance.

This also becomes apparent in Figure 2-11, where the variance of normalized times for particular portions of the pressure signal is illustrated (e.g. 10, 20, 30 % etc. of the initially injected pressure P_0). It is apparent that with increasing mean pressure of the system, the variance of the observed buildup rises. In order to accentuate this effect a linear time axis was chosen for Figure 2-11, while the pressure buildup in Figure 2-10 is plotted on semi-logarithmic scale.

For a detailed analysis of the induced flow field, a horizontal section through the block is analyzed in further detail. Figure 2-12 a shows the pressure buildup curves as recorded for the uppermost row of ports after applying a constant injection pressure. It is apparent that the curves are distributed in a bimodal pattern. Curves gathering at late times show late arrival times followed by a sharp pressure increase. However, most of the curves assembling at early dimensionless times with early arrival times show less sharp pressure increase.

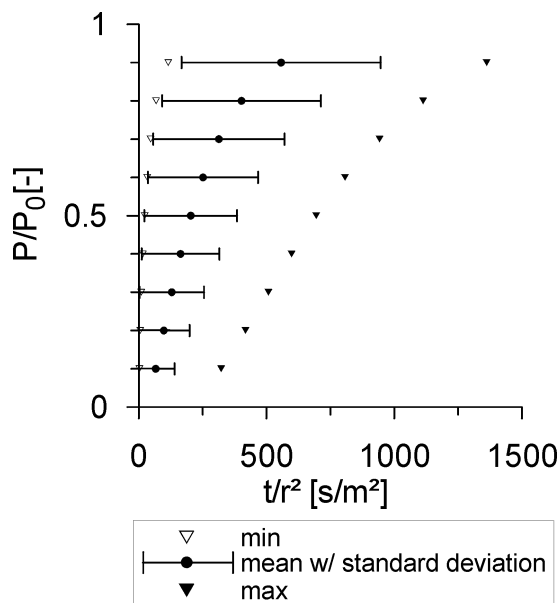


Figure 2-11. Variance of pressure buildup curves for a linear scale of normalized time for selected normalized pressures.

Single well tests (observation in the pumping well) will provide information about effective aquifer diffusivity, among other information (e.g. well efficiency). As in such tests radial flow fields are induced, no information on the aquifer anisotropy and any conductivity trends will be available [Streltsova, 1988], using traditional investigation and evaluation techniques.

Therefore, the pressure change recorded at the inlet of the borehole is used as a reference in the following, as this signal includes effects due to storage in the supplying pipe. Thus, by analyzing the pressure difference with respect to the pressure at the inlet of the borehole, information can be obtained that is solely affected by the properties of the considered system. In Figure 2-12 b the absolute difference between the observation at the inlet of the borehole and the external ports is presented.

The above-observed bimodal distribution also persists for the pressure difference curves. The presentation in Figure 2-12 b reveals more clearly various effects caused of the coupled fracture matrix-fracture system.

As described for the previous experimental series with a steady-state flow field, a detailed assessment of the integral system behavior can be obtained by using discrete information of the fractured porous system, which is available from the study of the physical and geometrical properties of the block. Those curves in Figure 2-12, which show the first pressure increase (Figure 2-12 a) and only minor difference from the pressure at the wellbore (Figure 2-12b) were recorded at ports directly connected to a fracture. The other curves originating from ports connected to the matrix. They show a delayed response, group at late times and display the largest deviations from the pressure changes at the wellbore (Figure 2-12b).

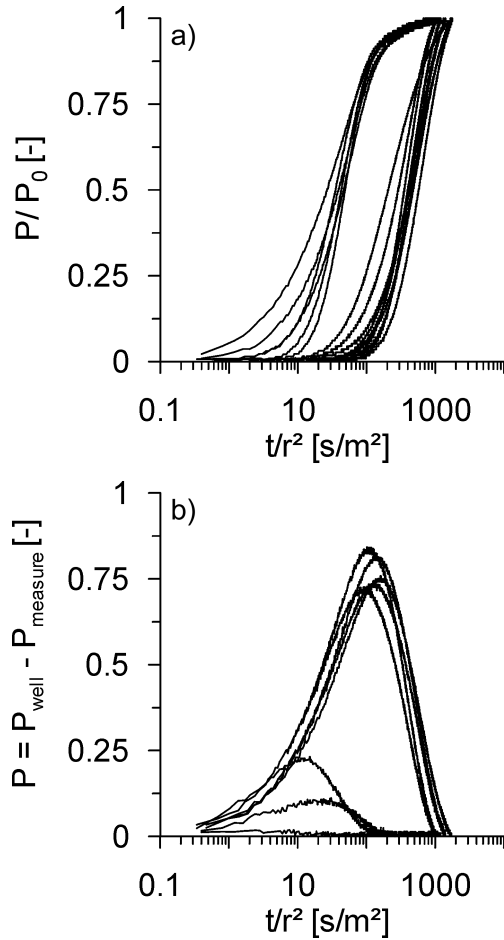


Figure 2-12. Pressure buildup curves recorded at the uppermost horizontal row of ports with constant injection pressure (a) and the absolute difference to the pressure buildup at the inlet of the wellbore (b); (P_{well} - pressure at the inlet of the borehole, $P_{measure}$ - pressure at external port).

The processes responsible for this behavior can be described as follows (Figure 2-13). Initially, the injected fluid, which theoretically expands with the speed of sound, flows along the pathways of the fracture network and only minor storage effects within the fracture system can be observed.

At later times, gas flows also to a larger extent through the matrix, while gas is stored in the matrix due to gas compression and some deformation of the matrix (increase in pore volume). The latter effect is

supposed to be of minor importance, since gas compressibility is orders of magnitude higher than the compressibility of the matrix. The change in storage effects can be deduced from the increasing pressure difference at the matrix-dominated port with respect to the inlet pressure, indicated by the curve ΔP_m .

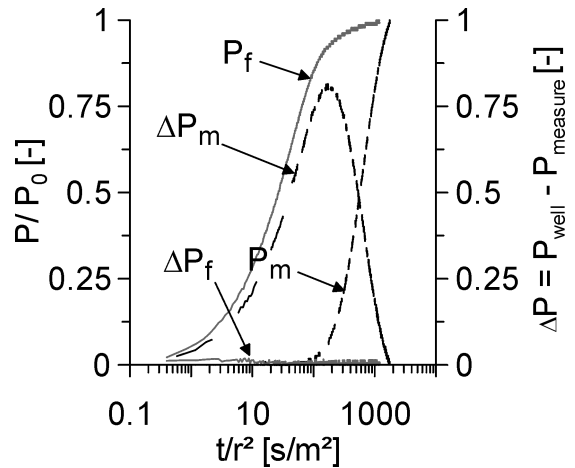


Figure 2-13. Selected pressure buildup curves for a fracture (P_f) and a matrix dominated port (P_m). The difference between the fracture (ΔP_f) and matrix (ΔP_m) dominated observation with respect to the pressure at the wellbore are obvious.

After storage due to fluid compression approaches asymptotically a physically defined limit, the pressure increase spreads through the matrix, which can be observed in the pressure increase at the matrix port (P_m). The transition from a storage-dominated phase to a pressure transfer within the matrix is indicated by maximum in the pressure difference ΔP_m (Figure 2-13). After maximum pressure difference, the absolute pressure in the matrix rapidly increases. Since the pressure difference ΔP_f reaches zero, no storage effects can be observed within the fracture system any longer.

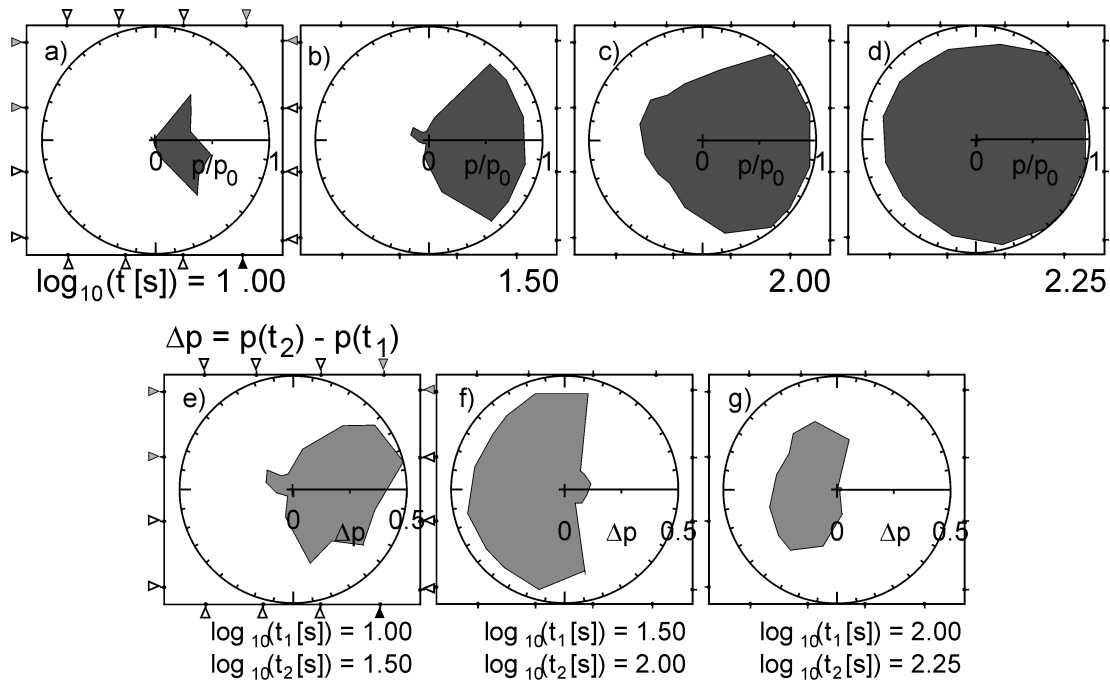


Figure 2-14. Pressure buildup recorded at the uppermost horizontal row of ports for four different times (a - d). The orientation of each plot in terms of the position and orientation is identical to Figure 2-9 (Symbols in (a) and (e) valid for all plots: Δ - matrix dominated connection, \blacktriangle - matrix connection in direct vicinity of fracture, \blacktriangle - direct fracture connection). The absolute difference between the pressure distributions at the particular time steps illustrates the affected domain within the block (e - g). Note the different scales between the plots of normalized pressure values (top; a - d) and the change in pressure (bottom, e - g).

5

The continuous spreading through the fracture system and the delayed response of the matrix-connected ports is also depicted in Figure 2-14 a - d. Pressure increases quickly in the region of the ports connected to a fracture or within the direct vicinity of a fracture, respectively (ports on the right hand side of the slice depicted in Figure 2-14). The position of the main vertical fracture (cf. Figure 2-2) is indicated in the graphs of Figure 2-14 a and e. Significant pressure buildup at matrix-dominated ports (on the left hand side) occurs after the pressure within the fractures almost reached injection pressure. The graphs in Figure 2-14 e - g illustrate the difference in pressure buildup between the particular time steps shown in Figure 2-14 a - d. This sequence of plots reveals more clearly the spatial increase of pressure within the distinct por-

tions of the fractured porous system. In Figure 2-14 e (pressure change between $\log_{10} t = 1.0$ and 1.5) it is clearly visible how the pressure increases predominantly in the fracture-dominated right area. Pressure change between $\log_{10} t = 1.5$ and 2.0 exposes that the pressure buildup is almost completed in the fracture system (on the right hand side) and that a further pressure increase takes place at the matrix dominated ports (left hand side in Figure 2-14 f). For late times, the pressure increase is limited to the portion of the porous matrix (Figure 2-14 g).

Nevertheless, some of the ports show a behavior, which is somewhat different from those described above, since some of the connections end in the matrix in the direct

vicinity of fractures (e.g. ports on the upper left hand side; Figure 2-14).

However, it could be shown that transient pressure build up measurements have a high sensitivity to the fracture network, since also matrix connection are influenced by the main matrix running from side I to III and intersects the ports on the right side in direct vicinity to side II. This is also apparent from the time series of pressure changes in Figure 2-14. Further effects due to specific properties of the fracture network are also discussed in the previous section.

2.7 Conclusions

The experimental series presented in this chapter intended to provide an insight into the effects of strongly heterogeneous media, such as fractured porous systems, on hydraulic or pneumatic measurements, respectively. In addition, an insight into the relevant processes for gas flow and pressure buildup in the heterogeneous media is given as well as these methods allow to distinguish between flow occurring in the porous matrix and along preferential pathways, i.e. in the fracture network. The experimental methods can be used to obtain high-resolution data sets, which can provide a basis for the validation of different modeling approaches as well as serve as a basis for further geostatistical investigations, which are subjects of ongoing research in the joint research project “Hard Rock Aquifer Analogue”.

The first experimental series with an induced stationary radial flow field and opened external ports provide mainly information on the heterogeneity in terms of preferential flow paths within the fractured sample, i.e. information can be gained on the

direction, respective proportions of flow, and the spatial extent of the fracture network. The effects of the porous matrix are of minor significance.

The transient pressure buildup experiments allow the examination of the effects of variable conductivity and storage capacity as summarized in the following: Because of the constant pressure injection the flow rate and therefore the injected fluid volume will decrease with time (Figure 2-15 a). Because of low storage capacity of the fracture system, pressure is increased rapidly in the fracture network and the pressure gradient toward the matrix increases to a definite value (e.g. Figure 2-13 and time step A - B in Figure 2-15). During this period the effect of matrix storage dominates and the pressure response at the matrix-connected ports will show a considerable delay (cf. Figure 2-11 through Figure 2-13 as well as Figure 2-15). During late times, after the storage capacity of the matrix is exhausted, the gradient towards the matrix decreases constantly, as the pressure in the matrix increases.

In general, both introduced methods reveal the very heterogeneous distribution of flow and pressure buildup, respectively, as result of the complexity of the system. The fracture network allows the focused flow and pressure spreading along distinct pathways leading to earlier arrival times with respect to an induced pressure stimulation. In addition, the enlarged fraction of flow along such pathways is evident.

The analysis of the distribution of the flow field (steady-state flow experiments) and the evolution of pressure buildup (diffusivity tests) during the hydraulic tests shows that the direction and the affected portion of

the flow field is highly dependent on the spatial formation of the fracture network and on the position of the observations with respect to highly conductive features. An examination of the pressure distribution in the sandstone block during the transient tests revealed how the response depends on the spatial position of the observation points at the block surface with respect to the type of connection, i.e. matrix or fracture dominated. The distinctive response to stimulation can be exploited to differentiate between matrix and fracture dominated flow.

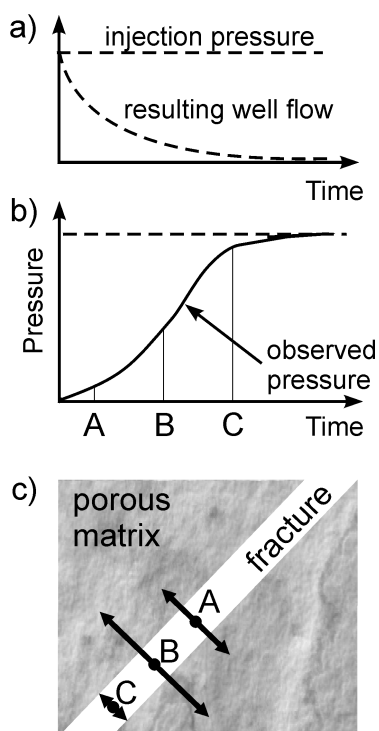


Figure 2-15. Relationship between the hydraulic disturbance of the system and the change of flow with time. (a) Evolution of the well flow at constant injection pressure. (b) Comparison of the injected pressure with the observed pressure at the external ports. (c) Arrows indicate the pressure gradient as difference between the injected and observed pressure within the matrix for three particular time steps (A - C).

In common, the presented experimental series expose two principle consequences:

→ The methods developed for the investigation of the strongly heterogeneous system of a fractured porous rock allows using practical measurements to reveal effects arising from the heterogeneity of the investigated system, as discussed above.

→ However, the comparison of the results from both experimental series (e.g. Figure 2-9 a and Figure 2-14 a - c) exemplifies the necessity of an improved understanding of the interrelation between an arbitrary parameter distribution and the response of a particular hydraulic measurement or measuring method, respectively. A promising concept to account for this interrelationship is the approach of sensitivity coefficients initially developed for the conception and interpretation of DC-geoelectric tracer experiments [Dietrich, 1999]. In the following chapters this approach is transferred and extended to groundwater hydraulics. To develop a fundamental understanding of the interrelationship between heterogeneity and the response of particular hydraulic measurements, the approach is applied to more general cases of heterogeneity, but can also be applied to strongly heterogeneous systems such as fractured porous aquifers.

3 The Approach of Sensitivity Coefficients

3.1 Introduction

The suitability of subsurface investigation methods for the characterization and the capability of the determination of variations in the distribution of hydraulic parameters is primarily controlled by the intrinsic characteristics of the measuring configuration. Therefore, concepts have to be utilized which can contribute to the understanding of effects of heterogeneities to an observed stimulus response. For this purpose the Sensitivity Coefficient Approach (SCA) is a useful tool allowing the analysis and evaluation of potential measurements providing an understanding of the influence of heterogeneities. The theory of the SCA is given in the following sections.

3.2 Governing equations

“Suppose that the ground consists of a uniform sand covered with an impermeable layer filled with water. Suppose further that the electrodes were to be replaced by wells terminated at the top of the sand by hemispherical screens, and electrical battery replaced by a pump connecting the two wells. Then, with the pump operating at a uniform rate, a water flow field would be created through the sand between the two wells. What would be the nature of the flow field, and what would be the equations describing the flow?” [Hubbert, 1969].

As described by Hubbert [1969] and Bredehoeft et al. [1966], among others, for many physical phenomena, which use potential fields, e.g. groundwater hydraulics, geoelectrics, and heat conduction, the relation between parameter distribution and measurable quantity can be described by the same differential equation. Table 3-1 lists relevant variables and quantities of analogies to groundwater flow.

Table 3-1. Analogies to groundwater flow, after Wang and Anderson [1982].

Problem	Parameter k	Potential u	Source function q
<i>Geoelectric</i>	Electric conductivity	Voltage	Current density
<i>Groundwater hydraulics</i>	Hydraulic conductivity	Hydraulic potential	Sink- / source term
<i>Heat conduction</i>	Heat conductivity	Temperature	Heat production rate

The relationship between the distribution of the parameter k , the potential u and the source function q can be described for steady-state conditions by

$$-\sum_{i=1}^n \frac{\partial}{\partial x^i} \left(k(x) \frac{\partial u(x)}{\partial x^i} \right) = q(x) \quad \text{Eq. 3-1}$$

with $x \in \Omega$, where Ω represents the domain of interest and n is the number of considered dimensions. To quantify the potential u for a given parameter distribution k the specification of boundary conditions is necessary to make the solution of Eq. 3-1 unique.

Three types of conditions are possible:

i) Boundaries of first type (Dirichlet): The head is known on the limits of the flow region. This can be expressed by

$$u(x) = h_D(x) \quad x \in \Gamma \quad \text{Eq. 3-2}$$

where Γ is the boundary of the flow domain Ω , and $h_D(x)$ is the function describing the potential on the boundary. For fixed head boundaries the function $h_D(x) = \text{const}$.

ii) Boundaries of second type (Neumann): The flow across the boundary of the region is known:

$$-k(x) \frac{\partial}{\partial n} u(x) = h_N(x) \quad x \in \Gamma_N \subset \Gamma \quad \text{Eq. 3-3}$$

where Γ_N is a subdomain of the boundary Γ , and h_N is a function giving the flow perpendicular to the boundary. For no-flow boundaries $h_N = 0$.

iii) Boundary of third type (Cauchy): For this type of boundary some combination of

the boundaries of first and second type is known on the limit of the flow domain:

$$\begin{aligned} u(x) &= h_D(x) & x \in \Gamma_D \\ k(x) \frac{\partial}{\partial n} u(x) &= h_N(x) & x \in \Gamma_N \end{aligned} \quad \text{Eq. 3-4}$$

where $\Gamma = \Gamma_D \cup \Gamma_N$ is the boundary of the flow domain Ω .

If the potential u changes with time, Eq. 3-1 has to be rewritten including the time coordinate t and the storage term S

$$\begin{aligned} S(x) \frac{\partial u(x,t)}{\partial t} \\ - \sum_{i=1}^n \frac{\partial}{\partial x^i} \left(k(x) \frac{\partial u(x,t)}{\partial x^i} \right) &= q(x,t) \end{aligned} \quad \text{Eq. 3-5}$$

with $x \in \Omega$ and $t \in \{0, T\}$

For a unique determination of the potential u the specification of boundary conditions analogous to Eq. 3-2, Eq. 3-3, and Eq. 3-4 is necessary:

i) First type

$$u(x,t) = h_D(x,t) \quad x \in \Gamma, t \in \{0, T\} \quad \text{Eq. 3-6}$$

ii) Second type

$$\begin{aligned} k(x) \frac{\partial}{\partial n} u(x,t) &= h_N(x,t) \\ x \in \Gamma; t \in \{0, T\} \end{aligned} \quad \text{Eq. 3-7}$$

iii) Third type

$$\begin{aligned} u(x,t) &= h_D(x,t) & x \in \Gamma_D \\ k(x) \frac{\partial}{\partial n} u(x,t) &= h_N(x,t) \\ x \in \Gamma_N, t &= \{0, T\} \end{aligned} \quad \text{Eq. 3-8}$$

with $0 < T < \infty$. In addition, the unique determination of u requires the specification of the initial state, where

$$u(x,0) = h_0(x) \quad x \in \Omega \quad \text{Eq. 3-9}$$

The transfer between applications of the potential field theory is possible based on the same mathematical formulation of the different physical relationships. An example for such a transfer is the application of the SCA for the analysis and evaluation of hydraulic measurements. This approach was originally utilized for the conception and interpretation of DC-geo-electrical measuring configurations [Dietrich, 1999]. It allows the analysis and evaluation of potential measurements and gives an understanding of the influence of heterogeneities on a measured value. In the following, the approach is transferred from DC-geo-electric (steady-state conditions) to groundwater hydraulics (steady- and transient-state conditions).

3.3 The Sensitivity Coefficient Approach

The effect of a particular deviation in the parameter distribution on the observation within a distinct domain can be expressed by

$$\Delta u = \sum_{j=1}^m I_j \cdot \Delta k_j \quad \text{Eq. 3-10}$$

where Δk_j corresponds to a change in the parameter distribution in the subdomain j causing a change in the observation Δu ; m is the total number of subdomains which potentially contain parameter changes. The coefficient I_j can be considered as a sensitivity coefficient, i.e. it is a measure for the

effect of a deviation in the parameter distribution on the measured quantity. While changes in the parameter distribution in some subdomain are supposed to be small compared to the absolute value of the parameter in the subdomain, the sensitivity coefficient can be approximated by

$$I_j \approx \frac{\partial u}{\partial k_j} \quad \text{Eq. 3-11}$$

which relates a change of the parameter k in the domain j to a particular change in the observation u . In groundwater hydraulics, I quantifies the change of the hydraulic head as result of a particular heterogeneity in the distribution of the hydraulic conductivity k .

This meaning of sensitivity coefficients corresponds to the definition used in inverse problem theory for parameter identification. Traditionally, the Gauss-Newton algorithm is used, where the elements of the Jacobian matrix consist of the partial derivatives of the observation with respect to the considered parameter. Generally, three different methods are commonly used for computing the Jacobian matrix, i.e. calculating the sensitivity coefficients [e.g. Yeh, 1986; Sun, 1994].

3.4 Calculation of the parameter derivative $\partial u / \partial k$

In this following section the main approaches for the calculation of the parameter derivative $\partial u / \partial k$, i.e. the sensitivity coefficients, are briefly sketched. All introduced methods allow the transformation from transient to the steady-state conditions without any restriction, thus only the formalisms for

the transient-state are preliminarily given. More detailed work is cited in the following section and can also be found in *Yeh* [1986], and *Sun* [1994], among others.

3.4.1 Influence coefficient method

The method of influence coefficients is based on the concept of parameter perturbation [*Becker and Yeh*, 1972]. This approach corresponds to the discrete description of the parameter derivative

$$\frac{\partial u}{\partial k_j} = \frac{u(k + \Delta k_j) - u(k)}{\Delta k_j}$$

Eq. 3-12

The values of $u(k)$ and $u(k + \Delta k)$ are obtained by solving the governing equation Eq. 3-1 and Eq. 3-5, respectively, subject to the imposed initial and boundary conditions. This method requires perturbing each parameter once at a time. For m subdomains, the governing equation has to be solved $(m + 1)$ times.

3.4.2 Sensitivity equation method

In this method, the parameter derivative $\delta u/\delta k$ is obtained by taking the partial derivatives with respect to each parameter in the governing equation Eq. 3-1 and Eq. 3-5, respectively, and initial and boundary conditions [*Yeh*, 1986]. Hence, the following set of sensitivity equation results

$$S \frac{\partial \partial u / \partial k_j}{dt} - \sum_{i=1}^n \frac{\partial}{\partial x^i} \left(\frac{k \partial u / \partial k_j}{\partial x^i} \right) = \sum_{i=1}^n \frac{\partial}{\partial x^i} \left(\frac{\partial k}{\partial k_j} \frac{\partial u}{\partial x^i} \right)$$

Eq. 3-13

where k_j is the parameter in the subdomain j . The number of simulations required for computation of the sensitivity coefficients is $(m+1)$, which is the same as for the influence coefficient method.

3.4.3 Adjoint state method

a. General formulation

The adjoint state method is based on the variational theory, and is applied in various fields, such as parameter estimation, reliability estimates, observation design, and sensitivity analysis [*Sun*, 1994]. While this method requires only one more simulation run than observation points are included, it is obviously the most advantageous approach in terms of the numerical effort, if the number of observation wells is small compared to the total number of subdomains m .

In literature, various concepts are discussed based on the variational theory [e.g. *Carter et al.*, 1974, *Chavent et al.*, 1975; *Kravaris and Seinfeld*, 1985; *Dietrich*, 1992; among others].

Following *Carter et al.* [1974, 1982], who extended the pioneer work of *Jacquard* [1964] and *Jacquard and Jain* [1965], the sensitivity coefficients with respect to the hydraulic conductivity can be calculated by

$$\begin{aligned}
 I_k(\Omega_j, t) &= \left. \frac{\partial u(x, t)}{\partial k} \right|_{\Omega_j} \\
 &= - \int_{\Omega_j} \int_0^t \sum_{i=1}^n \frac{\partial v'(x, t - \tau)}{\partial x^i} \frac{\partial u(x, \tau)}{\partial x^i} d\tau d\omega
 \end{aligned}$$

Eq. 3-14

where I_k is the sensitivity coefficient with respect to hydraulic conductivity. The sensitivity coefficient I_S in terms of the storage can be calculated by

$$\begin{aligned}
 I_S(\Omega_j, t) &= \left. \frac{\partial u(x, t)}{\partial S} \right|_{\Omega_j} \\
 &= - \int_{\Omega_j} \int_0^t v'(x, t - \tau) \frac{\partial u(x, \tau)}{\partial \tau} d\tau d\omega
 \end{aligned}$$

Eq. 3-15

where the sensitivity coefficients I_k and I_S , respectively, are expressed as functions of time t and spatial extension Ω_j of the subdomain j , in which a change in the parameter distribution is expected. The variable $v'(x, t)$ is the temporal derivative of $v(x, t)$ as the solution of the adjoint equation

$$\begin{aligned}
 S(x) \frac{\partial v(x, t)}{\partial t} - \\
 \sum_{i=1}^n \frac{\partial}{\partial x^i} \left(k(x) \frac{\partial v(x)}{\partial x^i} \right) = G(x) H(t)
 \end{aligned}$$

Eq. 3-16

The initial and boundary conditions for the calculation of $v(x)$ correspond to that imposed for the calculation of u . $G(x)$ is the continuous source function at the location of the observation well. Outside the specified location $G(x) = 0$; and

$$\begin{aligned}
 H(t) &= 0 & \text{for } t \leq 0 \\
 H(t) &= 1 & \text{for } t > 0
 \end{aligned}$$

Eq. 3-17

It is obvious that the adjoint equation for solving $v(x, t)$ is of the same form as Eq. 3-5 allowing the same numerical routine for calculating u and v . Practically, equation Eq. 3-5 is solved once for the calculation of u and Eq. 3-16 is solved once for each observation point. From this, the advantage of the utilized method becomes evident, as for a simple pumping test configuration, with one pumping and one observation well, only two computations are necessary for the whole model domain.

Carter et al. [1982] gave an interpretation of the adjoint equation, where the solution of Eq. 3-16 is given by the pressure responses to a constant withdrawal, which corresponds to the well known Heaviside unit step function $H(t)$. Compared to other solutions for the sensitivity coefficients using the adjoint equation method [cf. *Chavent et al.* 1975; *Kravaris and Seinfeld*, 1985; *Dietrich*, 1992; among others], it should be noted that in the cited approaches the temporal derivative of the solution for the adjoint equation is missing. This is because their solution can be interpreted as the pressure responses to a single pulse, a Dirac function-like withdrawal, where the Dirac function $\delta(t)$ equals the derivative of $H(t)$, at the time $\tau = t$ and the time τ runs backward from t to zero.

Furthermore, the adjoint state method introduced by *Carter et al.* [1974] is based on particular properties of equation Eq. 3-1 and Eq. 3-5, respectively:

i) Reciprocity, which exists, if the pumping and observation well in a hydraulic test would be interchanged and the same observation as in the original configuration would be made (Figure 3-1).

ii) The solutions can be described by convolution integrals and

iii) the parameters k and S are linear.

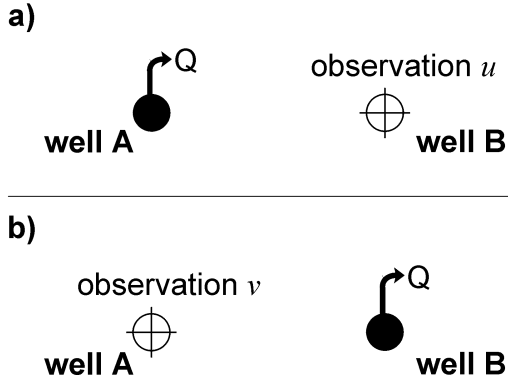


Figure 3-1. Principle of reciprocity. a) Initial positioning: pumping (Q = pumping rate) at well A leads to the observation u at well B. b) Situation with interchanged well positions: pumping at well B leads to the observation v at well A. Due to reciprocity observation v equals the observation u from the initial configuration.

In the present work, the adjoint state method is used to compute the derivative $\delta u/\delta k$ and $\delta u/\delta S$, respectively, to gain an understanding of the effect of heterogeneous parameter distributions on hydraulic measurements. For this purpose the adjoint state method is advantageous, because it can be utilized for the computation of sensitivity coefficients for arbitrary parameter distributions, as well as hydrogeologic systems with particular boundary conditions. Furthermore, this approach allows the computation of sensitivity coefficients using analytical solutions of Eq. 3-1 and Eq. 3-5, respectively, for known hydrogeologic situations.

b. The steady-state case

With $\partial u/\partial t = 0$ the time dependent Eq. 3-5 is transposed to Eq. 3-1 describing the steady-state condition. Consequently, the dependence of the observation of u from storage S will vanish and a reformulation of the parameter derivative $\partial u/\partial I_k$ for steady-state conditions has to be given.

Basically, all previously discussed approaches for the calculation of the parameter derivative $\partial u/\partial I_k$ can directly be utilized for steady-state conditions. *Dietrich* [1992] derives a solution for the calculation of $\partial u/\partial I_k$ for steady-state conditions, also based on the adjoint state method. Accordingly, the relation between the deviations in hydraulic head due to a deviation in the parameter distribution is given by

$$I_k(\Omega_j) = \left. \frac{\partial u}{\partial k} \right|_{\Omega_j} = - \int_{\Omega_j} \sum_{i=1}^n \frac{\partial u(x)}{\partial x^i} \frac{\partial v(x)}{\partial x^i} d\omega \quad \text{Eq. 3-18}$$

where the hydraulic head u is a solution of Eq. 3-1 and v is the solution of the adjoint equation

$$- \sum_{i=1}^n \frac{\partial}{\partial x^i} \left(k(x) \frac{\partial v(x)}{\partial x^i} \right) = G(x) \quad \text{Eq. 3-19}$$

with the appropriate boundary conditions corresponding to the conditions of Eq. 3-1, and $G(x)$ as the source function at the location of the observation well. As discussed in the previous section, the adjoint equation Eq. 3-19 for v is of the same form as Eq. 3-1, thus the same numerical algorithm can be utilized for the computation of

u and v . All other principles given in the general formulation of the previous section are valid in terms of implementation and realization.

3.5 Performance of the sensitivity coefficient approach

Generally, using the adjoint state method sensitivity coefficients can be derived from the superposition of two independent potential fields, i.e. two independent hydraulic tests with the same points of measurement at a given time t or for the steady-state case, respectively. The actual pumping test leads to the head distribution u . To gain the solution v of the adjoint equation, in practice a second pumping test is simulated, where the original observation well is used as pumping well. As discussed previously, this is based on reciprocity of hydraulic tests (e.g. Figure 3-1) and can also be derived from Eq. 3-14 and Eq. 3-18, respectively.

Practically, the calculation of the sensitivity coefficients can be implemented numerically, i.e. by using numerically simulated potential distributions with consecutive numerical differentiation and integration, or utilizing analytical solutions for known hydrogeologic conditions.

3.5.1 Numerical implementation

For the computation of sensitivity coefficients for arbitrary parameter distributions, numerical methods have to be utilized since appropriate analytical solutions are only known for specific hydrogeologic situations. The flow chart in Figure 3-2 illustrates the consecutive steps in computing sensitivity

coefficients in terms of a numerical implementation.

Step 1. Discretization and parameterization

In many practical hydrogeologic situations, information is available about general or specific boundary conditions and / or certain parameter distributions, e.g. preferential flow directions or macro-heterogeneities based on geophysical investigations. In practice, this information can be implemented most easily by the application of finite difference methods, since they allow a simple discretization and parameterization by appropriate zonation.

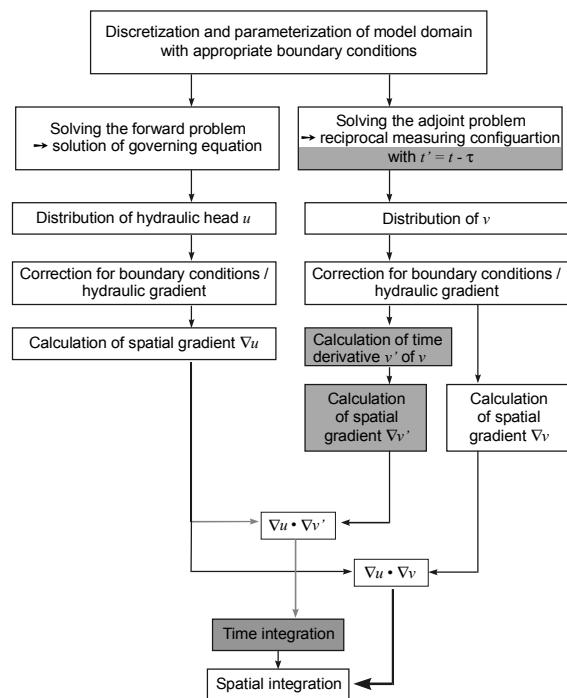


Figure 3-2. Flow chart of the consecutive steps for the computation of the sensitivity coefficients. Boxes in gray indicate steps necessary for computations for transient-state conditions.

Step 2. Solution of the forward problem and the adjoint equation

The analysis of equations Eq. 3-14 and Eq. 3-15 for transient conditions, and Eq. 3-18 for steady-state conditions, respectively, shows that the parameter derivatives $\partial u/\partial k$ and $\partial u/\partial S$ not only depend on the parameters k and S , respectively, and the hydraulic head u as response on the source term $q(x)$, but also on the response v as result of a hydraulic stimulation $G(x)$ at the location of the observation well. Hence, for the calculation of the sensitivity coefficients $\partial u/\partial k$ and $\partial u/\partial S$, equations Eq. 3-1 and Eq. 3-5, respectively, have to be solved once in each iteration step, and Eq. 3-16 or Eq. 3-19 have to be solved once in each iteration step for each observation point.

i) Transient conditions: For transient cases, only a limited number of data points out of the time series are available from each grid cell, therefore a spline interpolation algorithm [e.g. cubic spline interpolation, cf. *Press et al.*, 1996] can be utilized for calculating the solution with an adequate time discretization in the numerical realization. The calculation of the coefficients of the spline interpolation requires the computation of the derivatives at the beginning and the end of the interval $(0, t)$. Because at $t = 0$ the distribution of the hydraulic head can be regarded as the steady-state conditions, the derivatives equal zero. At the time $t = \tau$ the derivative is calculated by the difference quotient between $t = \tau$ and $t = (\tau - 1)$.

In addition, for the calculation of Eq. 3-5 and Eq. 3-16, the solution of the adjoint equation is required with the following transformation of the time coordinate

$$t' = t - \tau \tag{Eq. 3-20}$$

Since the resulting adjoint equation has the same form as the governing equation of the forward problem, it is possible to use the same numerical algorithm, as it is used for solving the forward problem. Furthermore, as reciprocity exists and the solution of Eq. 3-16 can physically be considered as the head response to a constant withdrawal at the observation well, for the source term $G(x)$, the value $q(x)$ from the solution of the original equation is used.

As described above, the numerical implementation is realized, using spline approximations for the solution of the adjoint equation.

ii) Steady-state conditions: For the calculation of the potential distribution under steady-state conditions, only two simulation runs of the finite difference model are required to solve Eq. 3-1 and Eq. 3-19.

Step 3. Correction for boundary conditions / hydraulic gradients

It can be shown that head changes due to parameter deviations during hydraulic tests are independent from the hydraulic gradient due to distinct boundary conditions. Hence for the calculation of sensitivity coefficients the potential field due to specific boundary conditions can be removed, e.g. using the method of singularity removal [e.g. *Lowry et al.*, 1989].

The potential distribution without hydraulic disturbance, i.e. pumping well (singularity), can be expressed following Eq. 3-5 by

$$S(x) \frac{\partial u(x,t)}{\partial t} - \sum_{i=1}^n \frac{\partial}{\partial x^i} \left(k(x) \frac{\partial u(x)}{\partial x^i} \right) = 0$$

Eq. 3-21

where u is the hydraulic head. The potential distribution resulting from pumping can be described by

$$S(x) \frac{\partial u'(x,t)}{\partial t} - \sum_{i=1}^n \frac{\partial}{\partial x^i} \left(k(x) \frac{\partial u'(x)}{\partial x^i} \right) = q$$

Eq. 3-22

with $u' = (u + s)$, which is the sum of the initial head u and the pumping induced head disturbance s , i.e. the quantity of draw-down. The difference between Eq. 3-21 and Eq. 3-22 is therefore appropriate for the calculation of the response due to a disturbance at a single spatial position and can be expressed by

$$S(x) \frac{\partial s(x,t)}{\partial t} - \sum_{i=1}^n \frac{\partial}{\partial x^i} \left(k(x) \frac{\partial s(x)}{\partial x^i} \right) = q$$

Eq. 3-23

For steady-state conditions, as the time derivative of the head, i.e. $\partial u/\partial t$ and $\partial s/\partial t$, respectively, equals zero the term on the left hand side quantifying the storage S will vanish.

In the same way the boundary conditions can be specified for the domain with and without hydraulic disturbance due to pumping. Accordingly, for transient-state the Dirichlet boundary based on Eq. 3-6 can be described using the method of singularity removal by

$$s(x,t) = 0 \quad x \in \Gamma, t \in \{0, T\}$$

Eq. 3-24

and Neumann boundaries following Eq. 3-7 by

$$k(x) \frac{\partial}{\partial n} s(x,t) = 0 \quad x \in \Gamma, t \in \{0, T\}$$

Eq. 3-25

For steady-state, the boundary conditions are defined according to Eq. 3-24 and Eq. 3-25 neglecting the time information.

Step 4. Calculation of temporal derivatives and gradients

i) Transient-state: Following equations Eq. 3-14 and Eq. 3-15 the calculation of the temporal derivative v' of the solution of the adjoint equation is required. As mentioned above the introduction of the temporal derivative results from the kind of the source term in Eq. 3-16. In practice, the same algorithm as for the interpolation of the time series of v can be utilized with appropriate conversions. In addition, the computation of the spatial gradients of the solution u of the forward problem and the temporal derivatives v' of the solution of the adjoint equation is required, whereby simple numerical algorithms can be utilized.

ii) Steady-state conditions: For steady-state conditions the spatial gradients of the solutions u and v are calculated using simple numerical algorithms.

Step 5. Calculation of the coefficients $\partial u/\partial k$ and $\partial u/\partial S$

i) Transient conditions: For the calculation of the parameter derivatives $\partial u/\partial k$ and

$\partial u/\partial S$ the calculated potential gradients are used with equations Eq. 3-14 and Eq. 3-15. For an increased accuracy, it is beneficial to calculate first the integral over the time domain $(0, t)$ before the spatial numerical integration is realized. For this purpose, the Romberg integration [cf. *Press et al.*, 1996] is one of the most suitable and powerful approximations of the integral in the time domain $(0, t)$.

ii) Steady-state conditions: For the calculation of the parameter derivative $\partial u/\partial k$ the calculated potential gradients are used with equations Eq. 3-18 performing a spatial integration.

3.5.2 Application of analytical solutions

For several definite hydrogeologic conditions analytical solutions of Eq. 3-1 and Eq. 3-5, respectively, can be derived. In this section the solution of Eq. 3-14 and Eq. 3-15 for the case of a transient pumping test in a two dimensional, homogeneous and isotropic, confined aquifer is given. From this case essential considerations with respect to effects from parameter distributions can be gathered.

The solution representing the specified hydrogeologic conditions is given by *Theis* [1935] by

$$s = \frac{Q}{4\pi T} \int_u^\infty \frac{e^{-z}}{z} dz \quad \text{and} \quad u = \frac{r^2 S}{4Tt} \quad \text{Eq. 3-26}$$

valid for a domain of infinite extent.

Using the parameter derivatives Eq. 3-14 and Eq. 3-15 given by the adjoint state method in combination with Eq. 3-26 and

replacing the hydraulic conductivity by the transmissivity T where

$$T = k \cdot b \quad \text{Eq. 3-27}$$

with b = aquifer thickness, the sensitivity coefficients for the observation with respect to a change in the transmissivity distribution can be calculated by

$$\begin{aligned} I_T(\Omega_i, t) &= \left. \frac{\partial s(t)}{\partial T} \right|_{\Omega_i} \\ &= - \int_{\Omega_j, 0}^t \frac{Q^2 S}{16\pi^2 T^3} \frac{e^{-\frac{S}{4T} \left(\frac{r_{ow}^2}{t-\tau} + \frac{r_{pw}^2}{\tau} \right)}}{(t-\tau)^2 r_{pw}^2} \cdot \\ &\quad (x_{pw} x_{ow} + y_{pw} y_{ow}) d\tau d\omega \end{aligned} \quad \text{Eq. 3-28}$$

Q is the pumping rate and $x_{pw}, y_{pw}, x_{ow}, y_{ow}$ are the distances to the pumping (PW) and observation well (OW) in x - and y -direction, respectively. The distance to the observation and pumping well is expressed by r_{ow} and r_{pw} . If the pumping well is located at $(\lambda, 0)$ and the observation well at $(-\lambda, 0)$ Eq. 3-28 can be expressed by

$$\begin{aligned} I_T(\Omega_i, t) &= \left. \frac{\partial s(t)}{\partial T} \right|_{\Omega_i} \\ &= - \int_{\Omega_j, 0}^t \frac{Q^2 S}{16\pi^2 T^3} \frac{e^{-\frac{S}{4T} \left(\frac{r_{ow}^2}{t-\tau} + \frac{r_{pw}^2}{\tau} \right)}}{(t-\tau)^2 r_{pw}^2} \cdot \\ &\quad (x^2 - \lambda^2 + y^2) d\tau d\omega \end{aligned} \quad \text{Eq. 3-29}$$

where

$$\begin{aligned} r_{pw} &= \sqrt{(x + \lambda)^2 + y^2} \\ r_{ow} &= \sqrt{(x - \lambda)^2 + y^2} \end{aligned} \quad \text{Eq. 3-30}$$

The sensitivity coefficient with respect to storage can accordingly be calculated by

$$I_S(\Omega_i, t) = \left. \frac{\partial s(t)}{\partial S} \right|_{\Omega_i} = - \int_{\Omega_j, 0}^t \left[\frac{Q^2}{16\pi^2 T^2} e^{\left[-\frac{S}{4T} \left(\frac{r_{ow}^2}{t-\tau} + \frac{r_{pw}^2}{\tau} \right) \right]} \right] d\tau d\omega$$

Eq. 3-31

From Eq. 3-29 and Eq. 3-31 it is evident that the sensitivity coefficients with respect to transmissivity and storage, respectively, are symmetrical about $x = 0$ and $y = 0$.

4 Analysis of Sensitivity Coefficients

4.1 Introduction

Based on the derivation of sensitivity coefficients an analysis of the sensitivity distribution with respect to variations of the governing parameters is given in this chapter. In order to evaluate the effects of parameter deviations on the hydraulic measurements it is most appropriate to analyze the distribution of sensitivity coefficients for a homogeneous parameter distribution. In this case, particular characteristics of the distribution of sensitivity coefficients are solely depending on the measuring configuration itself. Heterogeneous parameter distributions will be addressed in the following chapter 5.

In the following the distribution of sensitivity coefficients for the configuration of pumping test with one pumping and one observation well is analyzed based on the analytical solutions Eq. 3-28 and Eq. 3-31 given in the previous chapter

4.2 General considerations

A detailed analysis of the governing equations for the calculation of sensitivity coefficients and their solutions, e.g. Eq. 3-28 and Eq. 3-31), reveal some essential correlations that are independent from the actual measuring configuration: The values of sensitivity coefficients depend on

i) the parameter distribution of the domain of interest,

ii) the location of the points of measurement, i.e. pumping and observation wells,

iii) and on the spatial extension and magnitude of a potential discontinuity in the parameter distribution located in the domain of interest.

Furthermore, based on the equations for the calculation of sensitivity coefficients with respect to hydraulic conductivity (e.g. Eq. 3-18) the sensitivity coefficients can be considered as integral over the scalar product of the gradients ∇u and ∇v . With

$$\nabla u \cdot \nabla v = |\nabla u| \cdot |\nabla v| \cdot \cos\vartheta \quad \text{Eq. 4-1}$$

where ϑ is the angle between the gradients ∇u and ∇v . If ∇u and ∇v are perpendicular on each other, thus $\vartheta = 90^\circ$ or $\vartheta = 0^\circ$, the resulting coefficient equals zero. Accordingly, for angles of $0^\circ < \vartheta < 90^\circ$ the coefficients e.g. resulting from Eq. 3-18 are negative, and for angles of $90^\circ < \vartheta < 180^\circ$ the resulting coefficients are positive. It can be derived from Eq. 4-1 that with decreasing gradients ∇u and ∇v the influence on the measured quantity will decrease. Hence the value of sensitivity coefficient will decrease with increasing distance from the wells. The consequences for the spatial distribution of sensitivity will be shown in the following.

4.3 Sensitivity with respect to hydraulic conductivity

For a detailed analysis of sensitivity coefficients with respect to changes in hydraulic conductivity a two-dimensional distribution for a pumping test in a homogeneous, two-dimensional aquifer is given for three timesteps in Figure 4-1.

In order to obtain values that are independent from the distance between pumping and observation well, a normalization is introduced for the considerations with spatially separated pumping and observation positions using the transformation

$$\begin{aligned}x' &= x / r \\y' &= y / r\end{aligned}\tag{Eq. 4-2}$$

where r is the distance between the pumping and observation well. Hence, for the calculation of non-normalized sensitivity coefficients the following transformation is useful

$$I'(x', y') = I(x, y) \cdot r\tag{Eq. 4-3}$$

As the sensitivity distributions of a pumping test for homogeneous conditions under steady-state is of the same form as those for the transient-state at very late times, the steady-state case is not explicitly considered in this section. However, sensitivity distributions with respect to hydraulic conductivity for the steady-state case are

given and discussed in the following chapter 5.

From the spatial distribution of sensitivity coefficients in Figure 4-1, it is obvious that two domains of contrary sensitivity classify the spatial distribution. The transition zone between these domains is presented by a circle intersecting the pumping and observation well. Since the values of sensitivity on the transition zone approach zero, a parameter change on this line will have no impact on the observation.

The domain outside the transition zone represents a region having a negative sensitivity on drawdown with respect to a change in the parameter distribution. However, the domain between the pumping and observation well is characterized by positive sensitivity. Consequently, any heterogeneity of definite spatial extent and quantity could lead either to an increase or to a decrease of the observed value u , depending on the spatial position of the heterogeneity relative to the wells. Hence, a particular discontinuity at the same radial distance from the pumping well will not necessarily lead to the same observation.

For example, a discontinuity of higher conductivity in the domain of positive sensitivity will result in an increased drawdown, which contradicts the classical understanding of pumping tests, where increased drawdown is assumed to be the result of lowered conductivity.

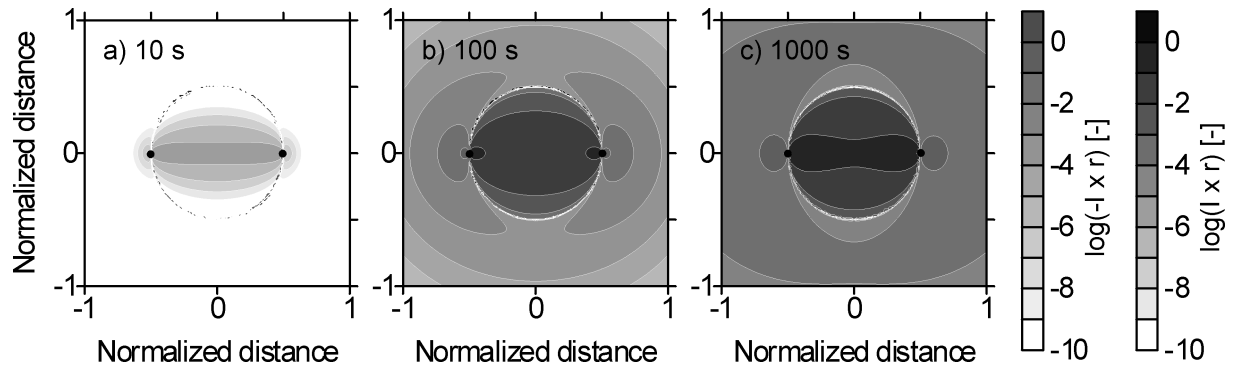


Figure 4-1. Two-dimensional sensitivity distribution for the times $t = 10, 100, 1000$ seconds. The black dots indicate the position of the pumping and observation well ($k = 10^{-4}$ m/s, $S = 10^{-4}$, $Q = 300$ m³/d).

The highest sensitivities with respect to a change in hydraulic conductivity are in the direct vicinity to the wells and are decreasing with increasing distance from the points of measurement. Hence, a small spatial discontinuity in direct vicinity of one well can lead to dramatic effects on the observed potential. However, although the domain of highest influence is located in vicinity of the wells, not every variation in hydraulic conductivity necessarily causes a noticeable influence on the observation u , e.g. if it lies near the line of zero influence, as discussed above.

The shape of the sensitivity distribution does not change for differing values of hydraulic conductivity and the symmetric form of the sensitivity distribution reflects reciprocity of the hydraulic test configuration.

Considering the temporal evolution of the sensitivity coefficients, it can be derived from Eq. 3-28, and consequently from Figure 4-1, that the above described distribution with two domains of contrary influence persists for all times. However, the absolute values of sensitivity are subject of

change over time within the domains. Highest values of sensitivity are situated in the direct vicinity of both wells for all time steps (Figure 4-2 a). However, these areas with highest but contrary (positive and negative) sensitivity are adjacent. At early times (Figure 4-1 a), the domain of positive sensitivity takes on high sensitivity values in contrast to the outer negative domain. Thus, for early times the drawdown is most sensitive for the domain in between the wells (Figure 4-1 a), however as discussed below its relative influence decreases with elapsing time.

The absolute values of sensitivity are rising in the domain of negative influence with elapsing time, while an increasing portion of the domain is covered with sensitivities of increasing value. In the distribution shown in Figure 4-1 and Figure 4-3 a, respectively, the sensitivity converges to constant values for the considered domain after $t = 1000$ seconds, i.e. the absolute contribution of this domain of stationary sensitivity remains constant as time proceeds.

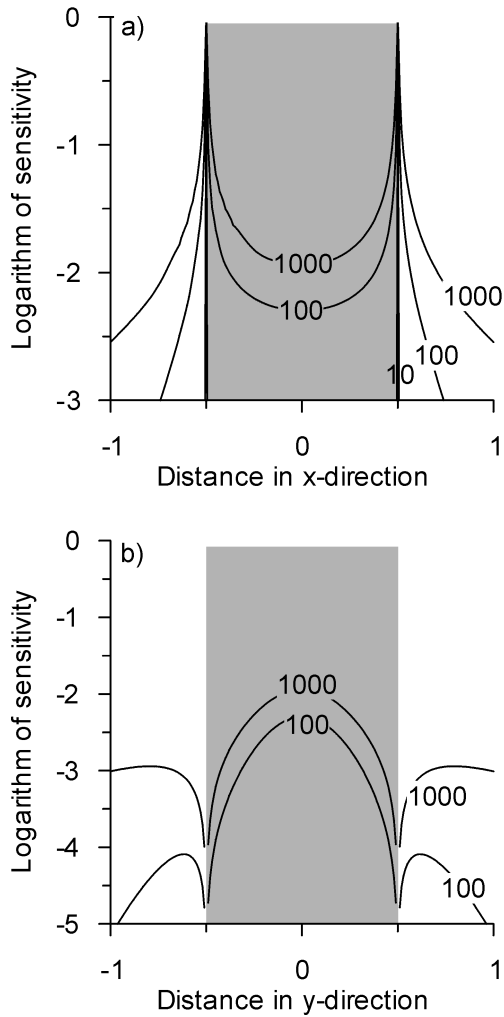


Figure 4-2. Sections through the two-dimensional distribution of sensitivity coefficients a) at $y' = 0$ intersecting the pumping and observation well, and b) at $x' = 0$. The numbers indicate the corresponding timesteps. The section with gray background indicates positive values of sensitivity. Note that the axes of ordinate have different scaling in a) and b) and the sensitivity coefficients at $t = 10$ s are only plotted in a) since the absolute values are very small compared to those at later timesteps (cf. Figure 4-1 a).

Figure 4-2 and Figure 4-3 a show the spatial and temporal distribution of sensitivity coefficients with respect to hydraulic conductivity for different one-dimensional sections. It is obvious how the sensitivity decreases with increasing distance from the wells. Both graphs in Figure 4-2 show the

relatively increasing influence of more distant areas with elapsing time. However, the domain of highest sensitivities remains in vicinity of the wells.

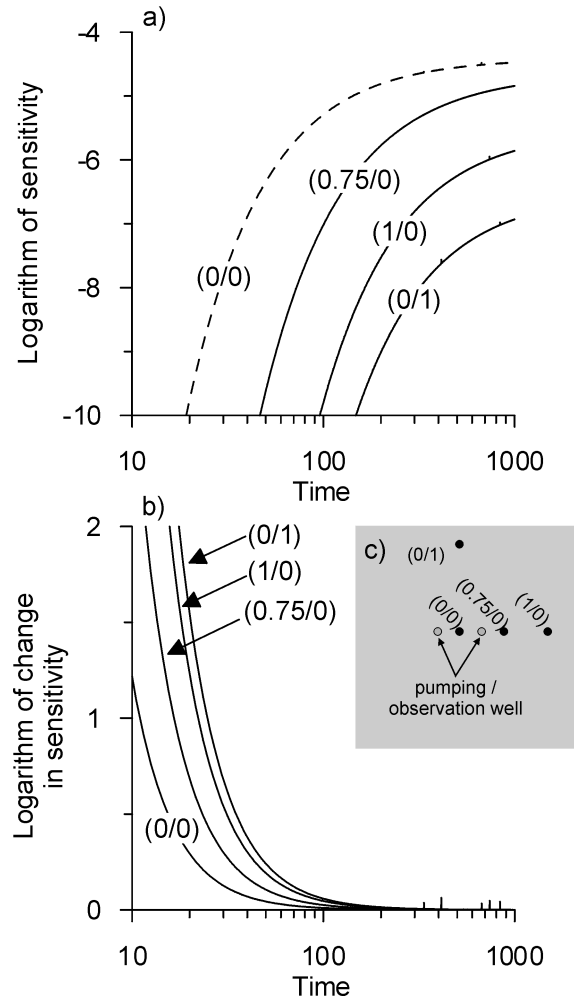


Figure 4-3. a) Evolution of sensitivity coefficients with respect to hydraulic conductivity at different spatial positions illustrated in (c). b) Time series of the relative change of sensitivity coefficients for the spatial positions given in (c).

Due to the described phenomena of sensitivity distribution various issues become relevant for the interpretation of hydraulic tests and for a reliable characterization of aquifer heterogeneities. The interpretation of draw-down data however is nonunique as different

heterogeneities might lead to identical drawdown behavior. E.g. a high conductivity zone in the positive domain can lead to the same observation as a low conductivity zone in the negative domain. Other problems associated with the ambiguity of results originate from the reciprocity and the symmetry of sensitivity distributions of hydraulic tests (Figure 4-1).

As discussed previously, the sensitivity coefficients reach constant values as the area of stationary sensitivity coefficients is increasing with time (e.g. Figure 4-1 a through c and Figure 4-3 a), thus the relative influence of parameter changes on the observation in those subdomains decreases. To account for this, the consideration of the relative change of sensitivity between consecutive time steps can be useful allowing a detailed assessment of results from hydraulic measurements as well as the possibility of a reliable interpretation based on sensitivity coefficients. Thereby the relative change of sensitivity coefficients is expressed by

$$\Delta I = \frac{I(t_k)}{I(t_{k+1})} \quad \text{Eq. 4-4}$$

where $I(t_k)$ and $I(t_{k+1})$ are the sensitivity coefficients at two consecutive timesteps.

Figure 4-3 b gives time series of relative changes in sensitivity for different spatial positions. It is evident, how the relative change of sensitivity decreases with elapsing

time and converges to the relative change of one, i.e. the logarithm of change equal zero. Mathematically, this corresponds to the transition of the governing equation from the parabolic to the elliptic form. Furthermore, with increasing distance from the center of the measuring configuration, i.e. from the midpoint between pumping and observation well, the value of relative change increases at a definite time step. This is also obvious from Figure 4-4. For early times the coefficients of relative change are elliptically distributed and tend to a radially symmetric distribution for later times (Figure 4-4 c).

From this distribution three distinct domains of relative sensitivity can be distinguished: 1) a domain where the sensitivity remains constant between the particular time steps, 2) a domain where a considerable change in the sensitivity distribution occurs, and 3) a domain, where changes in the sensitivity distribution occur, but the overall sensitivities are too small to affect the observation.

1. The domain where the sensitivity remains constant within a definite time frame, is represented by coefficients of relative change of $\log_{10}(\Delta I) \rightarrow 0$. In Figure 4-4 b and c, this domain corresponds to the innermost part of the domain with lowest values of relative change, and in Figure 4-3 b it is indicated by the abscissa-parallel section of the time curve. With ongoing time no further information is available from this area of the aquifer during the hydraulic test.

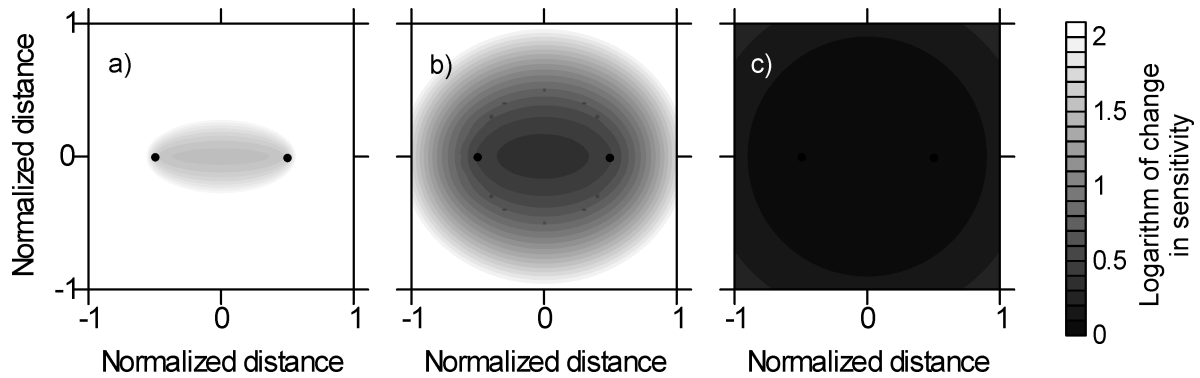


Figure 4-4. Logarithm of relative change in sensitivity between consecutive logarithmic time steps a) between $t = 10$ and 100 s, b) between $t = 100$ and 1000 s and c) between $t = 1000$ and 10,000 s.

2. A ring embracing the above-described domain represents that portion of the aquifer, where a considerable change in the sensitivity distribution occurs. In Figure 4-4 this area is characterized by coefficients of relative change of $\log_{10}(\Delta I) < 2$. In Figure 4-3 b this corresponds to the section of the curve, where the slope is flattening from high to low relative changes. With elapsing time, any changes in drawdown can be assigned to this portion of the aquifer. The chosen value of $\log_{10}(\Delta I) < 2$ given for the relative change is based on the fact that if the values of absolute sensitivity are less than two orders of magnitude for the time step t_{k-1} , it can be concluded that this area will not have a significant influence at the given time interval.

3. This is the domain, where a negligible or not measurable influence of parameter discontinuities on the drawdown can be expected, although considerable changes in the sensitivity distribution occur. This is due to the fact that the overall sensitivities in this

domain are too small in order to affect the observation.

4.4 Sensitivity with respect to storage

Based on the transient nature of the governing differential equation, the determination of storage and therefore the computation of sensitivity coefficients with respect to storage is possible.

Figure 4-5 shows the two-dimensional sensitivity distribution for three consecutive log-cycles. For all time steps, the entire domain is characterized by a negative sensitivity distribution. Consequently, any variation in storage has a reverse influence on the observation; i.e. heterogeneity of increased storage leads to a decreased drawdown, and vice versa, indifferent of the position of the parameter variation with respect to the well locations.

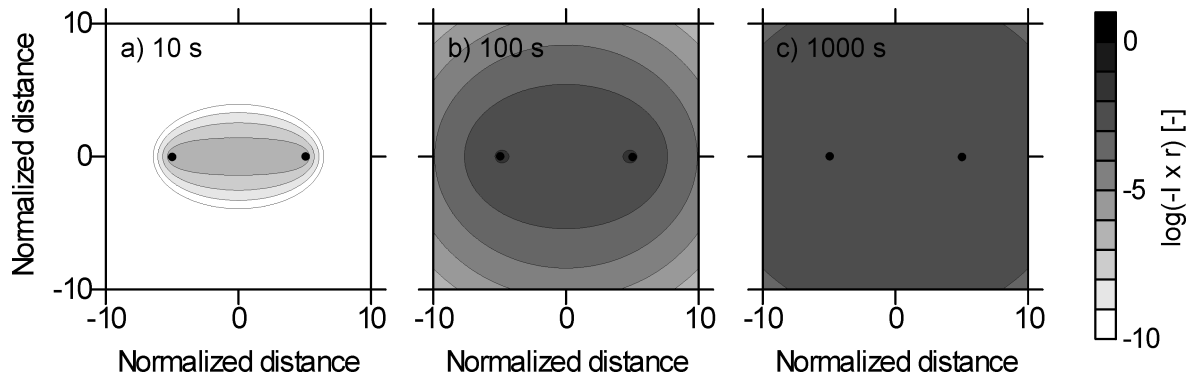


Figure 4-5. Two-dimensional distribution of sensitivity coefficients with respect to changes in storage for the three time steps. The black dots indicate the position of the pumping and observation well ($k=10^{-4}$ m/s, $S=10^{-4}$, $Q=300$ m³/d).

The distribution of the sensitivity coefficients is of elliptical form with foci at the position of the wells, and approaches a circular distribution at late times. With increasing sensitivities towards the wells, the highest influence for a change in storage is directly in the vicinity of the points of measurement.

The analysis of the temporal evolution reveals that with elapsing time the sensitivity increases at each point until a time is reached where

$$\frac{\partial}{\partial t}(I_s(\Omega, t)) = 0$$

Eq. 4-5

After the maximum is reached the sensitivity with respect to changes in storage decreases. This is also obvious from both graphs in Figure 4-6 showing the spatial and temporal distribution of sensitivity coefficients. The domain of highest sensitivities remains in the vicinity of the wells for all time steps. However, the overall sensitivity of the considered domain increases (Figure 4-6 b) thus the relative influence of the domain in vicinity of the wells will decrease.

4.5 Sensitivity distribution for different hydraulic tests

Following the principle of superposition [e.g. *Kruseman and DeRidder, 1994*] any arbitrary hydraulic measuring configuration can be derived from a summation of individual pumping test configurations with one pumping and one observation well. Consequently, the sensitivity distribution for any hydraulic measuring configuration can also be derived from a summation of sensitivity distributions of individual pumping test configurations.

In Figure 4-7 examples of two-dimensional sensitivity distributions for different measuring configurations are given, which are used in hydrogeologic practice. The configuration a) illustrates the case of a well doublet of pumping and injection well and an observation in the injection well. However, hydraulic tests in aquifers with high values of hydraulic conductivity or high values of storativity, respectively, would lead to very small potential changes,

thus this injection-extraction method requires precise measuring devices and is more suitable in aquifers of low conductivity.

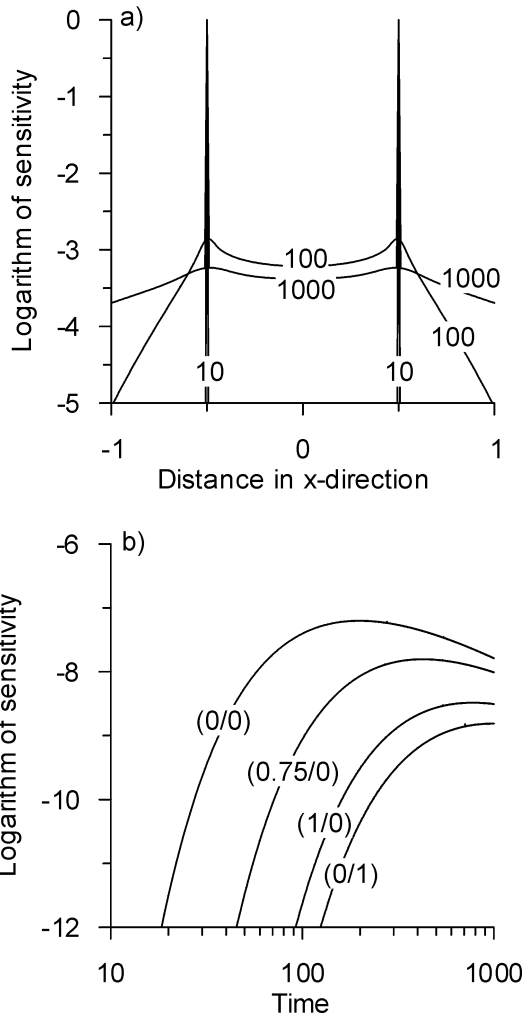


Figure 4-6. a) Section through the two-dimensional sensitivity distribution of Figure 4-5 at $y' = 0$ intersecting the wells. b) Evolution of sensitivity coefficients at different spatial positions that can be gathered from Figure 4-3 c.

The configuration given in d) has the same points of measurement as a) except that two extraction wells are used. The configuration g) is a classical pumping test with two observation wells, while the difference of head

is observed between the observation wells. The configurations illustrated in j, m, and p) are two well pumping tests with one observation well at different spatial positions. The configuration shown in m) corresponds to the DC-geoelectric configuration of the type AMA' [cf. Dietrich, 1999].

Applications of the cited configurations can be found in e.g. Molz *et al.* [1986], Lebbe *et al.* [1995], Zlotnik and Ledder [1996], Clement *et al.* [1997], and many others.

From the analysis of the sensitivity distribution for the different hydraulic measurement configurations some general statements can be given:

i) The conclusions of sensitivity distribution given for a standard pumping test (e.g. Figure 4-1) are reflected in the distributions of Figure 4-7: For the sensitivity with respect to changes in hydraulic conductivity the domain is divided in subregions of positive and negative sensitivity. The points of measurement lie on the transition zone between positive and negative sensitivity except for the cases where the observation takes place in the pumping or injection well.

ii) For the case of an observation in the pumping well, the well is surrounded by a radially symmetric negative sensitivity distribution with respect to hydraulic conductivity (Figure 4-7 d). Vice versa, if the observation occurs in an injection well, positive sensitivity is present around the corresponding well (Figure 4-7 b).

iii) Between a pumping and an observation well a domain of positive sensitivity is always present (middle column of Figure 4-7).

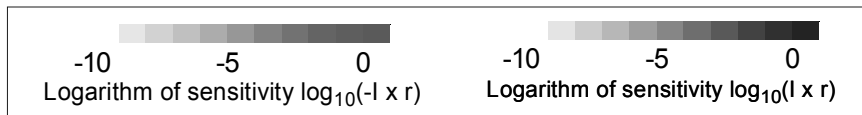
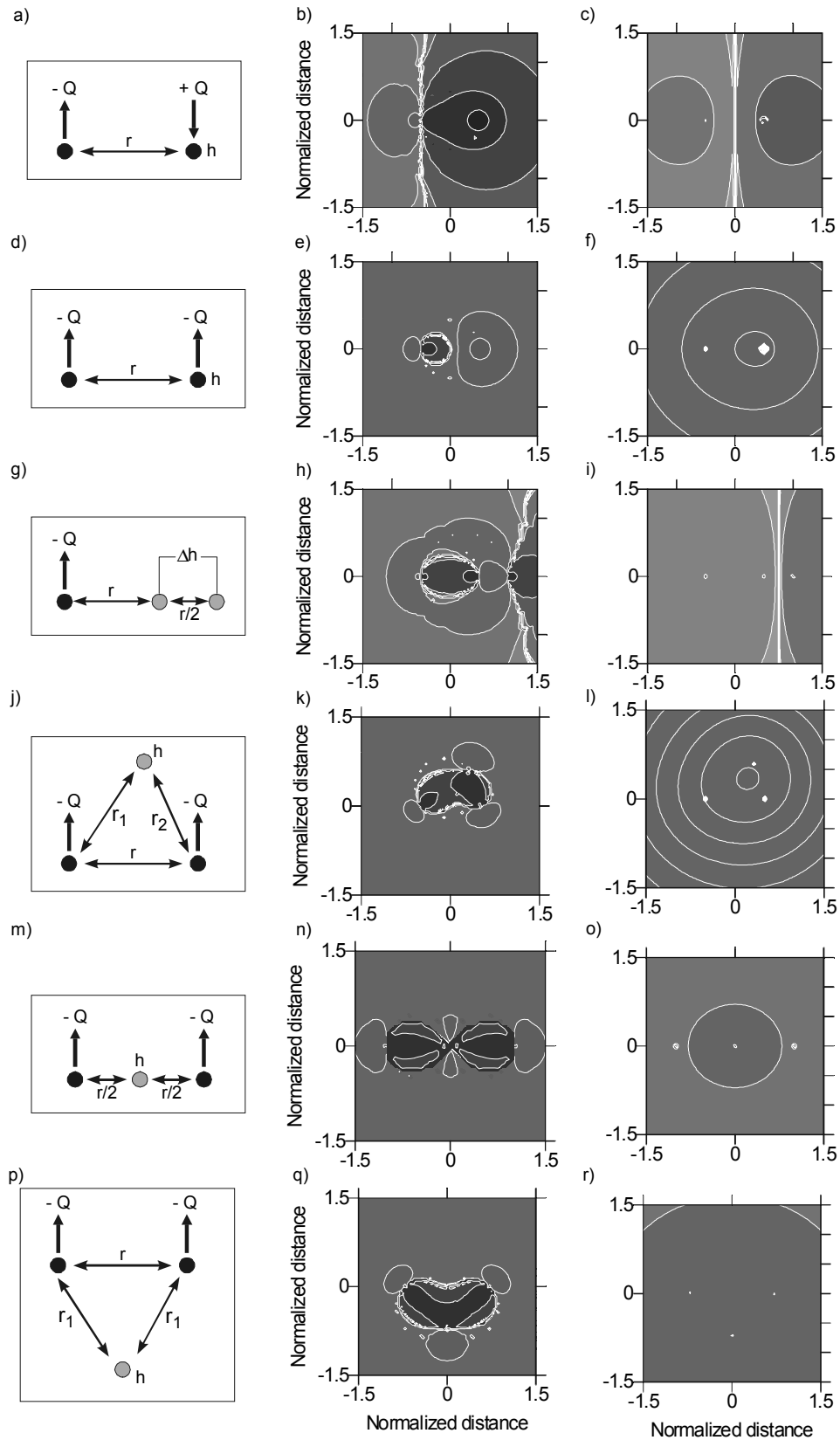


Figure 4-7. (Previous page): Two-dimensional sensitivity distribution at $t = 1000$ s for different hydraulic measuring configurations (left column) with respect to transmissivity (middle column) and with respect to storage (right column): a - c) Hydraulic dipole with one pumping ($-Q$) and one injection well ($+Q$), changes of the potential h are observed in the injection well. d - f) Two well pumping test with observation in one pumping well. g - i) Pumping test with two observation well at which the hydraulic gradient (Δh) is observed. j - l) Two well pumping test with arbitrarily located pumping well. m - o) Two well pumping test with observation well in between the pumping wells. p - r) Two well pumping test with an observation well located on the axis perpendicular to the axis of the pumping locations. The black dots in the sensitivity plots mark the position of the wells.

iv) If the hydraulic gradient is measured between two observation wells, the domain between these wells is represented by negative sensitivity. As the line of zero influence intersects the points of measurement, a line of zero influence also intersects the second observation well to which the head difference is measured.

v) The considered domain has an overall negative sensitivity with respect to changes in storage for the case of one or more pumping wells and a single observation well (Figure 4-7 f, l, o, r).

vi) For case of a doublet test with pumping and injection well (Figure 4-7 a), or if the hydraulic gradient is measured between two observation wells (Figure 4-7 g), the sensitivity distribution with respect to storage is divided in a domain of positive and negative influence (Figure 4-7 c and i). The transition zone of positive and negative sensitivity intersects the line between the respective wells at half distance.

In Figure 4-8 an example for the temporal development of the sensitivity distribution with respect to hydraulic conductivity

and storage, respectively, is given based on the hydraulic measuring configuration of Figure 4-7 g.

It is evident for the sensitivity distribution with respect to hydraulic conductivity that the transition zone between positive and negative sensitivity persists over time only for the closed line intersecting the pumping and the adjacent observation well. The line of zero influence intersecting the second observation well to which the head difference is measured does not persist with time. Thus any changes in hydraulic conductivity in the area over which this second line of zero influence moves with time can have a reverse influence on the observation at different times. For the change of coefficients with time within the distinct domains of sensitivity the findings from chapter 4.3 are applicable.

From the sensitivity distribution with respect to storage shown in Figure 4-8 b, d, and f) it is obvious that the division in the distribution persists for all times. However, the values of sensitivity vary over time, as discussed in the previous section 4.4.

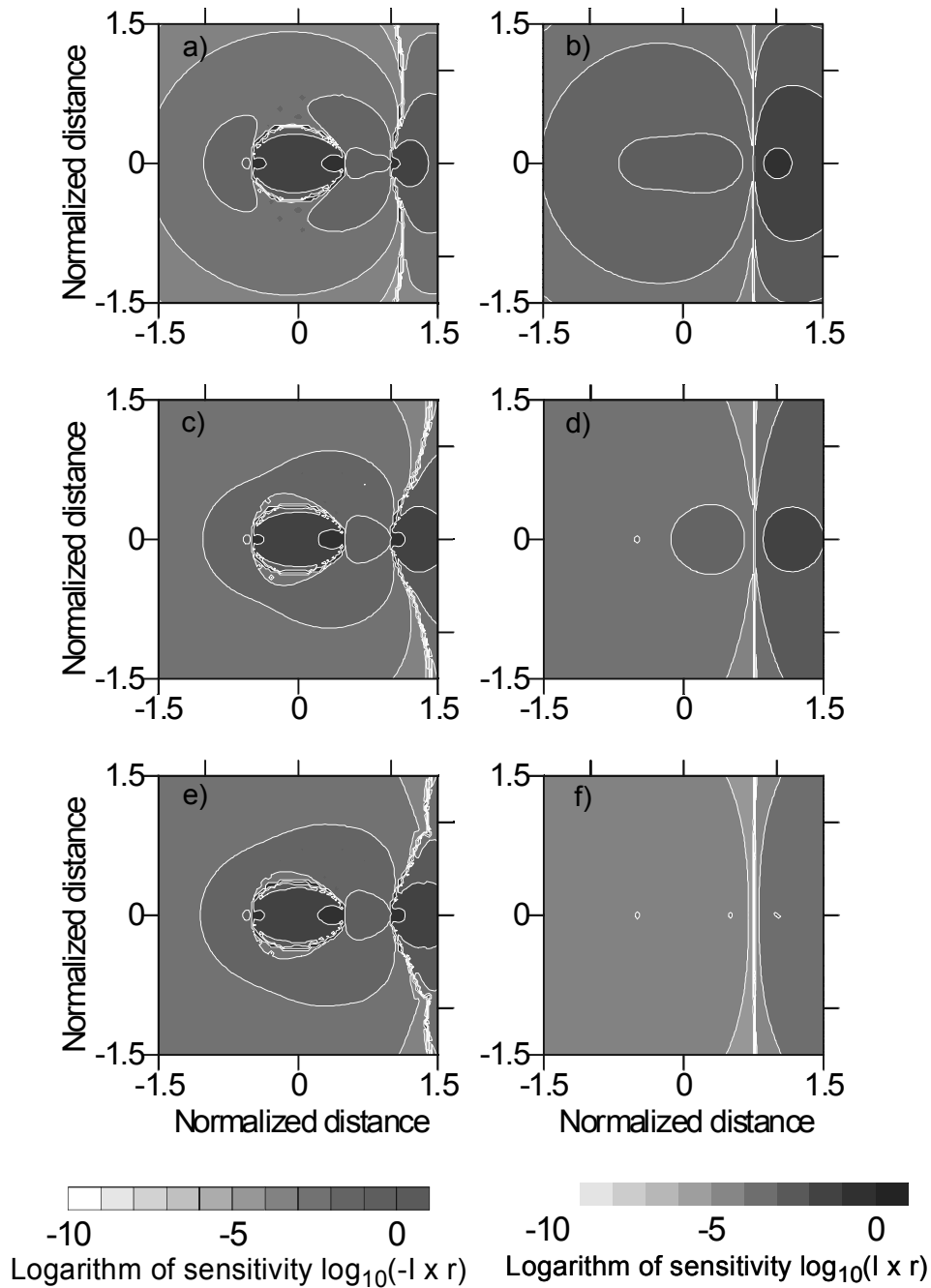


Figure 4-8. Sensitivity distribution for the hydraulic test configuration illustrated in Figure 4-7 g for three consecutive logarithmic time steps. a) and b) at $t = 10$ s, c) and d) at $t = 100$ s, e) and f) at $t = 1000$ s with respect to changes in hydraulic conductivity (left column) and with respect to storage (right column):

From analysis of the sensitivity distribution for different hydraulic measuring configurations some essential conclusions can be given:

For hydraulic measuring configurations with several wells, the distribution of sensitivity coefficients with respect to hydraulic conductivity can get complex, thus

the interpretation of observation from such tests can get difficult and equivocal. However, in terms of inversion of the observed data for parameter estimation purposes, distribution with highly variable sensitivity coefficients can be advantageous if several spatially different positioned measurements of the same configuration are available.

In terms of an estimation of effective parameters for the domain of interest, meas-

uring configurations can be chosen, which cover the domain homogeneously with average sensitivity values, i.e. configurations with a low variability of sensitivity coefficients (e.g. configuration d) in Figure 4-7 with respect to changes in hydraulic conductivity or configuration j) with respect to storage).

5 Application of the Sensitivity Approach for the Assessment of Heterogeneity and Anisotropy - The Steady-State Case

5.1 Introduction

In the last few decades, numerous efforts have been spent to improve the understanding of effects on hydraulic tests due to variations in the distribution of the governing hydraulic parameters. However, up to recent times there is still a lack in the exact spatial physical understanding of potential changes with respect to parameter variations, such as heterogeneity or anisotropy. For example, an exact assignment of parameter estimates derived from conventional pumping tests is still uncertain.

The focus of this chapter is to provide a better understanding of the effects caused by discrete parameter distributions on hydraulic tests. In literature, various studies have been investigated the effects arising from single heterogeneities of definite geometrical shape in a homogenous parameter distribution [Barker and Herbert, 1982; Butler, 1988, 1990; among others]. To provide a more general insight, the approach of sensitivity coefficients can be applied to common steady-state pumping tests in a homogeneous, anisotropic and heterogeneous aquifer, respectively.

According to Kabala [2001], two perspectives of sensitivity analysis are known. Firstly, approaches are used, which follow the *parameter estimation* perspective, such

as solving an inverse problem, which involves the calculation of sensitivity coefficients. Examples for this approach can be found in Butler and McElwee [1990], Butler and Liu [1991, 1993], Oliver [1993], McElwee et al. [1995a, b], and Vasco et al. [2000]. The second approach using sensitivity coefficients was introduced as *sensitivity-only* perspective with focus on the intrinsic nature of sensitivities, and does not involve parameter estimation. Kabala [2001] gave examples for this perspective. This approach usually provides information about optimal measurement design with respect of space and time. In the present chapter, the latter perspective is extended in order to clarify how particular parameter deviations affect hydraulic tests in homogeneous, anisotropic, and heterogeneous confined aquifers.

5.2 Numerical realization - An example under steady-state conditions

Considering pumping tests over extended periods of time, the introduced approach of sensitivity coefficients under steady-state conditions offers the possibility to analyze general effects of distinct parameter distributions on the observation during hydraulic tests. In order to calculate the sensitivity distribution for a standard pumping test with two wells, the computation of the solution of

equations Eq. 3-1 and Eq. 3-19 is required, as described in chapter 3. Figure 5-1 a illustrates a model domain with 168,750 equally spaced cells, which was used for the calculation of sensitivity coefficients in this chapter.

Figure 5-1 b shows the distribution of sensitivity coefficients for transmissivity for the homogeneous two-dimensional case for a pumping test configuration with one pumping and one observation well. Due to reciprocity the spatial position of pumping and observation well can arbitrary be interchanged as discussed in section 3.4.3.

As described in the previous chapter, two domains of contrary influence classify the sensitivity distribution, which are divided by a line of zero influence. As shown in the following, the circular shape of the division line persists only for the homogeneous case.

Figure 5-2 shows cross sections at $x' = 0$ and $y' = 0$ through the sensitivity distribution from Figure 5-1 b.

In the previous chapter an analysis of the sensitivity distribution was given for transient-states. The conclusions specified there are also valid for steady-state conditions and are discussed in the following section in further detail based on the numerical model given in Figure 5-1 a.

Due to reciprocity any heterogeneity of definite spatial extent and quantity can lead either to an increase or to a decrease of the observed value u depending on the spatial position of the heterogeneity.

As it is evident from Figure 5-3, a definite change in parameter distribution will lead to a contrary observation as if the

same discontinuity would lie in the domain of negative sensitivity relative to the homogeneous case.

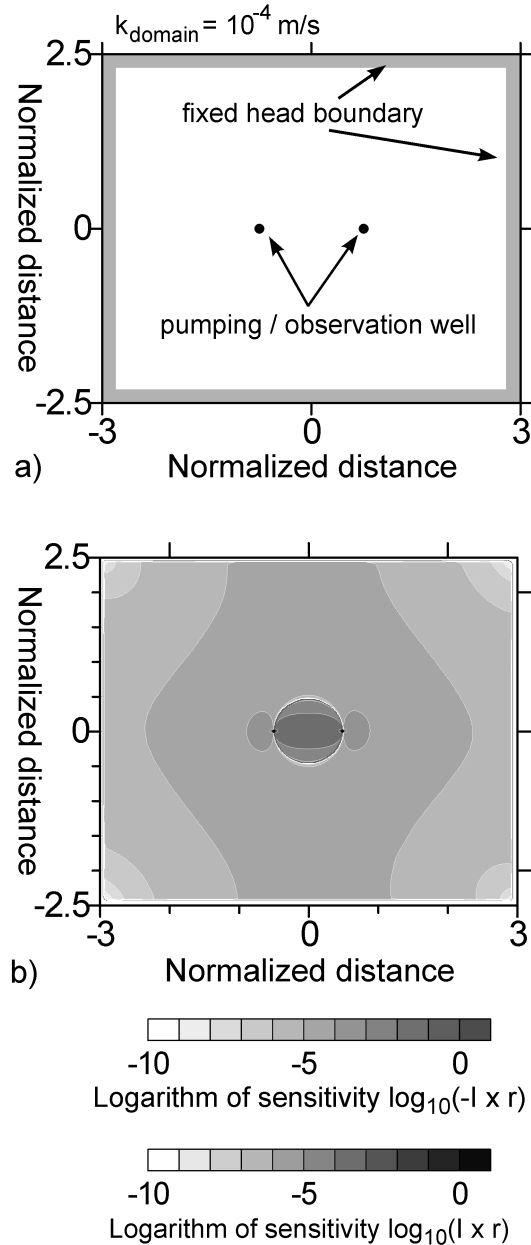


Figure 5-1. a. Model domain. b. Distribution of sensitivity coefficients for a homogeneous parameter field ($k=10^{-4} \text{ m/s}$, $Q=300 \text{ m}^3/\text{d}$).

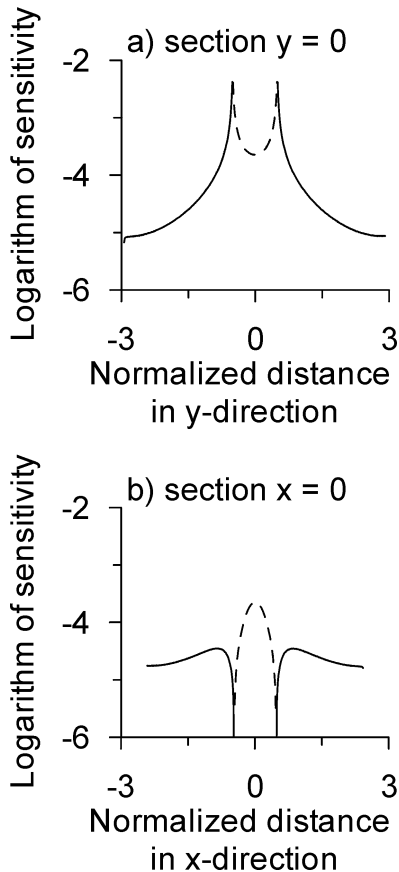


Figure 5-2. Section intersecting the wells, (a) perpendicular and (b) parallel the axis of the pumping test configuration as shown in Figure 5-1. In (a), the wells are located at $(0.5/0)$ and $(-0.5/0)$, respectively (dashed line: positive sensitivity: $\log_{10}(I \times r)$; solid line: negative sensitivity: $\log_{10}(-I \times r)$).

In the example of Figure 5-3, a discontinuity, which has an increased conductivity of one order of magnitude is considered. The drawdown observed at the observation well OW will be higher than for the homogeneous case, if the discontinuity is embedded in between the wells (dashed line in Figure 5-3). If the discontinuity of increased conductivity is lying outside the wells, a drawdown will result, which is less than the drawdown of the homogeneous case (dotted line in Figure 5-3). These findings are contrary to the often intuitively believed fact that pumping tests will lead to parameter

estimates dominated by the material between the pumping and observation well.

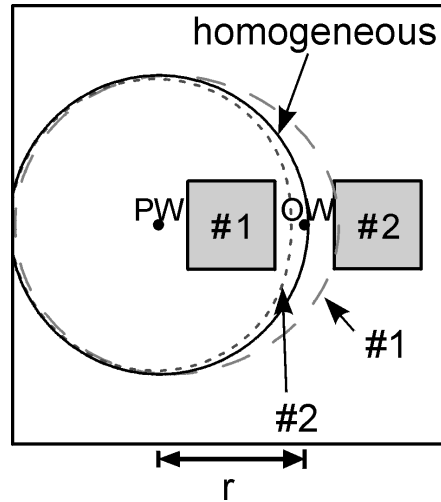


Figure 5-3. Isolines of drawdown for a pumping test in an aquifer with homogeneous parameter distribution (solid line) and with a discontinuity of increased conductivity (#1 - dashed line, #2 - dotted line).

Since the numerical computation of the stationary pumping test presented in Figure 5-1 includes effects caused by the boundary conditions, the distinct influence of the constant head boundary has to be taken into account. From Figure 5-1 b the effect of the constant head is evident as the gradient of sensitivity coefficients is aligned parallel to the boundaries in the spatial directions, except in the corners of the model domain. Here the sensitivity decreases toward the corners from both directions. For the following analyses the influence of the boundary conditions will be neglected, since only a subregion of domain shown in Figure 5-1 a is considered.

5.2.1 Anisotropic parameter distributions

In practice, pumping tests are conducted very often in aquifers of alluvial deposits. Such aquifers show significant horizontal anisotropy, i.e. correlating to sedimentological architectural elements formed under distinct depositional conditions. Generally, such systems cannot be characterized and investigated accurately by standard evaluation methods [Grimestad, 1995]. Therefore, in a first case study, the effects of anisotropic but homogeneous parameter distributions are analyzed. Figure 5-4 shows the case of a pumping test in a homogeneous aquifer with anisotropic parameter distributions.

Generally, in the sensitivity distribution for anisotropic parameter fields (Figure 5-4 a - d) the bimodal nature with two distinct domains of opposed sensitivity persists.

Although the line of zero influence intersects both wells, the shape of the bound depends strongly from the orientation of the principal axis of anisotropy relative to the centerline between pumping and observation well. This centerline is referred in the following as the 'pumping test axis' (PTA). Therefore, for a pumping test, whose PTA parallels the principal axis of highest conductivity the domain of positive influence

will be reduced in its width (Figure 5-4 a). The zonation of the distribution of negative sensitivities forms ellipsoids with their foci in the respective well. In contrast to this, a pumping test with its PTA perpendicular to the main axis of the hydraulic conductivity tensor (Figure 5-4 d) reveals a sensitivity distribution elongated in the corresponding direction. Figure 5-4 b and c show the distribution for anisotropy, where the principal axes are rotated with radians of $\pi/6$ and $\pi/3$, respectively, relative to the PTA. In both cases, the change due to differing anisotropy conditions is obvious.

In Figure 5-5 the effect of other ratios of anisotropy is illustrated with the PTA parallel to the main axis of anisotropy. As mentioned above the domain of positive influence will be reduced in its width, if the hydraulic conductivity is decreased perpendicular to the axis of test configuration (Figure 5-4 a and Figure 5-5).

Consequently, for pumping tests in strongly anisotropic aquifers (e.g. Figure 5-5 c), where the PTA parallels the main axis of the hydraulic conductivity tensor, the complex behavior for a deviation between the wells is strongly reduced. The resulting distribution corresponds more to the classical understanding of pumping induced drawdown, where e.g. for a decreased conductivity an increased drawdown can be expected.

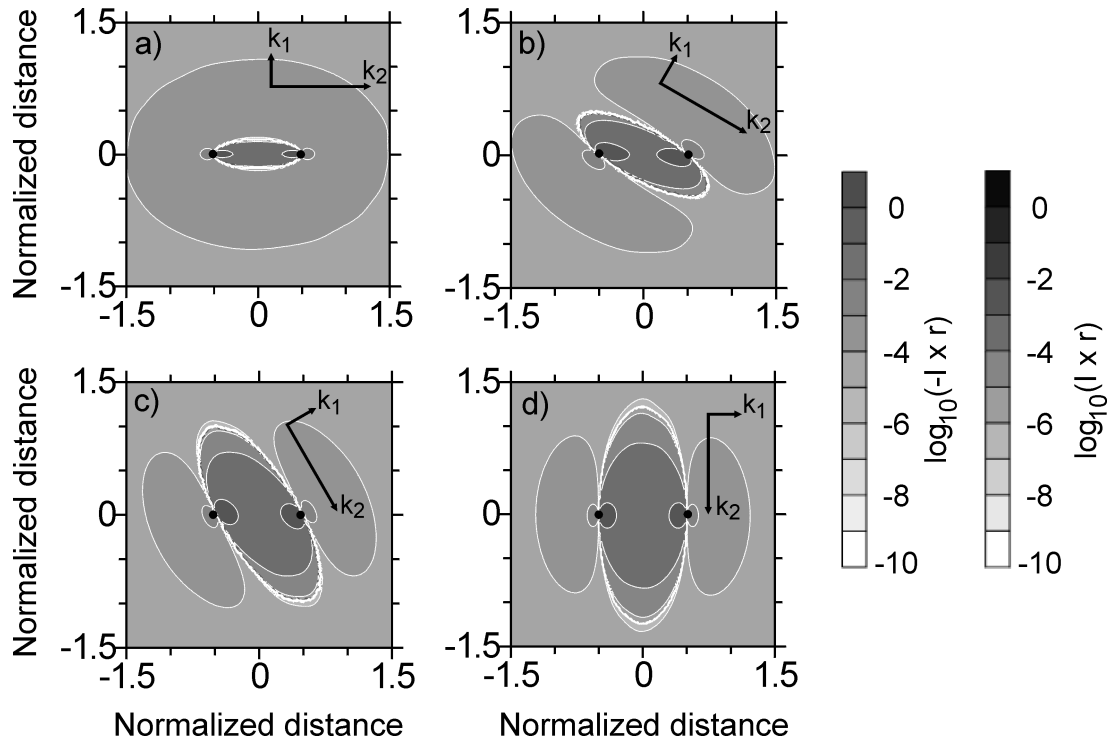


Figure 5-4. Sensitivity distribution for a pumping test for a homogeneous aquifer with different anisotropic parameter distributions. The arrows indicate the principal axis of anisotropy, with $k_1/k_2 = 1/3$. The black dots show the position of the wells.

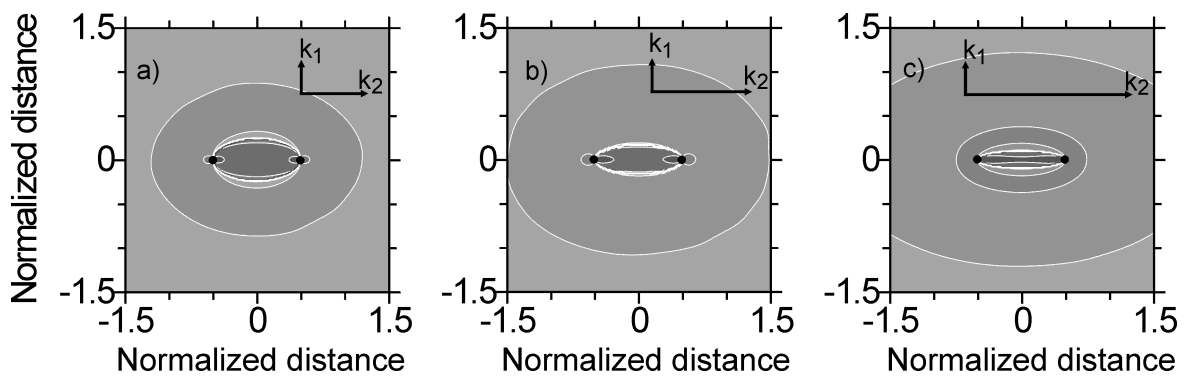


Figure 5-5. Sensitivity distribution for a pumping test in an anisotropic aquifer with (a) $k_1/k_2 = 1/2$, (b) $k_1/k_2 = 1/3$ and (c) $k_1/k_2 = 1/5$. The scaling of the sensitivity coefficients can be gathered from Figure 5-4. The black dots indicate the position of the pumping and observation well.

5.2.2 Heterogeneous parameter distributions

Most pumping test evaluation methods assume homogeneity, thus their applicability was critically discussed very often [Vandenberg, 1977; Barker and Herbert, 1982; Butler, 1990; Butler and Liu, 1993, among others]. However, the unreflected use of such evaluation methods is still common, although the effect of large-scale heterogeneities on the resulting observation is well known. In this section the effects of small-scale heterogeneities on a pumping test are analyzed in an aquifer, which is dominated by a large-scale heterogeneity. This scenario is often present in the field, where information is available from geophysical investigations allowing the detection and characterization of large-scale heterogeneities but detailed knowledge of small heterogeneity is required. For example, it has been recognized that the spreading of contaminants in the subsurface greatly depends on the spatial variability of the hydraulic parameters [e.g. Dagan, 1989].

The graphs in Figure 5-6 illustrate the resulting sensitivity distribution for a pumping test in an aquifer with a large-scale heterogeneity with increased and decreased conductivity, respectively.

i) *Large-scale heterogeneity of higher conductivity* (Figure 5-6 a - c):

Already for a large-scale heterogeneity with an increased conductivity by factor e (Euler's number $e = 2.7182\dots$), a considerable change in the sensitivity of the pumping test with respect to a change in the parameter distribution is evident (Figure 5-6 a). It is apparent that the sensitivity distribution is

disturbed by the limits of the heterogeneity. However, for the given distance between the limits of the heterogeneity and the wells, a determinable influence in the vicinity of the wells occurs for hydraulic contrast of approximately $\ln(k_1/k_2) = \pm 2$. With increasing conductivity, the influence of the corresponding domain decreases (Figure 5-6 a through c). The sensitivity distribution of the domain of lower hydraulic conductivity k_1 will become increasingly asymmetrical and leads to higher values approaching the areal extent of the heterogeneity (Figure 5-6 b and c). Hence, the influence on drawdown is considerably decreased for a large-scale heterogeneity with a conductivity of $k_2 > k_1$ as the corresponding domain is covered with decreased sensitivities. Therefore, the capability to reveal small-scale discontinuities within this domain of increased conductivity, i.e. decreased sensitivity, will be strongly reduced. In addition, the coverage with higher sensitivities is spatially more limited for larger contrasts in conductivity.

ii) *Large-scale heterogeneity of lower conductivity* (Figure 5-6 d - f):

For this case the pumping test is performed in the domain of higher conductivity compared to that of the large-scale heterogeneity. For a hydraulic contrast of $k_1/k_2 = e/1$ ($e = \text{Euler's number}$) no disturbance of the sensitivity distribution due to the heterogeneity is evident. However, the sensitivity distribution in the domain of the wells clearly changes, i.e. already for a given contrast the sensitivity in direct vicinity of the well adjacent to the large-scale heterogeneity is considerably affected resulting in an increasingly asymmetric distribution (Figure 5-6 d through f). With increasing conductivity in the domain incorporating the wells, a decreasing overall sensitivity arises. For a

contrast in hydraulic conductivity of two orders of magnitude (Figure 5-6 f with $k_1/k_2 = 1/100$), an insignificant influence of potential discontinuities may be expected, independently for the domain of the large-scale heterogeneity or the domain including the wells. In this case, only a major increase of the pumping rate, which is directly related to the absolute value of the sensitivity coefficients, would lead to an improved capability of capturing any discontinuity. In addition, in the distribution shown in Figure 5-6 e a region adjacent to the limit of the large-scale heterogeneity is evident that shows an increased and decreased sensitivity, respectively, on both side of the limiting bound. Further issues controlling the distribution of sensitivity coefficients will be discussed in the following section.

In alluvial aquifers, where heterogeneities follow the complex spatial distribution of structural or sedimentologic architectural elements, it is reasonable, that a pumping test is performed across or in the vicinity of a bound of changing conductivity. In Figure 5-7, the sensitivity distribution is given for a pumping test, where the position of the pumping and observation well, respectively, come to rest in the various zones of conductivity.

From all graphs in Figure 5-7, it becomes evident that the influence of parameter changes within the domain of higher conductivity affecting the observation is reduced, as ever smaller areas are covered by coefficients with values of higher sensitivity.

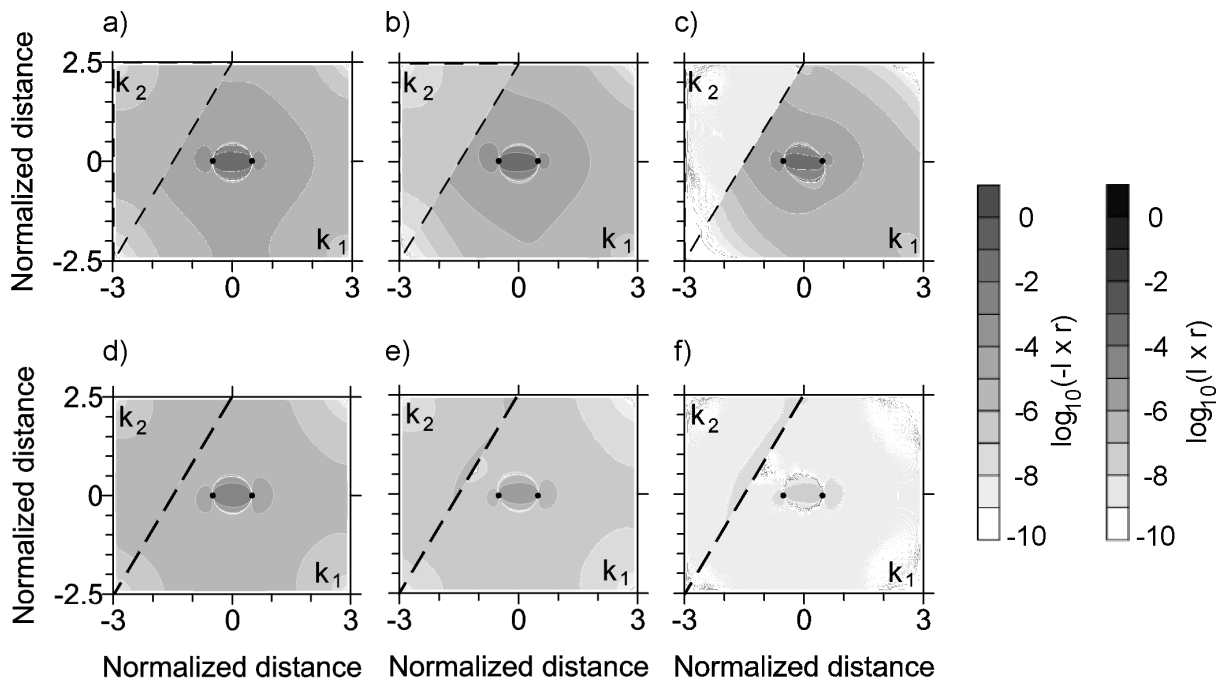


Figure 5-6. Sensitivity distribution for a pumping test in an aquifer with a large-scale heterogeneity with contrasts in hydraulic conductivity of (a) $k_1/k_2 = 1/e$, (b) $k_1/k_2 = 1/10$, (c) $k_1/k_2 = 1/100$, (d) $k_1/k_2 = e/1$, (e) $k_1/k_2 = 10/1$, (f) $k_1/k_2 = 100/1$ with $e = \text{Euler's number}$. The dashed line indicates the limit of the heterogeneity with conductivity k_2 . The black dots indicate the position of the wells.

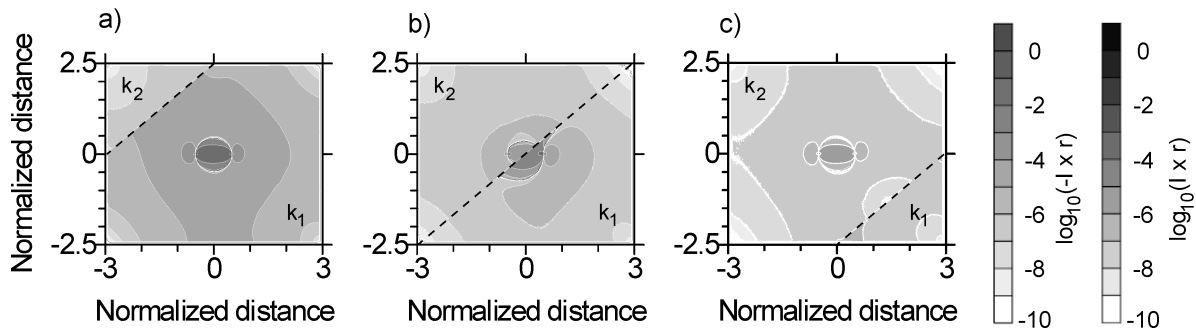


Figure 5-7. Sensitivity distribution for a pumping test in an aquifer with a large-scale heterogeneity with a contrast in hydraulic conductivity of $k_1/k_2 = 1/10$. The boundary of the heterogeneity (dashed line) is running outside the wells (a, c), and between the wells (b), respectively. The position of the wells can be gathered from Figure 5-6.

Therefore, the effect of a discontinuity on drawdown for a given parameter distribution highly depends on its relative position with respect to the zone of heterogeneity. In other words, the capability of a discontinuity to affect drawdown depends on its location in the domain of increased or decreased conductivity. Additionally, for higher hydraulic contrasts, the influence of the domain of higher conductivity will decrease continuously.

In Figure 5-7 b the lower right bound of the heterogeneity is moved toward the lower right edge cutting the model domain diagonally into half. In this case, the shape of the former circular line of zero influence is highly distorted. The domain of positive influence covers a more extensive area of the aquifer with lower conductivity k_1 compared to the domain with a conductivity k_2 . Furthermore, the distribution of positive sensitivity and therefore the line of zero influence in the domain of k_1 is elongated for a limited distance parallel to the bound of the heterogeneity. Figure 5-7 c shows a decreased overall sensitivity that corresponds to the explications given for Figure 5-6 d - f.

However, as the whole model domain is covered more uniformly by sensitivities of approximately same value, e.g. compared to Figure 5-7 a, effects caused by the model boundaries will get an increased influence on drawdown, except at the boundaries limiting the domain with k_1 .

This can also be illustrated by considering the depression cone of a pumping test at steady-state conditions. The cone of depression in an aquifer with a higher hydraulic conductivity expands more in the aquifer while the absolute drawdown is less compared to a pumping test employed in an aquifer of lower conductivity. In the latter case, the cone of depression is steeper but spatially more limited. This fact is also illustrated in Figure 5-8 where the relationship between the spatial extent of the depression cone at steady-state conditions and the hydraulic conductivity is shown. Note that the drawdown in Figure 5-8 is normalized to the maximum drawdown value, the absolute drawdown value of an aquifer with a conductivity of k_2 is ten times higher than for k_1 since k_1 is one order of magnitude higher than k_2 .

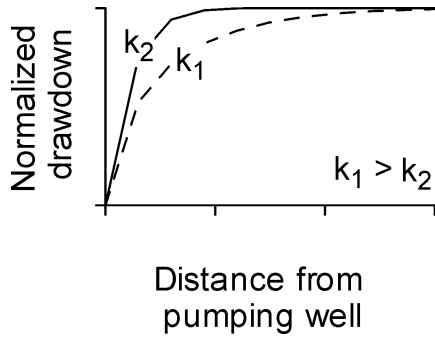


Figure 5-8. Illustration of the relationship between the spatial extent of the depression cone at steady-state conditions and the hydraulic conductivity. The absolute drawdown value for the case of k_1 is ten times smaller than for the case of low conductivity k_2 .

Considering the sensitivity distribution given in Figure 5-6 and Figure 5-7, another fact becomes evident: The capability to resolve or detect a heterogeneity is increased for the case where the actual measurement occurs in the domain of reduced hydraulic conductivity, i.e. based on the sensitivity distribution, heterogeneities of increased conductivity can result in an increased effect on the observation.

For example, considering a strongly heterogeneous aquifer such as a fractured porous system (cf. Chapter 2) a hydraulic measurement where the observation occurs within a fracture, will potentially not reveal parameter changes within the surrounding matrix. Furthermore, the observation would have only a minor sensitivity to parameter changes within the fracture. Vice versa, the same measurement occurring in the matrix of lower conductivity would reveal parameter changes as the sensitivity values would be increased in the matrix of lowered conductivity. In addition, considering Figure 5-7 a, the sensitivity to parameter changes within a fracture would be considerably decreased.

However, heterogeneities of higher hydraulic conductivity can be detected over a larger distance than such of lower conductivity (Figure 5-6 a vs. d). This is in accordance with *Dietrich* [1999] who found in terms of geoelectric measurements that discontinuities of lowered resistivity, i.e. higher electrical conductivity, are detectable over larger distances than such of higher resistivity.

The presented results of the analysis of effects due to parameter deviations can also be interpreted by separating the potential and parameter distribution in a primary and secondary field, where

$$u(x) = u_p(x) + u_s(x) \quad \text{Eq. 5-1}$$

$$k(x) = k_p + k_s(x) \quad \text{Eq. 5-2}$$

The variables u_p and k_p describe the primary field, which corresponds to the homogeneous reference case (Figure 5-1 b). The component u_s quantifies the deviation from the potential of the homogeneous conductivity distribution. It is caused by the deviation in the parameter distribution k_s . Thus, the relation between u_p and k_p can be expressed following Eq. 3-1 by

$$-\sum_{i=1}^n \frac{\partial}{\partial x^i} \left(k_p \frac{\partial u_p(x)}{\partial x^i} \right) = q(x) \quad \text{Eq. 5-3}$$

By subtracting Eq. 5-3 from Eq. 3-1 the differential equation of the potential of the secondary field can be derived

$$\begin{aligned}
 & - \sum_{i=1}^n \frac{\partial}{\partial x^i} \left(k(x) \frac{\partial u_s(x)}{\partial x^i} \right) \\
 & = \sum_{i=1}^n \frac{\partial}{\partial x^i} \left(k_s(x) \frac{\partial u_p(x)}{\partial x^i} \right)
 \end{aligned}$$

Eq. 5-4

The analysis of Eq. 5-4 reveals that any deviation from the (homogeneous) reference field u_p is significantly influenced by changes in the parameter distribution k_s . This means, that the deviations in the secondary parameter field can be considered as causal for the secondary potential. The absolute value of the secondary potential thereby depends on the distances to the wells.

According to *Dietrich* [1999], the capability of influencing the observation during a hydraulic test depends also on $\partial k_s / \partial x$, as a measure for the contrast in the parameter distribution. Following Figure 5-6 and Figure 5-7, the decreasing influence of the heterogeneity (k_2) with increasing conductivity can be seen, and vice versa.

Considering Figure 5-6 and Figure 5-7, another fact becomes apparent. The areas of increased sensitivity are located in the direct vicinity of the wells, which can be derived from the primary potential field. However, in the direct vicinity to the limits of the large-scale heterogeneity changes in the distribution are evident. For example, compared to the homogeneous case, the distribution in Figure 5-6 b and c is considerably disturbed with respect to an alignment of sensitivity distribution parallel the heterogeneity limit. Furthermore, changes in the distribution are evident for the region adjacent the heterogeneity limits with shortest distance to the wells (e.g. Figure 5-6 e). The origin of these disturbances in the sensitivity distribution can also be derived from the secondary potential that is caused by the

secondary parameter field, e.g. the (limit of) heterogeneity. With increasing distance from these sources of potential disturbance, i.e. from the heterogeneity, the capability of influencing the pumping test decreases.

A common application of this decomposition is the principle of superposition [*Ferris et al.*, 1962] where particular boundary conditions can be replaced by “image”-wells, which also will produce a secondary potential field.

5.3 Consequences for the assessment of hydraulic tests and conclusions

From the analysis presented in this chapter some substantial conclusions can be deduced, providing an insight in the effects arising from distinct parameter distributions. To summarize the main aspects, the sensitivity distribution for another pumping test under steady-state conditions is considered in further detail. Figure 5-9 shows the distribution of sensitivity coefficients for a steady-state pumping test in an anisotropic, heterogeneous, two-dimensional aquifer. The value of the main axis of the tensor of hydraulic conductivity differs by a factor of three from the value perpendicular to it, the hydraulic contrast between the large scale heterogeneity and the domain incorporating the wells is $k_1/k_2 = 1/10$. The effects of this parameter distribution on a pumping test are determined in Figure 5-9.

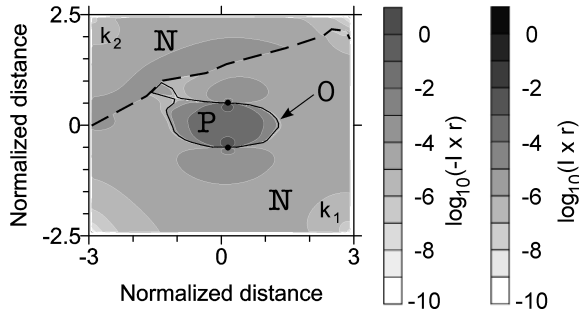
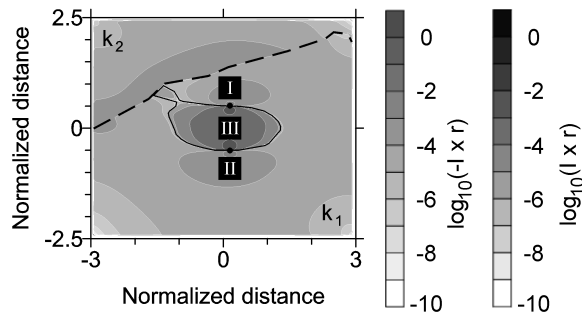


Figure 5-9. Sensitivity distribution for a pumping test in an anisotropic, and heterogeneous aquifer with $k_1/k_2 = 1/10$. The conductivity perpendicular to the PTA (x -direction) is three times higher than parallel to that axis (y -direction). The black dots indicate the position of the wells (P - domain of positive sensitivity, 0 - line of zero sensitivity, N - domain of negative sensitivity).

Generally, hydraulic tests with one pumping and one observation well, produce a division of the domain of interest in two subdomains of contrary sensitivity separated by a line of zero influence. This line contributing no information about the parameter distribution in the subsurface runs through the points of measurement and is of circular shape in the case of a homogeneous and isotropic parameter distribution (Figure 5-1 b). For anisotropic distributions (Figure 5-4 and Figure 5-5), an elliptical region is established. Thereby the elliptical region is elongated in direction of the axis of higher conductivity. In heterogeneous parameter distributions, this line can be highly irregular (Figure 5-7 b and Figure 5-9). Furthermore, the line of zero influence embraces a subdomain of the aquifer having a positive influence on the observation with respect to a change in the hydraulic conductivity. For anisotropic parameter distributions, the domain of positive sensitivity will diminish if the PTA parallels the main axis of the tensor of hydraulic conductivity. If the PTA parallels the axis of low conductivity, a widening of the domain

perpendicular to that direction will result (Figure 5-9).

On the contrary, negative influence of parameter discontinuities on drawdown exists for the region outside the line of zero influence. Therefore, it is essential, where the wells are positioned with respect to parameter discontinuities. Because of reciprocity, pumping and observation well are interchangeable. In Figure 5-10, the sensitivity distribution from Figure 5-9 is shown with a discontinuity of lowered conductivity (three orders of magnitude) at three different positions in the model domain. The table in Figure 5-10 gives values for drawdown observed at the observation well for the homogeneous case and for the three cases of a disturbed parameter distribution at the locations I, II and III. It is obvious, how a pumping test with a discontinuity of lowered conductivity outside the wells (I or II) would result in higher drawdown compared to the undisturbed case. Contrary to this, a pumping test with a discontinuity in between the wells (III) would result in a drawdown lower than that in the undisturbed case. This behavior results from the distribution of positive sensitivity. Besides, as it is evident from Figure 5-10 a smaller area covered by higher sensitivity values compared to the region where discontinuity II is located around discontinuity I. The spatial extent of decreased sensitivity will result in a smaller difference compared to the undisturbed case, which is given in the table in Figure 5-10.



Discontinuity	Drawdown at observation well	Discontinuity within domain
undisturbed	0.297	—
I	0.3453	negative sensitivity
II	0.3541	negative sensitivity
III	0.2821	positive sensitivity

Figure 5-10. Sensitivity distribution and results of a simulated pumping test with a discrete discontinuity of lowered conductivity at three spatial positions. The sensitivity distribution given for the undisturbed case corresponds to that shown in Figure 5-9.

The capability of a discontinuity to have a detectable effect on the observation during a pumping test is greatly affected by its distance from the wells as well as by the contrast of hydraulic conductivity between the heterogeneity and the surrounding material. The sensitivity of the observation with respect to changes in the parameter distribution is again highest in the direct vicinity of the wells, i.e. the absolute sensitivity coefficient is highest (Figure 5-2 a). This is why skin effects, i.e. head losses in the vicinity of the wells due to e.g. damage to the aquifer during drilling or head losses in the gravel pack [cf. *Kruseman and DeRidder, 1994*], attain a significant influence on observations of pumping tests.

Regarding the intrinsic characteristics of sensitivity distribution of arbitrary parameter fields, the pumping and observation well should be placed as close as possible to

each other, thus the domain of positive sensitivity diminishes. These findings are in accordance to *Butler and McElwee [1990]* who stated that in radial flow fields an observation well placed near the pumping well allows during transient-states “a record to be established of the properties of the material through which the front of the cone of depression has passed during pumping test”. In addition, the effects of anisotropic structures will be reduced. Although, the sensitivity distribution of a pumping test in a heterogeneous aquifers still includes effects of the secondary potentials arising from the heterogeneity itself.

Furthermore, any hydraulic test, which is aimed on high-resolving investigations, the wells should be positioned as close as possible to the domain of interest, while it should be covered by as many different permutations of sensitivity distribution as possible for a reduction of ambiguousness and for an improvement of the resolution of potential discontinuities.

For the characterization of a definite domain in terms of effective parameters, several tests, spatially different positioned, should be performed in the way of getting a nearly homogeneous coverage of the domain of interest with average sensitivity values.

For a known anisotropy, the well configuration needs to be determined carefully, because for anisotropic parameter distributions the sensitivity patterns are basically changed. Mainly for high factors of anisotropy, the results of a pumping test depend strongly on the positioning of the wells with respect to the principal axis of anisotropy.

6 A Theoretical Investigation Based on the Analysis and Application of the SCA

6.1 Introduction

An accurate knowledge of the parameter distribution of the subsurface is a prerequisite for the handling and solution of many problems in hydrogeology and related fields, such as contaminant site remediation. Here the parameter of hydraulic conductivity is assumed to be the most important variable. In hydrogeologic practice, the characterization of aquifers is mostly performed using classical test methods, such as constant rate pumping tests evaluating the hydraulic parameters most often by means of homogeneous interpretation models following the classical work of *Theis* [1935] and *Cooper and Jacob* [1946]. However, these methods are used frequently in an inattentive way, i.e. idealized homogeneous models are applied to naturally heterogeneous systems. This can lead to misinterpretations, as these methods are assumed to give parameters averaged over a domain of uncertain extend and unknown weighting. Additionally, in heterogeneous systems the evaluation of transient groundwater flow to a pumped well may reveal varying hydraulic parameters with time. The observed drawdown can be interpreted as the result of a scaling up of the hydraulic properties over an increasing averaging volume during the temporal evolution of the depression cone [*Schad and Teutsch*, 1994]. Furthermore, hydraulic parameters acquired from pumping tests are not only dependent on distinct spatial prop-

erties in the area of the wells, but are also considered to be an average value of a representative volume of the aquifer [e.g. *Sánchez-Vila et al.*, 1999].

As a consequence, various issues can arise using classical test and evaluation methods. These facts can lead to the problem of how a definite parameter estimate can be related to a certain parameter distribution. Additionally, considering transient groundwater flow, the problem is extended, as the time dependent information, e.g. distinct intervals in the time-drawdown curve, can be connected to definite spatial information, i.e. spatially varying hydraulic parameters.

In order to illustrate and resolve these difficulties the approach of sensitivity coefficients can be applied as it allows on the one hand the investigation of the intrinsic characteristics of hydraulic tests giving a better understanding of the response of hydraulic test methods due to aquifer heterogeneity. In addition, this approach can be used for an optimization and improvement of the classical concept of pumping tests. On the other hand, the SCA allows the assessment of information from distinct time periods during a hydraulic test, e.g. data from definite sections of the time-drawdown curve of a pumping test, and the assignment of estimated parameters to particular spatial information.

This chapter is guided by standard hydrogeologic evaluation techniques, i.e. using classical evaluation methods that are commonly applied without the use of sophisticated inversion techniques. Besides the fact that inverse parameter estimation techniques are rarely applied to evaluate pumping tests in hydrogeologic investigations, they also require a considerable amount of test data. In addition, difficulties may arise, due to extensive computations [Vasco *et al.*, 2000].

Various studies address the above-mentioned issues in discrete or stochastic approaches. The discrete approaches define distinct patterns of heterogeneity using simplified aquifer geometries with singular discontinuities [e.g. Barker and Herbert, 1982; Hunt, 1985; Butler, 1988; 1990; Streltsova, 1988; Butler and McElwee, 1990; Butler and Liu, 1991]. More detailed analyses, which use sensitivity coefficients, e.g. based on McElwee [1987], for the investigation of the influence of lateral discontinuities are limited to numerical solutions of homogeneous and radial aquifers, or to approximated analytical solutions for particular time intervals [e.g. Butler and Liu, 1993].

However, hydraulic parameter distributions can also be described with stochastic processes, characterized by statistical parameters. Statistical methods can be applied by defining apparent effective parameters, e.g. effective transmissivities, which are a function of the radial distance to the well [Naff, 1991; Neuman and Or, 1993; Indelman and Abramovich, 1994, Indelman *et al.*, 1996; among others]. Furthermore, methods are utilized to assign values of equivalent transmissivity to blocks of finite size (block transmissivity) by empirical and / or analytical approaches [Desbarats, 1992; Indelman and Dagan, 1993 a, b; Tiedeman *et al.* 1995;

Renard and deMarsily, 1997]. Here the equivalent parameter reproduces the average behavior at a certain scale and should converge to the value of the effective parameter for very large geometries [Sánchez-Vila *et al.*, 1995]. The above-mentioned approaches considering stochastic processes are mainly dealing with steady-state conditions. Extensions to transient groundwater flow conditions are given by Lachassagne *et al.* [1989] Butler [1991], Schad and Teutsch [1994], Schad [1997], Serranso [1997], Sánchez-Vila *et al.* [1999].

Oliver [1993] investigated the influence of nonuniform transmissivity and storativity distributions on drawdown for continuously varying parameter fields by using the kernels of the Fréchet derivative, which is the “Hilbert space equivalent to sensitivity coefficients”. In the sophisticated first-order analytical approach Oliver found a similar expression for the Fréchet derivatives with respect to lognormal and normal distribution of transmissivity and storage, respectively as given for the sensitivity coefficients in Eq. 3-28 and Eq. 3-31.

6.2 Numerical example

A pumping test simulation is used to illustrate the issues connected with classical pumping test interpretation and aquifer characterization in a two-dimensional heterogeneous confined aquifer. In order to achieve comparability, the distance between the pumping and observation well is kept constant. The whole model domain (2000×2000 length units) comprises 182,329 cells, with the central region with equally grid spacing (100×100 length units) solely including a heterogeneous parameter distribution. The model domain and the utilized

pumping configuration are shown in Figure 6-1. As only the influence of changes in hydraulic conductivity will be addressed, and the variability of storage in natural systems is supposed to be small, a constant storativity of $S = 5.0 \times 10^{-2}$ [-] is assumed throughout the whole domain. Although this value is somewhat unrealistic for confined aquifer conditions, this assignment has principally no influence on the results and was chosen out of numerical considerations. The hydraulic conductivity within the central part of the model domain varies over one order of magnitude. The minor variability of hydraulic conductivity already allows demonstrating that the proposed concept will succeed. Furthermore, in terms of transport processes, significant consequences for the spreading of contaminants can arise in aquifers with such conductivity contrasts.

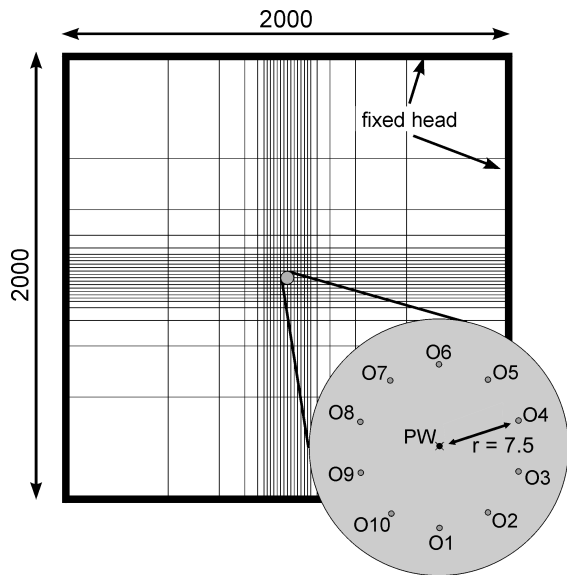


Figure 6-1. Schematic illustration of the model domain showing the configuration of the simulated pumping test. The distance between the pumping well PW and each observation well (O1 - O10) is $r = 7.5$ scale units. The squared model domain exists of 182,329 elements, with a central equally spaced sub-domain of 100×100 units. Only the central sub-domain includes aquifer heterogeneity.

In order to address the resulting drawdown data in objective manner, the aquifer is treated as a black box, i.e. without any information on heterogeneity, which is connected to the central domain. Figure 6-2 shows the time-drawdown curves recorded at the observation wells O1 - O10. For parameter evaluation the type curve method following Theis [1935] was used.

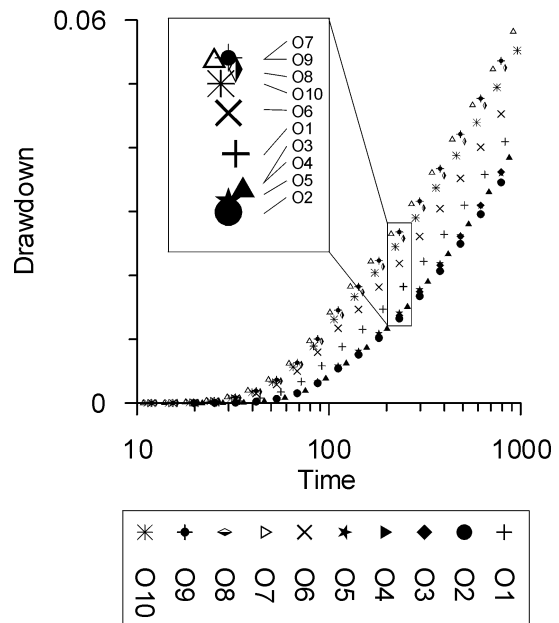


Figure 6-2. Time-drawdown curves for a pumping test in a heterogeneous aquifer. The observation wells O1 - O10 are in a radial distance of $r = 7.5$ units from the pumping well (cf. Figure 6-1).

Analyzing the curves in Figure 6-2, no effects of wellbore storage due to the definite size of the grid cells (straight line in a log-log plot with unit slope) have been observed at the observation wells and the early drawdown phase was evaluated with a duration to approximately 100 time units. The changing slope of the drawdown curves starting at approximately $t = 100$ (a break in the curve in a log-log plot, cf. Figure 6-3) indicates increasing effects of the constant head

boundaries which would lead to unrealistic high values transmissivity, as constant head boundaries behave like discontinuities of high conductivity at some distance to the wells. The classical type curve matching method using the *Theis* solution was applied to estimate the hydraulic parameters for each drawdown curve individually, leading to the values given in Table 6-1.

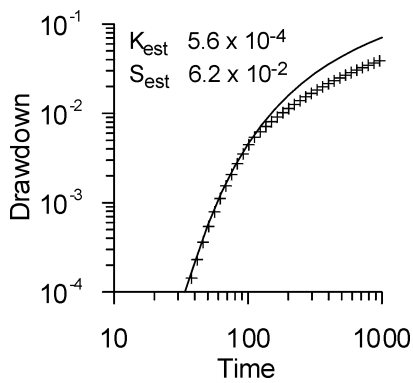


Figure 6-3. Time-drawdown curve observed at well O2 (symbols) and the corresponding Theis fitting curve (solid line) for early times (k_{est} - estimated conductivity, S_{est} - estimated storativity).

It should be pointed out, that the intention of this part of the study is not to find effective parameters, rather than illustrate the problem, which will arise for pumping tests with one or more observation wells as a variety of parameter sets can be obtained, and their spatial dependence is unknown. Considering the values in Table 6-1, several questions may arise:

1. Although the storativity is kept constant throughout the model domain, the estimated storativities vary over a considerable range, approximately in the same range as the transmissivity.

2. Knowing the model hydraulic conductivities vary over one order of magnitude, the variability of the estimated conductivity is much less.

Table 6-1. Parameter estimates for a pumping test in a heterogeneous aquifer (k - hydraulic conductivity in length per time unit, S - storativity [-], min - minimum, max - maximum, $mean$ - arithmetic mean, std - standard deviation, geo - geometric mean, read $5.5 e-4$ as 5.5×10^{-4}).

Pumping at central well <i>PW</i>		
Well	Early time fit	
	k	S
<i>O1</i>	6.1 e-4	5.1 e-2
<i>O2</i>	5.6 e-4	6.2 e-2
<i>O3</i>	4.7 e-4	5.5 e-2
<i>O4</i>	5.2 e-4	6.2 e-2
<i>O5</i>	5.6 e-4	6.2 e-2
<i>O6</i>	8.6 e-4	5.1 e-2
<i>O7</i>	4.8 e-4	2.8 e-2
<i>O8</i>	4.8 e-4	3.2 e-2
<i>O9</i>	5.0 e-4	3.2 e-2
<i>O10</i>	7.1 e-4	4.0 e-2
<i>min</i>	4.7 e-4	2.8 e-2
<i>max</i>	8.6 e-4	6.2 e-2
<i>range</i>	3.9 e-4	3.4 e-2
<i>mean</i>	5.8 e-4	4.8 e-2
<i>std.</i>	1.2 e-4	1.3 e-2
<i>geo</i>	5.6 e-4	4.6 e-2

3. From the comparison of the time-drawdown curves (Figure 6-2) and the corresponding parameter estimates (Table 6-1) it is evident that apparently no correlation exists between drawdown amplitude and parameter estimate, i.e. curves with highest drawdown can coincide with values of low or high conductivity, and vice versa (e.g. wells *O7* and *O10*). For wells with the highest drawdown, the response time of measurable amplitude is shortest, i.e. the measurable drawdown starts at significantly earlier times. However, considering for example wells *O7* - *O9* the parameter estimates con-

tradict the findings from the response times, as in the conventional understanding the response time increases with decreasing conductivity (Figure 6-4).

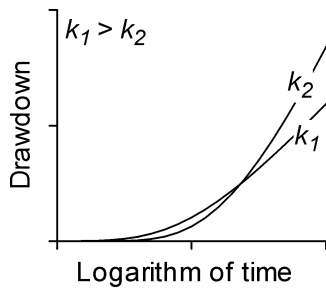


Figure 6-4. Illustration of the relation between response time of drawdown and hydraulic conductivity for the early time of a pumping test with constant storage.

The main question is how heterogeneities affect the response of an aquifer to the pumping test and how the temporal information, e.g. time intervals from the time-drawdown-curve can be related to information about the spatial distribution of a heterogeneity.

a. Effects of varying storativity

The effect of varying storativity on drawdown behavior was observed in several numerical experiments and field studies and is discussed extensively e.g. in *Schad and Teutsch* [1994], *Meier et al.* [1998], *Sánchez-Vila et al.* [1999]. All these studies reveal a reduction of the variability in the estimates of storage and transmissivity values at late times depending on the well distance. Additionally, transmissivity approaches a constant value, the effective transmissivity of the domain. In contrast the geometric mean of the estimated S -values converges to the true value of storativity.

The estimated value of S can provide some information about the connectivity between the pumping and observation wells, since the time to measurable drawdown response is directly related to the intrinsic hydraulic aquifer property between pumping and observation wells. This is in accordance with *Vasco et al.* [2000], who used arrival time sensitivities in an asymptotic inversion approach and showed that arrival times are equally sensitive to structures between the pumping and observation wells. Hence, the initial drawdown response is not influenced at all by variations in the vicinity of the wells, which is contrary to the above-described approach of head sensitivities (Chapters 3 and 4). Consequently, the pumping test evaluation using *Theis* [1935] will produce significantly lower storativity values for drawdown curves with early initial response behavior compared to the correct value, in order to account for the initial drawdown response from the actual drawdown curves (cf. Table 6-1 vs. Figure 6-2). This leads to the problem that hydraulic parameters will be estimated that contradict the normal assumption of the hydraulic conductivity in between the wells if the initial response behavior of drawdown is considered.

b. Variability of hydraulic conductivity

From Table 6-1 it is evident that the variability of estimated conductivities is considerably smaller than that of the actual parameter variability. Two reasons can be given for this fact: Firstly, observed drawdown is the result of an ever increasing averaging process which addresses growing volumes as the depression cone expands with time. Therefore, a decreasing variability with increasing time can be expected as discussed in the previous section, which finally results in an effective parameter rep-

representing the overall property of the investigated domain. However, uncertainty exists about the actual extent of the domain and the weighting within the spatially varying parameter field. Considering the sensitivity distribution of Figure 4-1, the contribution of different areas of the aquifer in sign as well as in quantity to the observation cause further difficulties in the spatial assessment of the pumping test results.

c. Spatial assignment of parameter estimates

Since the assignment of time dependent parameter estimates from conventional pumping tests to different areas of the aquifer is equivocal, a reliable description and characterization of aquifer heterogeneity will fail. The frequently discussed concept of defining a radius of investigation will only succeed within some limitations, as the estimated parameters are averaged over a non-radial domain for early times and limited distances (cf. Figure 4-1 or Figure 4-4). Only for large times where averaging occurred about an increased aquifer volume this concept might provide more consistent estimates. Several descriptions have been proposed for defining a radius of investigation. Either it can be based on magnitudes of drawdown, or on the magnitude of flux at a certain radius, or on the location at which a maximum value is reached at a given time [Streltsova, 1988], thus emphasizing the uncertainty of the issue of a spatial assignment of distinct parameter estimates.

As a consequence, a reliable resolution of the described issues connected to conventional pumping test evaluation may succeed solely by the use of numerical inversion

techniques [e.g. Sun and Yeh, 1985; Yeh, 1986; McLaughlin and Townley, 1996; Vasco et al. 2000]. However, in hydrogeologic practice such methods are sparsely applied, since these partially sophisticated techniques require a considerable amount of data as well as an extensive computational effort. Alternatively, in the following a modification of the classical concept of pumping tests is given based on the distribution of sensitivity coefficients to resolve the issues cited, without complex inverse modeling.

6.3 Modification of the pumping test configuration based on sensitivity coefficients

Considering the sensitivity distribution of Figure 4-1, the domain of positive influence will diminish, if pumping and observation well are moved towards the same spatial position. A distribution of negative sensitivities will solely remain. Figure 6-5 shows a time series of sensitivity distribution for a pumping test, where the observation takes place at the pumping well location. Hence, the whole domain of interest has a negative influence with respect to any discontinuity in the distribution of hydraulic conductivity and the ambiguousness due to domains of contrary influence will vanish. Consequently, any heterogeneity of definite spatial extent and quantity will get the same influence on drawdown for same radial distances, i.e. a discontinuity of higher conductivity will lead to the same reduced drawdown s^* , compared to the homogeneous case, for all spatial positions in a radial distance r^* .

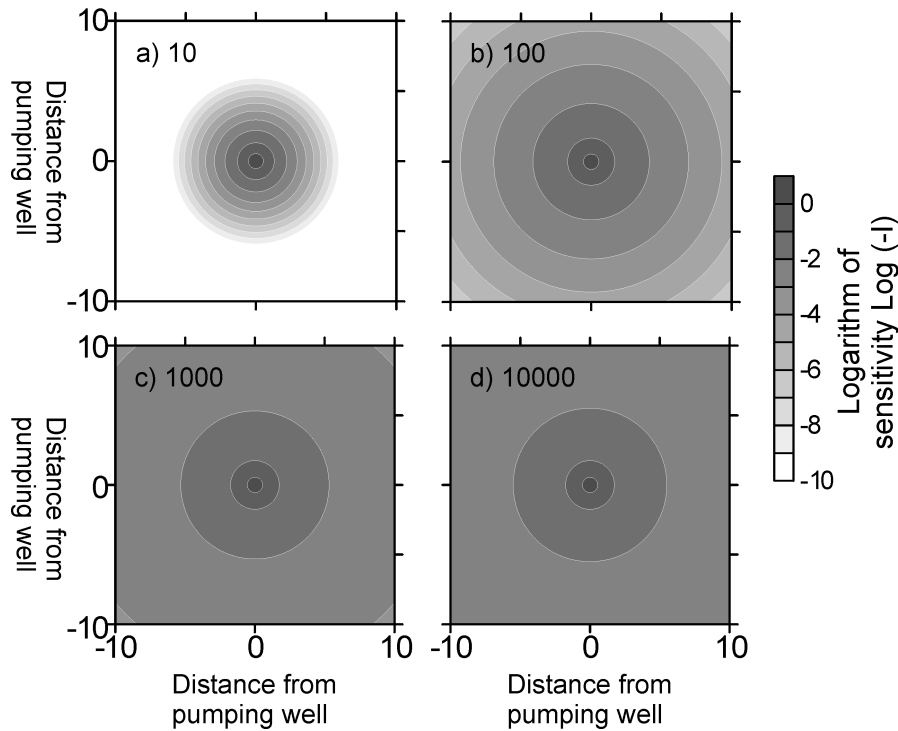


Figure 6-5. Sensitivity distribution of a pumping test with observation in the pumping well at $t = 10, 100, 1000,$ and $10,000$ seconds after start of pumping. The values of the hydraulic parameters are the same as for the distribution shown in Figure 4-1.

It is obvious how the sensitivity coefficients develop over time for observations of drawdown in the pumping well. The domain of highest sensitivity is in the direct vicinity of the well and the distribution in this region remains constant throughout all time steps. Figure 6-6 illustrates sections through the pumping well for several time steps and clearly shows this behavior in the direct vicinity of the pumping well. However, at late times the overall sensitivities increase, thus the relative influence of the region near the well will decrease. As a consequence, parameter estimates that rely on information for medium to late time will better represent effective values due to the increasing volumes of influence and the increase of absolute values of sensitivity (Figure 6-5 and Figure 6-6).

For a reliable application of the sensitivity distributions for single well pumping tests, it is appropriate to consider the relative change of sensitivities, as their values remain constant for an increasing portion of the domain of interest with increasing time (Figure 6-5 and Figure 6-6). With the relative change of sensitivity

$$\Delta I = \frac{I(t_k)}{I(t_{k-1})}$$

Eq. 6-1

the division of the domain of interest in several parts of differing influence is possible where $I(t_k)$ and $I(t_{k-1})$ quantify the sensitivity coefficients at two consecutive time steps.

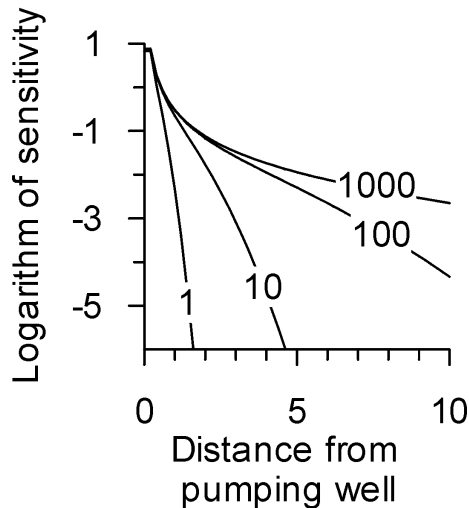


Figure 6-6. One-dimensional sensitivity distribution for a single well pumping test for different time steps ($t = 1, 10, 100, 1000$ s). Note that the illustrated sensitivity coefficients are negative ($\log_{10}(|I \times r|)$).

As proposed in chapter 4.3 for standard pumping tests three areas can be distinguished if considering the relative change of sensitivity coefficients: 1) A domain where the sensitivity remains constant between the particular time steps, 2) a domain where a considerable change in the sensitivity distribution occurs, and 3) a domain, where changes in the sensitivity distribution occur, but the overall sensitivities are too small to affect the observation. In Figure 6-7 the distribution of coefficients of relative change are given for three intervals.

In addition, Figure 6-8 shows time series of the evolution of sensitivity coefficients and their relative changes for several positions in the domain of interest. The proposed characterization was discussed for standard pumping tests in chapter 4.3 in detail and is summarized for the sensitivity distribution of a single well pumping test in the following.

Because of the radially symmetric distribution of sensitivity coefficients with respect to hydraulic conductivity, the coefficients of change in sensitivity are also distributed radially symmetric around the well. The domain where the sensitivity remains constant within a definite time frame, is represented by coefficients of relative change of $\log_{10}(\Delta I) \rightarrow 0$. In Figure 6-7 a through c, this domain corresponds to the innermost part of the domain with lowest values of relative change, and in Figure 6-8 b it is indicated by the abscissa-parallel section of the time-sensitivity curve. At later times, no further information is available from this portion of the aquifer. The radial symmetric area around the above-described domain represents that portion of the aquifer, where a considerable change in the sensitivity distribution occurs, given by coefficients of relative change of $\log_{10}(\Delta I) < 2$. With time, any changes in drawdown can be assigned to this portion of the aquifer.

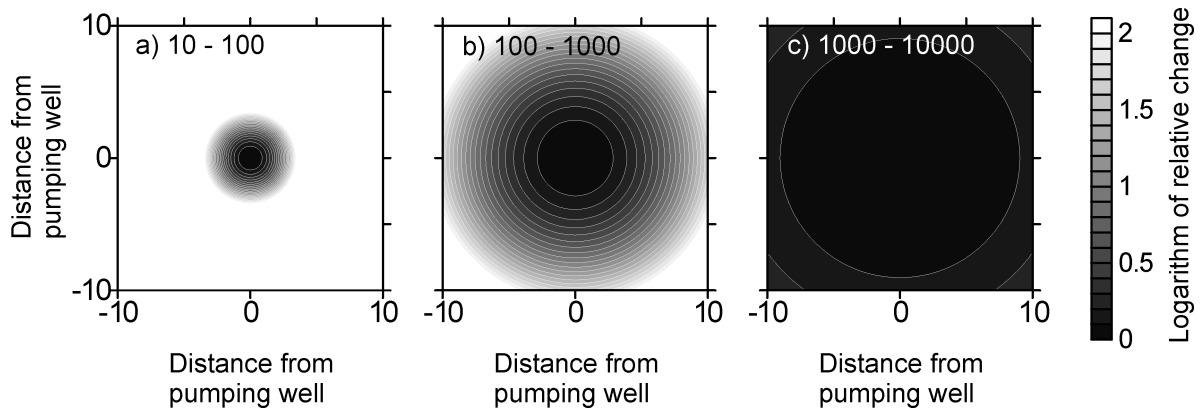


Figure 6-7. Distribution of relative changes of sensitivity for three intervals between (a) 10 and 100, (b) 100 and 1000, and (c) 1000 and 10,000 seconds.

From the domain with $\log_{10}(\Delta I) > 2$ no influence of parameter discontinuities on drawdown can be expected as the overall sensitivities in this domain are too small in order to affect drawdown.

With this information, a reliable characterization of the spatial variations of aquifer heterogeneity can be accomplished, as a link between temporal and spatial information is given.

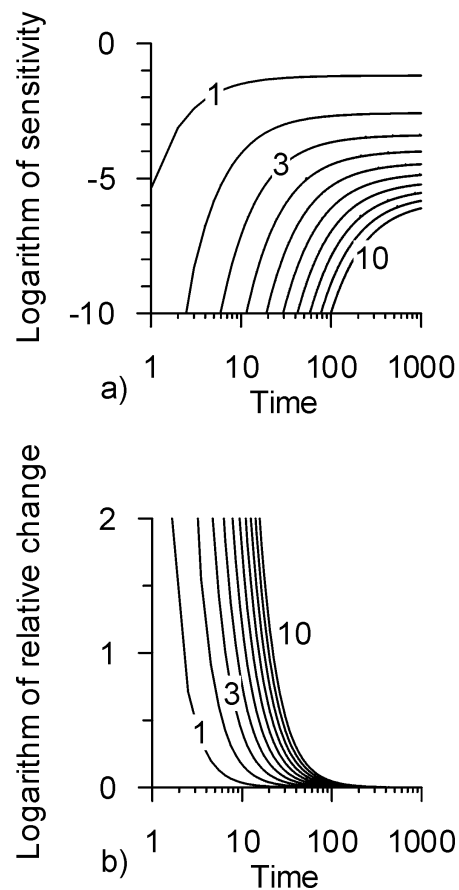


Figure 6-8. Time-sensitivity curves series at different radial distances from the well (a) and the relative change of sensitivity (b) for a single well test. The numbers indicate the radial distance; the interval between two curves is one meter.

6.4 Single well pumping tests

When dealing with single well pumping tests, some important restrictions have to be considered. Firstly, the drawdown measured in a pumping well may be influenced by well bore storage, as any well has a finite radius and thus a certain intrinsic storage capacity. In time-drawdown curves it can easily be determined whether the early-time drawdown data are dominated by well storage, since such a behavior will yield a line of unit slope in a log-log plot of time versus drawdown [Gringarten *et al.*, 1979]. Secondly, well losses have to be taken into account. The phenomena of well losses consist of a linear and a non-linear component [Kruseman and DeRidder, 1994]. The first component is caused by damage or stimulation of the well (known in petroleum engineering as skin effects). The latter is caused by friction losses inside the well screen, and by turbulent flow in the zone in direct vicinity of the well and in the suction hoses. The sum of the well losses leads to a deviation of the actual drawdown from the theoretically expected. This latter restriction leads to the fact that a reliable estimation of the storage coefficient S is practically not possible unless the total well loss is known precisely [Clark, 1977; Kawecki, 1995]. Therefore, the estimated values of S based on the observation in the pumping well should be treated very carefully. This is because the actual effective well radius, i.e. the radius that is extended by effects from well losses, is usually unknown. Applying the *Theis* solution incorrect radii lead to large errors in the determination of S , as r^2 enters the formula

$$S = \frac{4Tt}{r_w^2}$$

Eq. 6-2

However, both described phenomena can be introduced in the concept of sensitivity coefficients, e.g. using a corresponding analytical solution [e.g. Papadopoulos and Cooper, 1967] or a numerical implementation.

For a detailed illustration of the application of the sensitivity approach, the flow model is used, which was introduced in section 6.2. In the following, the wells *PW* and *O1 - O10* are used as pumping wells for consecutive single well pumping tests. Figure 6-9 shows the corresponding time-drawdown curves from each well. For the estimation of the hydraulic parameters, the *Theis* matching procedure was applied, where the distance r from Eq. 3-26 is replaced by the equivalent well radius r_w based on the size of actual grid spacing. From Figure 6-9 and Figure 6-10 it can be seen that different sections with different slopes can be observed in the time-drawdown curves. The first section is assigned to well bore storage, caused by the grid spacing (A-B in Figure 6-10), and can be identified by a straight line of unit slope in the log-log plot. With elapsing time, the influence of well storage effects will diminish as the cone of depression moves through the aquifer. The observed drawdown is the result of the averaging of the hydraulic properties over an increasing volume of investigation. Changes in the slope of the observed drawdown indicate significant changes in the parameter distribution of the subsurface. In order to obtain values for hydraulic parameters that represent averaged parameters of small domains, the first phase of drawdown after which no well bore stor-

age effects have been observed anymore was used for estimation (B-C in Figure 6-10).

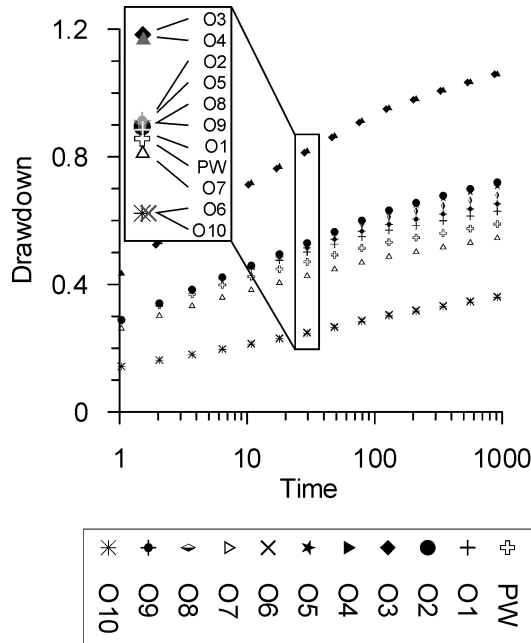


Figure 6-9. Time-drawdown curves for consecutive single well pumping tests at the wells PW, O1 - O10 (cf. Figure 6-1).

The resulting hydraulic parameters are given in Table 6-2. A comparison of the estimated parameters with the time-drawdown curves in Figure 6-9 shows a good agreement between parameter estimates and the amplitudes of drawdown, i.e. values of highest drawdown coincide with values of lowest conductivity, and vice versa. Furthermore, no differences between the response times of drawdown (time where the first drawdown occurs) have been observed. Theoretically, in a confined aquifer drawdown response starts with pumping. The variability of estimated conductivity values k approaches the actual range of one order of magnitude. A comparable variability for the storage coefficients can be observed as such is the case where pumping well and observation well

are spatially separated, but the geometric mean of estimated S agrees very well with the actual value of 5.0×10^{-2} .

These findings have substantial consequences for the interpretation of the drawdown curves and the corresponding estimates of hydraulic parameters.

1. Highest values of hydraulic conductivity are estimated for wells where lowest drawdown is observed, and vice versa. For the case of spatially separated pumping and observation wells (c.f. previous section 6.2) this behavior was found to be valid only in some cases.
2. No relationship between response time and hydraulic conductivity exists, as compared to cases of spatially separated pumping and observation wells.

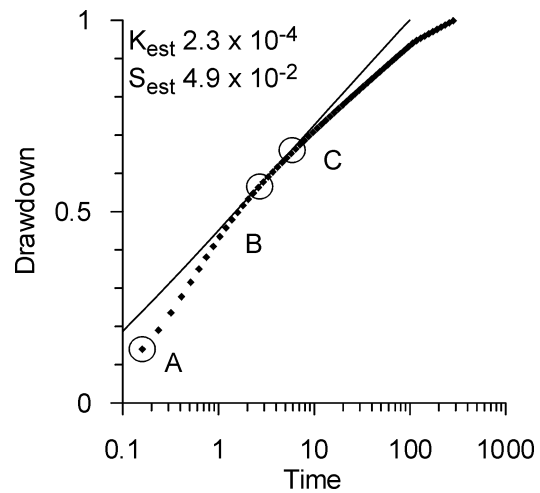


Figure 6-10. Time drawdown curve recorded for the single well pumping test performed at well O3. A-B: Early drawdown phase with well bore storage, B-C: Evaluated section of drawdown curve based on the analysis of sensitivity coefficients. Increasing effects of the heterogeneous distribution of hydraulic conductivity influence the following time drawdown behavior.

3. The geometric mean of estimated S -values will give a more accurate approximation than in the case of spatially separated pumping and observation wells. This is due to the fact, that early time data are considered. In addition, as described e.g. by *Schad and Teutsch* [1994] and *Meier et al.* [1998], the variability depends on the distance between the pumping and observation well. Therefore, for a single well pumping test a minor variability can be expected. The restrictions in terms of estimating values for S apply, as cited above.

Table 6-2. Estimates of the hydraulic parameters of the single well pumping tests.

Pumping at well	K	S
<i>PW</i>	4.5 e-4	3.8 e-2
<i>O1</i>	3.9 e-4	5.7 e-2
<i>O2</i>	3.9 e-4	5.0 e-2
<i>O3</i>	2.3 e-4	4.9 e-2
<i>O4</i>	2.3 e-4	5.0 e-2
<i>O5</i>	3.9 e-4	5.1 e-2
<i>O6</i>	9.1 e-4	7.1 e-2
<i>O7</i>	5.2 e-4	3.3 e-2
<i>O8</i>	3.8 e-4	6.2 e-2
<i>O9</i>	4.1 e-4	4.0 e-2
<i>O10</i>	9.1 e-4	7.1 e-2
<i>min</i>	2.3 e-4	3.2 e-2
<i>max</i>	9.1 e-4	7.1 e-2
<i>range</i>	6.8 e-4	3.9 e-2
<i>mean</i>	4.7 e-4	5.2 e-2
<i>std.</i>	2.3 e-4	1.3 e-2
<i>geo</i>	4.3 e-4	5.1 e-2

In order to address drawdown data from distinct time intervals to the corresponding spatial distribution of hydraulic parameters, the approach of sensitivity coefficients is applied to the data set gathered from the single well pumping tests.

As described in the beginning, sensitivity coefficients are calculated using Eq.

3-14 and Eq. 3-26 leading to Eq. 3-29. In the following, homogeneity is assumed - as implemented in Eq. 3-26 - for the time interval, for which the hydraulic parameters are estimated. Thus, the calculation of the sensitivity distribution is based on these parameters. Finally, for the time interval relative changes of sensitivity coefficients are calculated following Eq. 6-2, leading to a link of temporal and spatial information. For purpose of simplification, well bore storage is neglected in the further analysis. Figure 6-11 shows the distribution of relative changes for the single well pumping tests at the wells *O3* and *O10*. It is evident that for values of higher conductivity the “radius of investigation” is increased.

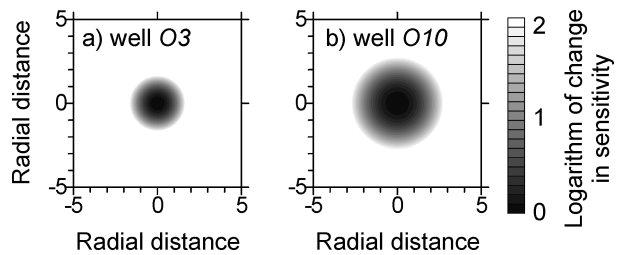


Figure 6-11. Distributions of coefficients of the relative change within the time interval for which the hydraulic parameters were fitted (a) for well *O3*, (b) for well *O10*.

As a consequence, a spatial distribution of hydraulic parameters can be given including the calculations of sensitivity coefficients. Figure 6-12 shows the distribution of the hydraulic conductivity based on the estimated parameters of the single well pumping tests (Table 6-2) and the relative changes of sensitivities (Figure 6-11). A bimodal distribution with lowest values on the left and right hand side at wells *O3*, *O4*, and *O8*, *O9* is evident. Highest values can be found on an axis between *O6* and *O10*. The circles

around the well positions illustrate the portion of the aquifer from which no additional information can be gained for further time steps. It is evident, how the radius of the circles decreases with decreasing conductivity, and vice versa.

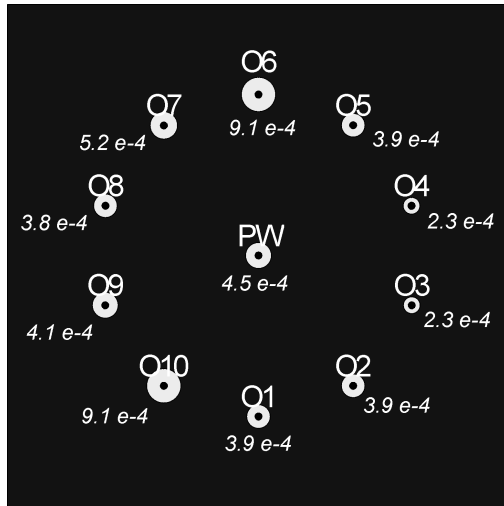


Figure 6-12. Distribution of hydraulic conductivity based on the estimated parameters from the single well pumping tests in connection with the sensitivity coefficient approach. The circles around the well positions illustrate the portion of the aquifer from which no additional information can be gained for further time steps.

Figure 6-13 shows the model parameter distribution for the simulation of the pumping test and single well pumping tests. For purpose of comparison, the values of the actual conductivity distribution and the estimated parameters from the conventional and the single well pumping tests are given in Table

6-3. It is obvious that the results from the single well pumping test and the actual distribution show a close agreement.

Table 6-3. Comparison of model input parameters (K_{model}) and parameters estimated for the single well pumping test (K_{sw}) and conventional pumping test (K_{pt}).

Well	K_{model}	K_{sw}	K_{pt}
PW	4.0 e-4	4.5 e-4	-
O1	4.0 e-4	3.9 e-4	6.1 e-4
O2	4.0 e-4	3.9 e-4	5.6 e-4
O3	2.0 e-4	2.3 e-4	4.7 e-4
O4	2.0 e-4	2.3 e-4	5.2 e-4
O5	4.0 e-4	3.9 e-4	5.6 e-4
O6	1.0 e-3	9.1 e-4	8.6 e-4
O7	4.0 e-4	5.2 e-4	4.8 e-4
O8	4.0 e-4	3.8 e-4	4.8 e-4
O9	4.0 e-4	4.1 e-4	5.0 e-4
O10	1.0 e-3	9.1 e-4	7.1 e-4

Furthermore, if the results of the conventional pumping test with pumping at well *PW* (Table 6-3) are compared to the model input parameters, the effects discussed previously get apparent. Highest storage was observed for the cases where a region of high conductivity was in between the pumping and observation well (wells *O6* and *O10*). In addition, these wells show highest drawdown, although a portion of high conductive material is lying in between. Only the response time of drawdown would indicate higher conductivity between the wells, however, the spatial assignment of the estimated parameters is equivocal.

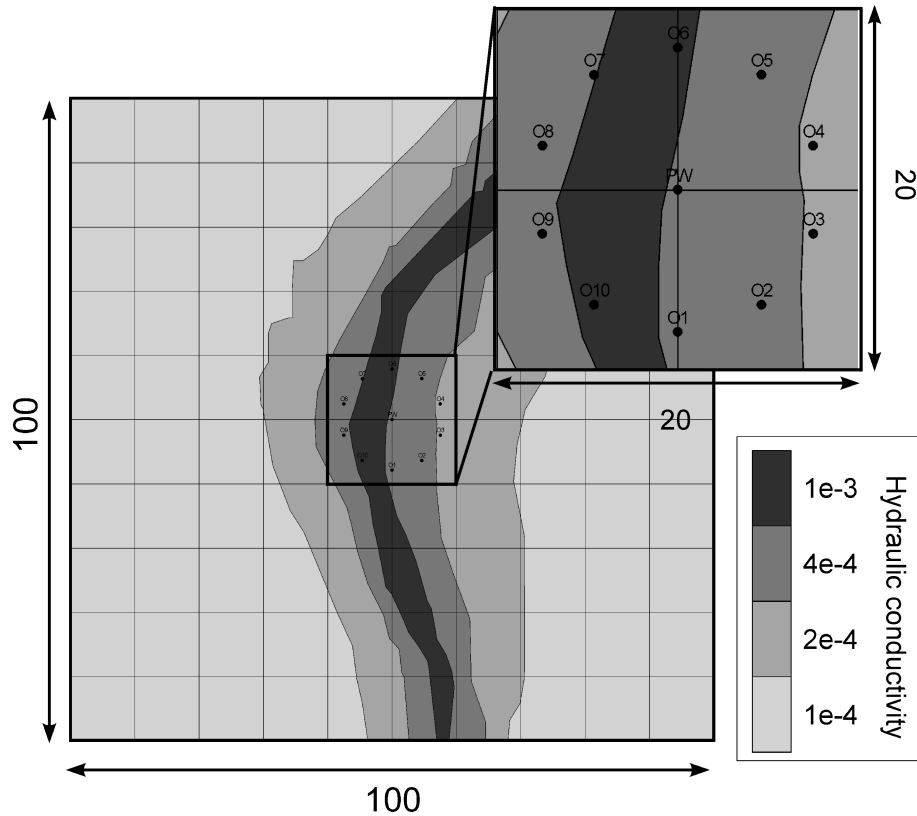


Figure 6-13. Distribution of hydraulic conductivity of the model domain.

6.5 Further considerations and conclusions

In this section, a further investigation is presented illustrating the suitability and applicability of the concept of single well pumping tests in connection with an analysis of sensitivity coefficients. In practical situations a certain amount of a priori information is often available, e.g. including knowledge about preferential flow directions or trends in the parameter distribution. If such information is available, the placement of wells can be performed appropriately. For example, in the aquifer model used for the considerations (Figure 6-13) an appropriate well placement would be perpendicular to

the main structure, i.e. across the channel of increased hydraulic conductivity. Figure 6-14 shows a row of wells that are used for single well pumping tests and the corresponding drawdown curves.

From Figure 6-14 b it is evident that the curves of drawdown evolve with differing slope with time. Applying the procedure used in the previous section, hydraulic parameters can be estimated for the consecutive intervals with different slope utilizing traditional evaluation methods like *Theis* curve matching. After calculation of the sensitivity distribution and their relative changes with the corresponding parameters for each well position, the temporal information, i.e. the hydraulic parameter estimated at different times, can be linked to the spa-

tial variability of heterogeneity. Accordingly, Figure 6-15 shows the distribution of hydraulic conductivity estimated for three different time intervals. For early and intermediate times the estimated hydraulic conductivities are close to the real values. The late time curve reveals clearly the effect of the averaging process over an increasing domain with time. The bars in Figure 6-15 indicate the radius of that area around the respective well from which no further information can be gained with ongoing time.

As the concept of sensitivity coefficients allows to include boundary effects, such as well bore storage or skin effects, a reliable quantification using classical evaluation methods can succeed. By considering the evolution of changes in the sensitivity distribution, a direct link between temporal and spatial information is given. Thus, any deviations in the drawdown curve, indicated

by a changing slope, can be assigned to particular areas of the aquifer.

The proposed application of single well pumping tests comprises several advantages compared to conventional pumping tests. Because the observation takes place within the pumping well, the pumping rate can be reduced. For single well tests in high permeable zones or aquifers with high conductivity, the signal, i.e. drawdown will reach amplitudes high enough for a reliable interpretation compared to the configuration with spatially separated pumping and observation well. Furthermore, the single well pumping tests allow the utilization of wells with a small diameter. Thus, boundary effects such as wellbore storage can be reduced in addition. With a given budget, the number of wells can be increased leading to an improved coverage of the domain of interest.

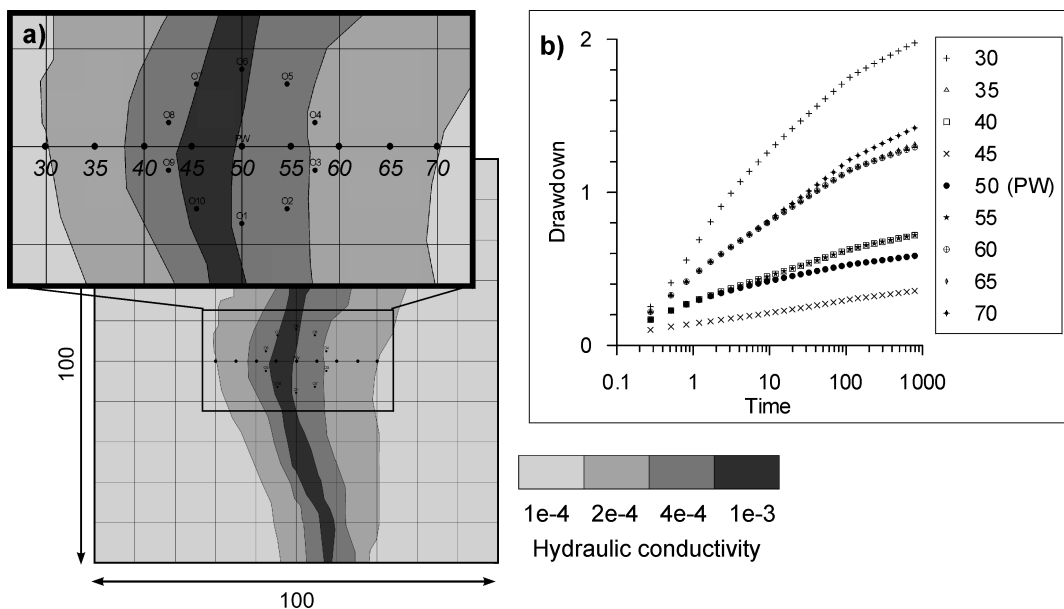


Figure 6-14. a) Section of wells perpendicular to the main structure of heterogeneity and b) the time-drawdown curves for single well pumping tests.

As illustrated in the previous section of by the results given in Figure 6-15, the performance of short term pumping tests may be sufficient for a high resolving characterization of the aquifer. However, as the early time drawdown phase is also most sensitive to measuring errors, e.g. induced by a fluctuating pumping rate, the performance of several short term pumping tests at each well may be advantageous. The stacking of the resulting time-drawdown curves may allow the removal or reduction of such measuring errors.

aquifer heterogeneity is improved using the proposed single well method in connection with the application of sensitivity coefficients. Already using the most commonly utilized evaluation techniques, e.g. based on the solution of *Theis* [1935], a reliable description will succeed. Thereby any other evaluation method, including definite boundary conditions, e.g. skin effects, well bore storage [e.g. *Gringarten et al.* 1979], can be included in this approach leading to a further improvement of the characterization and quantification procedure.

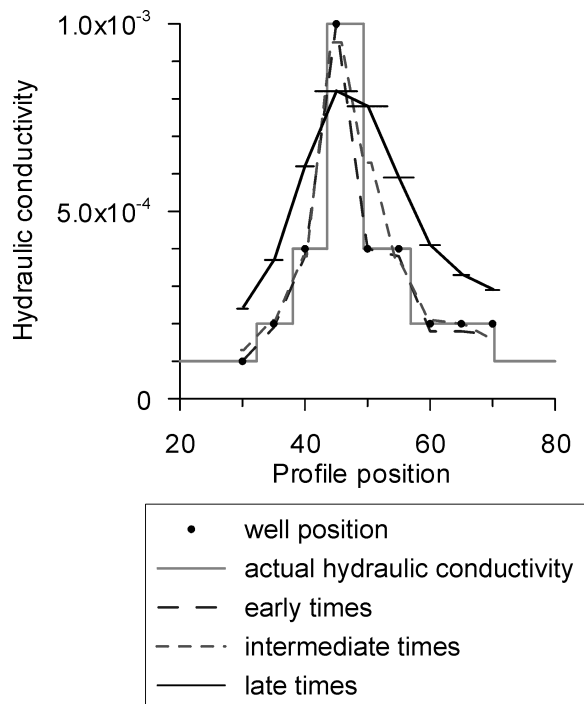


Figure 6-15. Profiles of hydraulic conductivity based on the estimated parameters for three different time intervals. For early and intermediate times the estimated hydraulic conductivities are close to the model parameters. The late time curve includes bars indicating the radius of that portion from that no further information can be gained with ongoing time.

Besides these technical advantages, the reliability of characterizing and quantifying

7 Application of the Concept of Sensitivity Coefficients - A Field Example from the “Boise Hydrogeophysical Research Site”

7.1 Introduction

The previous chapters dealing with sensitivity coefficients have been based on considerations of numerical simulations of pumping tests in hypothetical aquifers. In order to illustrate the suitability and applicability of the approach of sensitivity coefficients a field experiment at the Boise Hydrogeophysical Research Site (BHRS) is described in this chapter. The BHRS is the test site of the *Center of Geophysical Investigation of the Shallow Subsurface (CGISS)* at Boise State University (Idaho, USA). It is being developed as a three-dimensional control volume in a natural heterogeneous aquifer to support research on developing methods for combining non-invasive geophysical techniques with hydrologic measurements to map variations in permeability in shallow alluvial aquifers [Barrash and Clemo, 2000].

7.2 Description of the test site

The BHRS (Figure 7-1) is a wellfield located on a gravel bar adjacent to the Boise River. The wellfield includes 13 wells in a central area of approx. 20 m diameter for detailed testing, and five wells at some distance for information on hydraulic boundary conditions.

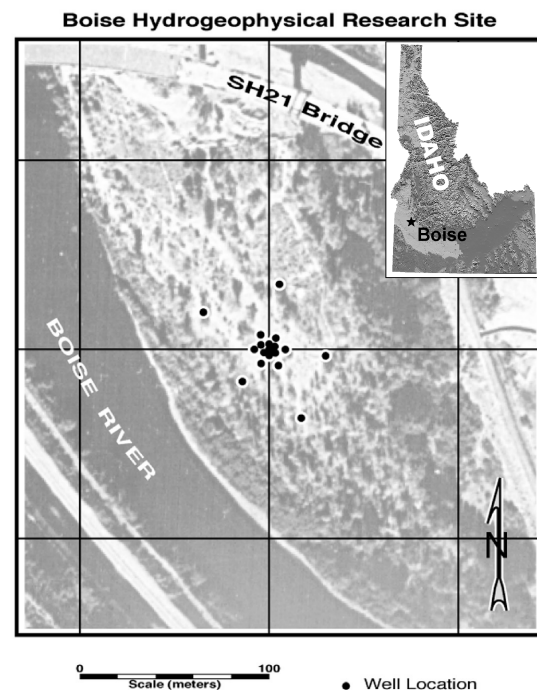


Figure 7-1. Photomap of the Boise Hydrogeophysical Site (BHRS) showing locations of 13 wells in the central portion of the site and 5 wells for information on hydraulic boundary conditions [from Barrash et al. 1999].

The wells in the central area are in two concentric rings at offset radial angles around a central well. Exact locations of the wells were selected using a Monte Carlo process to find the optimal well arrangement with similar numbers and azimuthal distributions of well pairs at 1 m lag through expected horizontal ranges of spatial correlation of

hydrologic and geophysical parameters [Barrash and Knoll, 1998]. Further details of the wellfield design can be found in Barrash et al. [1999].

From borehole data it is known that cobble and sand alluvial sediments are present to a depth of 18.5 to 21.5 m, and underlain by red clay continuous beneath the site. The deposits appear to be similar to slightly older Quaternary, coarse, braided-stream deposits observed in nearby outcrops and quarries [e.g. Figure 7-2].



Figure 7-2. Quarry exposure of analogue coarse, braided-stream deposits showing disconnected sand lenses (S) and a variety of cobble-dominated facies ranging from poorly sorted massive units (Gm), to moderately sorted horizontally-bedded units (Gh) and trough cross-bedded units (Gt). Heavy lines identify bounding surfaces between depositional sequences. For scale, quarry face is approx. 12 m high. Photograph and interpretation from Barrash and Knoll [1998].

Important data sets from the BHRS are given from core analyses and geophysical well logs from all the wells in order to characterize aquifer heterogeneity. In the following results of different geophysical investigations (well logging and ground penetrating radar) are given employed through CGISS. These studies will support findings

given later when presenting results from hydraulic testing.

a. Porosity logs

Porosity values are derived from neutron well logs in the 18 wells at the BHRS measured at 6 cm intervals in the saturated portion of the cobble and sand deposits. Generally, the porosity logs can successfully be interpreted for lithologic units where units of lowered porosity are cobble-dominated deposits and units of increased porosity are sand or relatively sand rich portions of cobble deposits. The stratigraphic interpretation of the units is given in Figure 7-3: Unit 1, the lower low-porosity cobble-dominated unit overlying a very thin portion of a basalt flow and a tight red clay; Unit 2, the lower variable-porosity cobble-dominated unit; Unit 3, the upper low-porosity cobble-dominated unit; Unit 4, the upper variable-porosity cobble-dominated unit; and Unit 5, channel sand.

From the porosity logs and their interpretation, plots of the spatial distribution of the stratigraphic units are calculated. The main feature dominating the two-dimensional distribution of hydraulic conductivity is supposed to be Unit 5 that is interpreted as sand dominated channel structure. Figure 7-4 shows the thickness distribution of Unit 5 that thickens towards the Boise River (southwest) and pinches out in the center of the well field.

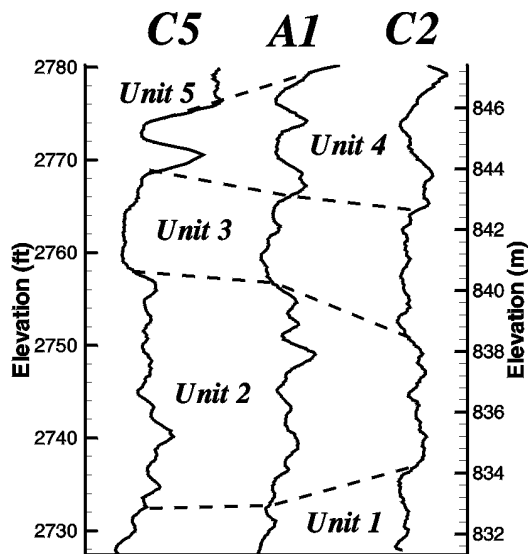


Figure 7-3. Section of stratigraphic units at the BHRS based on porosity logs perpendicular to the main depositional direction [from Barrash and Clemo, 2000].

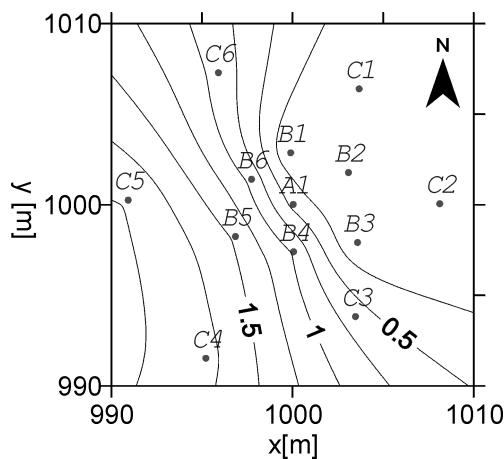


Figure 7-4. Spatial distribution of Unit 5 (channel sand) thickening towards southwest (thickness in meters).

A series of three-dimensional ground penetrating radar data sets were acquired over the central wellfield area at the BHRS. The goal of the surveys was to image the

complex stratigraphy around the well field. These images were used to construct 3-D models of the sedimentary architecture. Data sets were acquired using antennas of various frequencies enabling investigations with different depth penetration and resolution. The obtained images resulting from the GPR investigations suggest that the deposits can be subdivided laterally and vertically into several distinct surfaces (Figure 7-5). Time slices and vertical cuts through the data volumes were performed to identify the shape and orientation of the different architectural elements. These data are being used to construct a 3-D model of the hydrogeologic zonation of the aquifer [Peretti *et al.*, 1999]. Further information on data acquisition, processing, and detailed interpretation can be found in Peretti *et al.* [1999]. From Figure 7-5 major bounding surfaces and many internal reflectors can be traced laterally and vertically providing an image of the nature of the radar facies and architectural elements.

Note the reflector in the vertical slice at profile line 5.6 m in the chair image given in Figure 7-5 dipping from the central well field towards the wells C4 and C5. This reflection is interpreted as part of Unit 5 (channel structure). As discussed in the previous section, this unit is supposed to be dominant in terms of the two-dimensional distribution of hydraulic conductivity.

7.3 Single well pumping tests

Based on the analysis and application of sensitivity coefficients it was shown in the previous chapters that conventional pumping tests with spatially separated pumping and observation wells can lead to non-unique results since different domains of the inves-

tigated system contribute with contrary influence to the observation.

As discussed in Chapter 6, the domain of positive sensitivity will diminish, if the observation takes place in the pumping well.

Therefore, in the following the application of the sensitivity approach in connection with single well pumping tests employed at the BHRS is illustrated. Figure 7-6 shows the time drawdown curves from single well pumping tests at the wells in the central wellfield. All curves show more or less clearly the effect of unconfined conditions with delayed yield. More obviously these conditions have been observed in drawdown data in observation wells during conventional short time pumping tests (Figure 7-7 a).

In general, the effect of unconfined conditions with delayed yield can be divided in three phases [e.g. *Kruseman and deRidder, 1994*]:

i) Early time drawdown phase: The aquifer reacts in the same way as a confined aquifer, i.e. water is released instantaneously from storage. The drawdown curve follows a *Theis* type curve for corresponding values of T and S . ii) Intermediate time drawdown phase: The drawdown curve reflects the dewatering of the aquifer with falling water table. iii) Late time drawdown phase: The drawdown curve reflects the situation where flow in the aquifer is horizontal again. The drawdown curve follows a *Theis* type curve with corresponding values for T and S_y , the latter reflecting the specific yield of the aquifer.

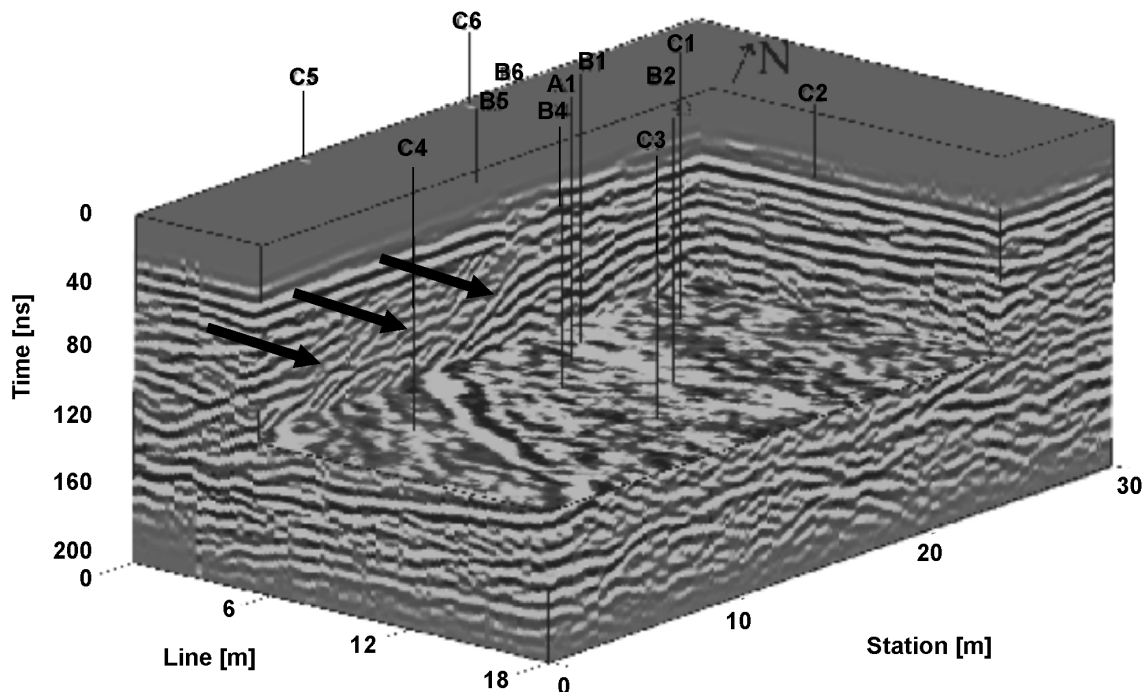


Figure 7-5. Chair image from the 200 MHz GPR data showing time slices at 134 ns (~ 6.8 m depth), and vertical sections along the 5.6 m line and the 24.0 m station line [from: *Peretti et al., 1999*]. Note the reflector interpreted as part of unit 5 (arrows).

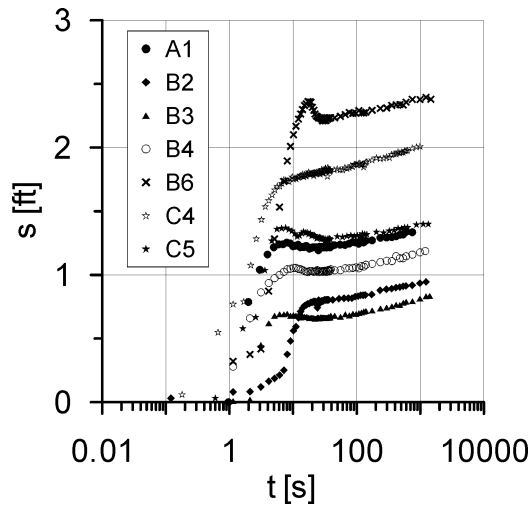


Figure 7-6. Time-drawdown curves from single well pumping tests employed at the wells in the central area of the BHRS.

Therefore, the early and late time phase of the drawdown curve can also be analyzed using the method of *Cooper and Jacob* [1946] and *Theis* [1935] (e.g. Figure 7-7 b) yielding the hydraulic conductivity k , storage S and the specific yield S_y , respectively. In addition, if an unconfined aquifer does not show the effect of delayed yield, the drawdown curve only follows the late time segment of the S-shaped curve [*Kruseman and deRidder*, 1994] that might be the case in few of the curves plotted in Figure 7-6.

Based on these facts the drawdown curves recorded in the individual pumping wells were evaluated using the method following *Cooper and Jacob* [1946]. The derived values of hydraulic conductivity are summarized in Table 7-1.

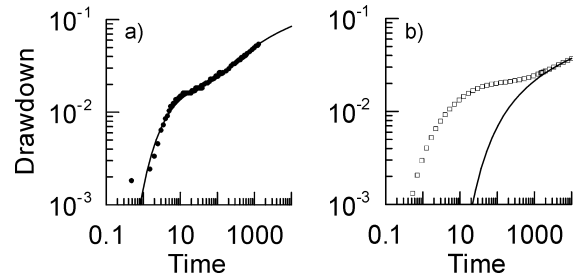


Figure 7-7. a) Time drawdown curve (dots) recorded at an observation well during a conventional short time pumping test with a best fit of the solution after *Neuman* [1974] indicating unconfined conditions with delayed yield. b) Calculated drawdown curve (symbols) after *Neuman* [1974] and a fitting curve (solid line) after *Theis* [1935] for late time data.

In order to obtain a spatial relation to the parameters given in Table 7-1, the distribution of sensitivity coefficients and their relative change for the considered time interval is calculated for the individual wells. Figure 7-8 gives the distribution of coefficients for the relative change of sensitivity at the central well *A1* for the interval of late time drawdown data.

Table 7-1. Hydraulic conductivities derived from single well pumping tests at the BHRS.

well	k [m/s]
A1	4.90 e-3
B2	3.03 e-3
B3	3.04 e-3
B4	3.49 e-3
B6	3.76 e-3
C4	5.43 e-3
C5	4.98 e-3

It is evident that information in terms of the evaluated drawdown signal (late time data) at *A1* is obtained from a portion in direct vicinity of the well. Using the estimated data (Table 7-1) and the corresponding change of sensitivity distribution (e.g. Figure 7-8) the

spatial variability of the two-dimensional hydraulic conductivity can be calculated and is given in Figure 7-9.

Compared to the distribution of Unit 5 that is supposed to be the dominating feature of the two-dimensional distribution of hydraulic conductivity based on the porosity logs (Figure 7-4) and the interpretation of the three-dimensional GPR measurements, a close agreement to Figure 7-9 can be recognized. In other words, the assumption that Unit 5 (sand channel) will act as the dominating feature controlling the two dimensional distribution of hydraulic conductivity is proven.

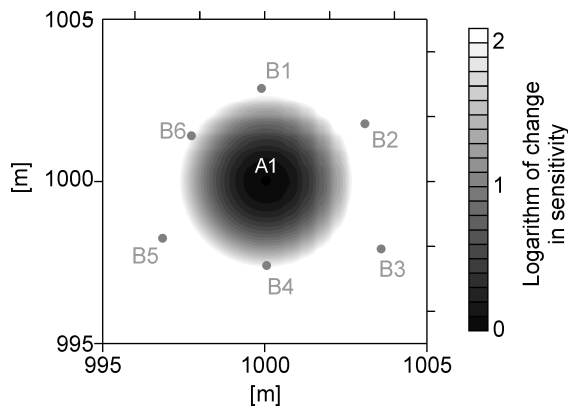


Figure 7-8. Distributions of coefficients of change in sensitivity for the single well pumping test at the central well *A1* of the BHRS for the interval between 100 and 1000 s.

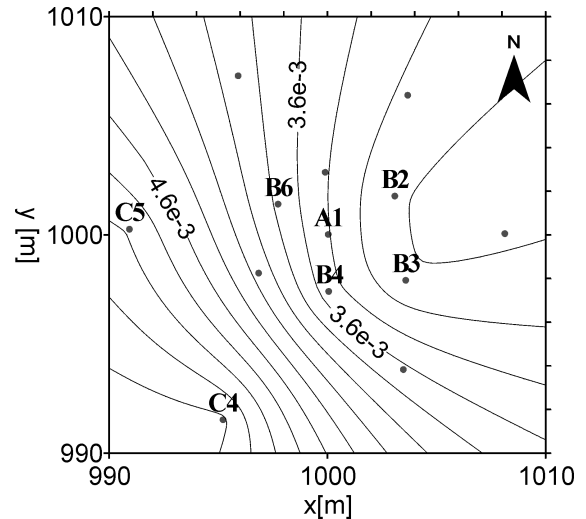


Figure 7-9. Distribution of hydraulic conductivity utilizing the connection of coefficients of relative change in sensitivity and parameter estimates using the method of *Cooper and Jacob* [1946]. An agreement with the distribution of the sand channel (Figure 7-4) is evident.

7.4 Final remarks

The field application of the SCA in combination with the proposed concept of single well pumping test was successfully performed at the BHRS. The field example illustrates the suitability and applicability of the SCA for aquifer characterization and for an improvement of the understanding of effects on hydraulic tests resulting from heterogeneity. This field example of the SCA was the first application to field data known to the author. The work presented in this chapter was funded by grants from the German Academic Exchange Service (DAAD, D/01/049/14) and the U.S. Army Research Office (DAAH04-96-1-0318).

8 Summary and Conclusion

The present thesis was motivated by the requirement of an improved understanding and insight in the interrelationship of effects resulting from heterogeneity on particular measurements, and by the importance of a detailed characterization and quantification of aquifer heterogeneity for a reliable identification and prediction of flow and transport in heterogeneous aquifers. Consequently, the general objective of this thesis was to improve the understanding of effects that may arise from aquifer heterogeneity on hydraulic measurements. Thereby two approaches, an experimental and a theoretical, have been applied.

In the experimental approach gas flow and pressure buildup experiments based on the aquifer analogue approach have been conducted at a fractured sandstone block on laboratory scale. This approach allows the practical investigation of the system in terms of an examination of the effects due to the strongly heterogeneous nature of the fractured sample. A theoretical approach based on the analysis of sensitivity coefficients was chosen as it enables the improvement of the theoretical comprehension of effects arising from aquifer heterogeneity. This approach allows the extension to more general considerations, i.e. regarding arbitrary parameter distributions. To provide a general statement, the approach was based on considerations of the hydraulic configuration of a conventional pumping test.

The experimental investigations provide an insight into the effects of the

strongly heterogeneous fractured porous system on the employed pneumatic measurements. In addition, an insight into the relevant processes for flow and pressure buildup in the heterogeneous media was given. Experiments with an induced stationary radial flow field provide mainly information on the heterogeneity in terms of preferential flow paths within the fractured sample. The effects of the porous matrix are of minor significance. Experiments with transient pressure buildup allow the examination of the effects of variable conductivity and storage capacity. Both experimental series reveal the very heterogeneous distribution of flow and pressure buildup, respectively, as result of the complexity of the system. The fracture network allows the focused flow and pressure spreading along distinct pathways leading to faster response with respect to an induced stimulation. In addition, the enlarged fraction of flow along such pathways gets evident from the employed experiments.

The methods developed for the investigation of the strongly heterogeneous system of a fractured porous rock using practical measurements allow revealing effects arising from the heterogeneity of the investigated system. However, the comparison of the results from both experimental series exemplified the necessity of an improved understanding of the interrelation between an arbitrary parameter distribution and the response of a particular hydraulic measurement or measuring method, respectively. A promising concept to account for this inter-

relationship is the Sensitivity Coefficient Approach (SCA).

This approach, which was initially developed in DC-geoelectrics, was transferred and extended to groundwater hydraulics. To develop the principle understanding of the interrelationship between heterogeneity and the response of particular hydraulic measurements, the approach is applied to more general cases of heterogeneity. Based on the derivation of sensitivity coefficients an analysis of the sensitivity distribution with respect to variations of the governing parameters was given. In order to evaluate the effects of parameter deviations on the hydraulic measurements the distribution of sensitivity coefficients for a homogeneous parameter distribution was analyzed in detail. This analysis revealed the intrinsic characteristics of sensitivity distributions with a division of the domain of interest in two subdomains of contrary sensitivity separated by a line of zero influence. For anisotropic parameter fields, an elliptical distribution of sensitivity coefficients can be expected. The elliptical sensitivity distributions are elongated in direction of the axis of higher conductivity. In heterogeneous parameter distributions, the sensitivity distribution can be highly irregular.

The analysis of sensitivity coefficients in terms of heterogeneous parameter distributions showed that the capability of a discontinuity to have a detectable effect on the observation during a pumping test is greatly affected by its distance from the wells as well as by the contrast of hydraulic conductivity between the heterogeneity and the surrounding material. The sensitivity of the observation with respect to changes in the parameter distribution is highest in the direct vicinity of the wells.

Consequently, for any hydraulic test, which is aimed on high-resolving investigations, the wells should be positioned as close as possible to the domain of interest, which should be covered by as many different permutations of sensitivity distribution as possible for a reduction of ambiguousness and for an improvement of the resolution of potential discontinuities. For the characterization of a definite domain in terms of effective parameters, several tests, spatially different positioned, should be performed in the way of getting a nearly homogeneous coverage of the domain of interest with average sensitivity values.

In hydrogeologic practice, the characterization of aquifers is mostly performed using classical test methods, such as constant rate pumping tests evaluating the hydraulic parameters most often by means of homogeneous interpretation models. This can lead to misinterpretations, as these methods are assumed to give parameters averaged over a domain of uncertain extent and unknown weighting as revealed by the SCA.

As a consequence, various issues can arise using classical test and evaluation methods. These facts can lead to the problem of how a definite parameter estimate can be related to a certain parameter distribution. Considering transient groundwater flow, the problem is extended, as the time dependent information, e.g. distinct intervals in the time-drawdown curve, can be connected to definite spatial information, i.e. spatially varying hydraulic parameters.

In order to illustrate and resolve these difficulties the approach of sensitivity coefficients was applied to investigate the intrinsic characteristics of hydraulic tests giving a

better understanding of the response of hydraulic test methods due to aquifer heterogeneity. As the approach allows the assessment of information from distinct time periods during a hydraulic test, e.g. data from definite sections of the time-drawdown curve of a pumping test, the assignment of estimated parameters to particular spatial information can succeed.

Based on the SCA the modification of the classical pumping test configuration to a single well pumping test with observation in the pumping well was suggested. With this optimization, the ambiguity due to domains of contrary influence will diminish. The suitability and applicability of the proposed configuration is illustrated by a numerical example and by field measurements.

Generally, both approaches, the experimental as well as the theoretical approach revealed that the effects resulting from aquifer heterogeneity greatly depends on the spatial positions of the measuring configuration relative to the spatial position and extent of the heterogeneity. For exam-

ple, the analysis of the distribution of the flow field (steady-state flow experiments) and the evolution of pressure buildup (diffusivity tests) during the hydraulic tests shows that the direction and the affected portion of the flow field is highly dependent on the spatial formation of the fracture network and on the position of the observation points with respect to highly conductive features.

Furthermore, both approaches show clearly that the capability to affect hydraulic measurements is also depending on the parameter distribution in terms of absolute values of the considered parameter. In this context from both approaches it became apparent that for hydraulic measurements in high conductive zones, e.g. fractures, only a reduced capability to detect parameter changes exists. For some measurements in a domain of lower conductivity, the capability to detect parameter changes is increased relatively. However, in both cases no information will be gained from parameter changes within a heterogeneity of increased conductivity.

9 References

- Baraka-Lokmane, S., 1999. Comparison of hydraulic conductivities derived from theoretical modelling based on discrete geometrical characterisation of fractured sandstone cores with laboratory measurements, *Tübinger Geowissenschaftliche Arbeiten (TGA)*, C51, 113 p.
- Barker, J.A., and Herbert, R., 1982. Pumping tests in patchy aquifers, *Ground Water*, 20(2), 150-155.
- Barrash W., and Clemo T., 2000. Hierarchical geostatistics of porosity derived from neutron logs at the Boise Hydrogeophysical Research Site, Boise, Idaho. In: Dassargues A. (ed.), *Tracers and Modelling in Hydrogeology*, IAHS Publ., 262, 333-338.
- Barrash, W., and Knoll, M.D., 1998. Design of research wellfield for calibrating geophysical methods against hydrologic parameters. In: 1998 Conference on Hazardous Waste Research, Snowbird, UT, Great Plains / Rocky Mountains Hazardous Substance Research Center, Kansas State University, 296-318.
- Barrash, W., Clemo, T., and Knoll, M.D., 1999. Boise Hydrogeophysical Research Site (BHRS): Objectives, design, initial geostatistical results. *Proceedings of the Symposium on the Application of Geophysics to Engineering and Environmental Problems (SAGEEP99)*, Oakland (CA), 389-398.
- Becker, L., and Yeh, W.G., 1972. Identification of parameters in unsteady open channel flows. *Water Resources Research*, 8(4), 956-965.
- Bengelsdorf, K., 1997. Fazies- und Reservoirgeologie im Stubensandstein von Pliezhausen-Rübgarten, Diplomarbeit an der Geowissenschaftlichen Fakultät der Universität Tübingen, 61 p.
- Billaux, D., Chiles, J.P., Hestir, K., and Long, J., 1989. Three-dimensional statistical modeling of a fractured rock mass - an example from the Fanay-Augère mine. *International Journal of Rock Mechanics and Mining Sciences and Geomechanics Abstracts*, 26, 281-299.
- Bloomfield, J.P., and Williams, A.T., 1995. An empirical liquid permeability - gas permeability correlation for use in aquifer properties studies, *Quarterly Journal of Engineering Geology*, 28, 143-150.
- Bodvarsson, G.S., Boyle, W., Patterson, R., and Williams, D., 1999. Overview of scientific investigations at Yucca Mountain - the potential repository for high-level nuclear waste. *Journal of Contaminant Hydrology*, 38, 3-24.

- Bredehoeft, J.D., Cooper, H.H., and Papadopoulos, I.S., 1966. Inertial and storage effects in well-aquifer systems: An analogue investigation. *Water Resources Research*, 2, 697-707.
- Butler, J.J., 1988. Pumping Tests in Nonuniform Aquifers – The radially symmetric case. *Journal of Hydrology*, 101, 15-30.
- Butler, J.J., 1990. The role of pumping tests in site characterization: Some theoretical considerations. *Ground Water*, 28(3), 394-402.
- Butler, J.J., 1991. A stochastic analysis of pumping tests in laterally nonuniform media. *Water Resources Research*, 27(9), 2401-2414.
- Butler, J.J., and Liu, W., 1991. Pumping tests in nonuniform aquifers: The linear strip case. *Journal of Hydrology*, 128, 69-99.
- Butler, J.J., and Liu, W., 1993. Pumping tests in nonuniform aquifers: The radially asymmetric case. *Water Resources Research*, 29(2), 259-269.
- Butler, J.J., and McElwee, C.D., 1990. Variable-rate pumping tests for radially symmetric nonuniform aquifers. *Water Resources Research*, 26(2), 291-306.
- Butler, J.J., McElwee, C.D., and Bohling, G.C., 1999. Pumping test in networks of multilevel sampling wells: Motivation and methodology. *Water Resources Research*, 35(11), 3553-3560.
- Carter, R.D., Kemp, L.F., and Pierce, A.C., 1982. Discussion of comparison of sensitivity coefficient calculation methods in automatic history matching. *Society of Petroleum Engineers Journal*, 22, 205-208.
- Carter, R.D., Kemp, L.F., Pierce, A.C., and Williams, D.L., 1974. Performance matching with constraints. *Society of Petroleum Engineers Journal*, 14, 187-196.
- Chavent, G., Dupuy, M., and Lemmonier, P., 1975. History matching by use of optimal theory. *Society of Petroleum Engineers Journal*, 15, 74-86.
- Clark, L., 1977. The analysis and planning of step drawdown tests. *Quarterly Journal of Engineering Geology*, 10, 125-143.
- Clauser, C., 1992. Permeability of crystalline rocks. *EOS, Transactions, American Geophysical Union*, 73 (21), 233-240.
- Clement, T.P., Truex, M.J., and Hooker, B.S., 1997. Two-well test method for determining hydraulic properties of aquifers. *Ground Water*, 35(4), 698-703.
- Cooper, H.H., and Jacob, C.E., 1946. A generalized graphical method for evaluating formation constants and summarizing well field history. *Transactions, American Geophysical Union*, 27, 526-534.
- Dagan, G., 1989. Flow and transport in porous formations. Springer Verlag, Berlin, 465 p.

- Desbarats, A.J., 1992. Spatial averaging of the hydraulic conductivity in three-dimensional heterogeneous porous media. *Mathematical Geology*, 24 (3), 249-267
- Dietrich, P., 1992. Impedanztomographie: Entwicklung eines Rechnerprogramms zur Bestimmung der Durchlässigkeitsverteilung des Untergrundes mittels hydraulischer Tomographie. Diplomarbeit an der Bergakademie Freiberg, 61 pp.
- Dietrich, P., 1999. Konzeption und Auswertung gleichstrom-geoelektrischer Tracerversuche unter Verwendung von Sensitivitätskoeffizienten. *Tübinger Geowissenschaftliche Arbeiten (TGA)*, C50, 130 p.
- Ferris, J.G., Knowless, D.B., Brown, R.H., Stallman, R.W., 1962. Theory of aquifer tests. U.S. Geological Survey, Water Supply Paper 1536E, 174 p.
- Flint, S.S., and Bryant, I.D., 1993. The geological modelling of hydrocarbon reservoirs and outcrop analogues. *Special Publication of the International Association of Sedimentologists*, 15, 269 p.
- Freeze, R.A., and Cherry, J.A., 1979. Groundwater. Englewood Cliffs, Prentice Hall, 604 p.
- Grimestad, G., 1995. Analysis of data from pumping tests in anisotropic aquifers: Equations and graphical solutions. *Water Resources Research*, 31(4), 933-941.
- Gringarten, A.C., Bourdet, D.P., Landel, P.A., and Kniazeff, V.J., 1979. A comparison between different skin and wellbore storage type-curves for early-time transient analysis. *SPE paper 8205*, presented at the SPE-AIME 54th Annual Technical Conference and Exhibition, Las Vegas, Nevada, Society of Petroleum Engineers.
- Guglielmi, Y., and Mudry, J., 2001. Quantitative measurements of channel-block hydraulic interactions by experimental saturation of a large, natural, fissured rock mass. *Ground Water*, 39(5), 696-701.
- Heling, D., 1963. Zur Petrologie des Stubensandsteins. Dissertation an der Geowissenschaftlichen Fakultät der Universität Tübingen.
- Hornung, J., and Aigner, T., 1999. Reservoir and aquifer characterization of fluvial architectural elements: Stubensandstein, Upper Triassic, southwest Germany, *Sedimentary Geology*, 129, 215-280.
- Hubbert, M.K., 1969. The theory of groundwater motion and related papers. Hafner, New York. 310 p.
- Huggenberger, P., 1993. Radar facies: recognition of facies patterns and heterogeneities within Pleistocene Rhine gravels, NE Switzerland. Braided Rivers, *Geological Society Special Publication*, 75, 163-176.
- Hunt, B., 1985. Flow to a well in a multiaquifer system. *Water Resources Research*, 21(11), 1637-1641.
- Indelman, P., and Abramovich, B., 1994. Nonlocal properties of nonuniform averaged flows in heterogeneous media. *Water Resources Research*, 30(12), 3385-3393.

- Indelman, P., and Dagan, G., 1993 a. Upscaling of permeability of anisotropic heterogeneous formations, 1. The general framework. *Water Resources Research*, 29(4), 917-923.
- Indelman, P., and Dagan, G., 1993 b. Upscaling of permeability of anisotropic heterogeneous formations, 2. General structure and small perturbation analysis. *Water Resources Research*, 29 (4), 925-933.
- Indelman, P., Fiori, A., and Dagan, G., 1996. Steady flow toward wells in heterogeneous formations: Mean head and equivalent conductivity. *Water Resources Research*, 32(7), 1975-1983.
- Jacquard, P., 1964. Théorie de l'interprétation des mesures de pression. *Revue IFP*, Vol. XIX, 297-338.
- Jacquard, P., and Jain, C., 1965. Permeability distribution from field pressure data. *Society of Petroleum Engineers Journal*, 5, 281-294.
- Jaritz, R., 1999 - Quantifizierung der Heterogenität einer Sandsteinmatrix (Mittlerer Keuper, Württemberg), *Tübinger Geowissenschaftliche Arbeiten (TGA)*, C45, 106 p.
- Kabala, Z.J., 2001. Sensitivity analysis of a pumping test on a well with wellbore storage and skin. *Advances in Water Resources*, 24, 483-504.
- Karasaki, K., Freifeld, B., Cohen, A., Grossenbacher, K., Cook, P., and Vasco, D., 2000. A multidisciplinary fractured rock characterization study at Raymond field site, Raymond, CA. *Journal of Hydrology*, 236, 17-34.
- Kawecki, M.W., 1995. Meaningful Interpretation of step-drawdown tests. *Ground Water*, 33(1), 23-32.
- Keller, A.A., Roberts, P.V., and Blunt, M.J., 1999. Effect of fracture aperture variations on the dispersion of contaminants. *Water Resources Research*, 35 (1), 55-63.
- Kickmaier, W., and McKinley, I., 1997. Forschungsarbeiten in europäischen Felslabors. *NAGRA informiert (NAGRA bulletin)*, 29, 29-36.
- Kravaris, C., and Seinfeld, J.H., 1985. Identification of parameters in distributed parameter systems by regularization. *SIAM J. Control and Optimization*, 23, 217-241.
- Kruseman, G.P., and de Ridder, N.A., 1994. Analysis and evaluation of pumping test data. *ILRI publication*, 47, Wageningen, 377 p.
- Lachassagne, P., Ledoux, E., and deMarsily, G., 1989. Evaluation of hydrogeological parameters in heterogeneous porous media. *Groundwater Management: Quantity and Quality. IAHS Publ.*, 188, 3-18.
- Lebbe, L., Tarhouni, J., Van Houtte, and De Breuck, 1995. Results of an artificial recharge test and a double pumping test as preliminary studies for optimizing water supply in the western Belgian coastal plain, *Hydrogeology Journal*, 3(3), 53-63.

- Long, J.C.S., and Witherspoon, P.A., 1985. The relation ship of the degree of interconnection to permeability in fracture networks. *Journal of Geophysical Research*, 90, 3087-3098.
- Lovelock, P.E., 1977. Aquifer properties of permo-triassic sandstones in the United Kingdom. *Bulletin of the Geological Survey of Great Britain*, 56, 1-40.
- Lowry T., Allen, M.B., and Shive, P.N., 1989. Singularity removal: A refinement of resistivity modeling techniques. *Geophysics*, 54(6), 766-774.
- Mauch, S., 1993. Bestimmung von Matrixdiffusionskoeffizienten und hydraulischer Leitfähigkeit verschiedener Sandsteine Süddeutschlands. Diplomarbeit an der Geowissenschaftlichen Fakultät der Eberhard Karls Universität Tübingen.
- McDermott, C.I., 1999 - New experimental and modelling techniques to investigate the fractured porous system, *Tübinger Geowissenschaftliche Arbeiten* (TGA), C52, 170 p.
- McDermott, C.I., Sauter, M., and Liedl, R., 1998. Investigating Fractured-Porous Systems - The Aquifer Analogue Approach, in: Rossmannith (ed.), *Mechanics of Jointed and Faulted Rock*, Balkema, Rotterdam, 607-612.
- McElwee, C.D., 1987. Sensitivity analysis of groundwater models. *Advances in Transport Phenomena in Porous Media*. In: Bear, J., and Corapcioglu, M.Y. (eds.), *NATO ASI Series. Series E: Applied Sciences*, 128, 751-817.
- McElwee, C.D., Bohling, G.C., and Butler, J.J., 1995 a. Sensitivity Analysis of Slug Tests, Part 1. The Slugged Well. *Journal of Hydrology*, 164, 53-67
- McElwee, C.D., Bohling, G.C., Butler, J.J., and Liu, W., 1995 b. Sensitivity Analysis of Slug Tests, Part 2. Observation Wells. *Journal of Hydrology*, 164, 69-87
- McLaughlin, D., and Townley, L.R., 1996. A reassessment of groundwater inverse problem. *Water Resources Research*, 32(5), 1131-1161.
- Meier, P.M., Carrera, J., and Sánchez-Vila, X., 1998. An evaluation of Jacob's method for the interpretation of pumping tests in heterogeneous formations. *Water Resources Research*, 34(5), 1011-1025.
- Miralles-Wilhelm, F., and Gelhar, L.W., 1996. Stochastic analysis of sorption macrokinetics in heterogeneous aquifers. *Water Resources Research*, 32(6), 1541-1549.
- Molz, F.J., Güven, O., Melville, R.D., Crocker, R.D., and Matteson, K.T., 1986. Performance, analysis, and simulation of a two well tracer test at the Mobile site. *Water Resources Research*, 22(7), 1031-1037.
- Naff, R.L., 1991. Radial flow in heterogeneous porous media: An analysis of specific discharge. *Water Resources Research*, 27(3), 307-316.
- Neuman S.P., 1974. Effect of partial penetration on flow in unconfined aquifers considering delayed gravity response. *Water Resources Research*, 10 (2), 303-312.

- Neuman, S., and Orr, S., 1993. Prediction of steady state flow in nonuniform geologic media by conventional moments: Exact nonlocal formalism, effective conductivities, and weak approximation. *Water Resources Research*, 29(2), 341-364.
- Oliver D.S., 1993 - The Influence of Nonuniform Transmissivity and Storativity on Drawdown, *Water Resources Research*, 29(1), 169-178.
- Papadopoulos, I.S. and H.H. Cooper, 1967. Drawdown in a well of large diameter, *Water Resources Research*, 3, 241-244.
- Peretti W.R., Knoll M.D., Clement W.P., Barrash W., 1999. 3-D GPR imaging of complex fluvial stratigraphy at the Boise Hydrogeophysical Research Site. *Proceedings of the Symposium on the Application of Geophysics and Environmental Problems (SAGEEP99)*, 555-564.
- Press, W.H. (ed.), Teukolsky, S.A., Vetterling, W.T., and Flannery, B.P., 1996. Numerical recipes in Fortran 90: The art of parallel scientific computing. Cambridge University Press, Cambridge, 963 p.
- Rasmussen, T.C., Evans, D.D., Sheets, P.J., and Blanford, J.H., 1993. Permeability of Apache Leap Tuff: Borehole and Core Measurements Using Water and Air, *Water Resources Research*, 29, 1997-2006.
- Renard, P., and deMarsily, G., 1997. Calculating equivalent permeability: A review. *Advances in Water Resources*, 20(5-6), 253-278.
- Romm, E.S., 1966. Flow characteristics of fractured rocks (in Russian). Nedra, Moscow.
- Sampath, K., and Keighom, C.W., 1982. Factors affecting gas slippage in tight sandstones of cretaceous age in the Uinta Basin. *Journal of Petroleum Technology*, 2715-2720.
- Sánchez-Vila, X., Girardi, J.P., and Carrera, J., 1995. A synthesis of approaches to upscaling of hydraulic conductivities. *Water Resources Research*, 31(4), 867-882.
- Sánchez-Vila, X., Meier, P.M., and Carrera, J., 1999. Pumping tests in heterogeneous aquifers: An analytical study of what can be obtained from their interpretation using Jacob's method. *Water Resources Research*, 35(4), 943-952.
- Sauter, M., 1992. Quantification and forecasting of regional ground water flow and transport in a karst aquifer (Gallusquelle, Malm, southwestern Germany). *Tübinger Geowissenschaftliche Arbeiten (TGA)*, C13, 150 p.
- Savage, D. (ed.), 1995. The scientific and regulatory basis for the geological disposal of radioactive waste. John Wiley & Sons, Chichester.
- Schad, H., 1997. Variability of hydraulic parameters in non-uniform porous media: Experiments and stochastic modelling at different scales. *Tübinger Geowissenschaftliche Arbeiten (TGA)*, C35, 233 p.
- Schad, H., and Teutsch, G., 1994. Effects of the investigation scale on pumping test results in heterogeneous porous aquifers. *Journal of Hydrology*, 159, 61-77.

- Schulze-Makuch, D., and Cherkauer, D.S., 1997. Method Developed for Extrapolating Scale Behavior. *EOS, Transactions, American Geophysical Union*, 78 (1), 3.
- Schulze-Makuch, D., Carlson, D.A., Cherkauer, D.S., and Malik, P., 1999. Scale dependency of hydraulic conductivity in heterogeneous media. *Ground Water*, 37, 904-919.
- Scott, D.W., 1992. Multivariate Density Estimation: Theory, practice, and visualization. John Wiley & Sons, New York, 317 p.
- Serrano, S.E., 1997. The Theis solution in heterogeneous aquifers. *Ground Water*, 35(3), 463-467.
- Streltsova, T.D., 1988. Well testing in heterogeneous formations. Exxon monographs, John Wiley & Sons, 419 p.
- Sudicky, E.A., and Huyakorn, P.S., 1991. Contaminant migration in imperfectly known heterogeneous groundwater systems. *Review of Geophysics.*, 29, 240-253.
- Sun, N.Z., 1994. Inverse problems in groundwater modeling. Kluwer Acad. Publ., Dordrecht, 337 p.
- Sun, N.Z., and Yeh, W.W., 1985. Identification of parameter structure in groundwater inverse problem. *Water Resources Research*, 21(6), 869-883.
- Theis, C.V., 1935. The relation between the lowering of the piezometric surface and the rate and duration of discharge of a well using groundwater storage. *Transactions, American Geophysical Union*, 16, 519-524.
- Tiedeman, C.R., Hsieh, P.A., and Christian, S.B., 1995. Characterization of a high-transmissivity zone by well test analysis: Steady state case. *Water Resources Research*, 31(1), 27-37.
- Tompson, A.F., and Gelhar, L.W., 1990. Numerical simulation of solute transport in three-dimensional, randomly heterogeneous porous media. *Water Resources Research*, 26(10), 2591-2602.
- Vandenberg, A. 1977. Pump testing in heterogeneous aquifers. *Journal of Hydrology*, 34, 45-62.
- Vasco, D.W., Keers, H., and Karasaki, K., 2000. Estimation of reservoir properties using transient pressure data: An asymptotic approach. *Water Resources Research*, 36(12), 3447-3465.
- Vesselinov, V.V., and Neuman, S.P., 2001. Numerical inverse interpretation of single-hole pneumatic tests in unsaturated fractured tuff. *Ground Water*, 39 (5), 685-695.
- Wang, H.F., and Anderson, M.P., 1982. Introduction to groundwater modeling: Finite differences and finite element methods. W.H. Freeman and Company, New York, 237 p.
- Wang, Y., and Dusseault, M.B., 1991. The effect of quadratic term on the borehole solution in poroelastic media. *Water Resources Research*, 27, 3215-3223.

- Yeh, W.W., 1986. Review of parameter identification procedures in groundwater hydrology: The inverse problem. *Water Resources Research*, 22(2), 95-108.
- Zlotnik, V., and Ledder, G., 1996. Theory of dipole flow in uniform anisotropic aquifers. *Water Resources Research*, 32(4), 1119-1128.

Appendix

Appendix A-1 Photographs and maps of the fractured sandstone block

Appendix A-2 The multi purpose measuring device

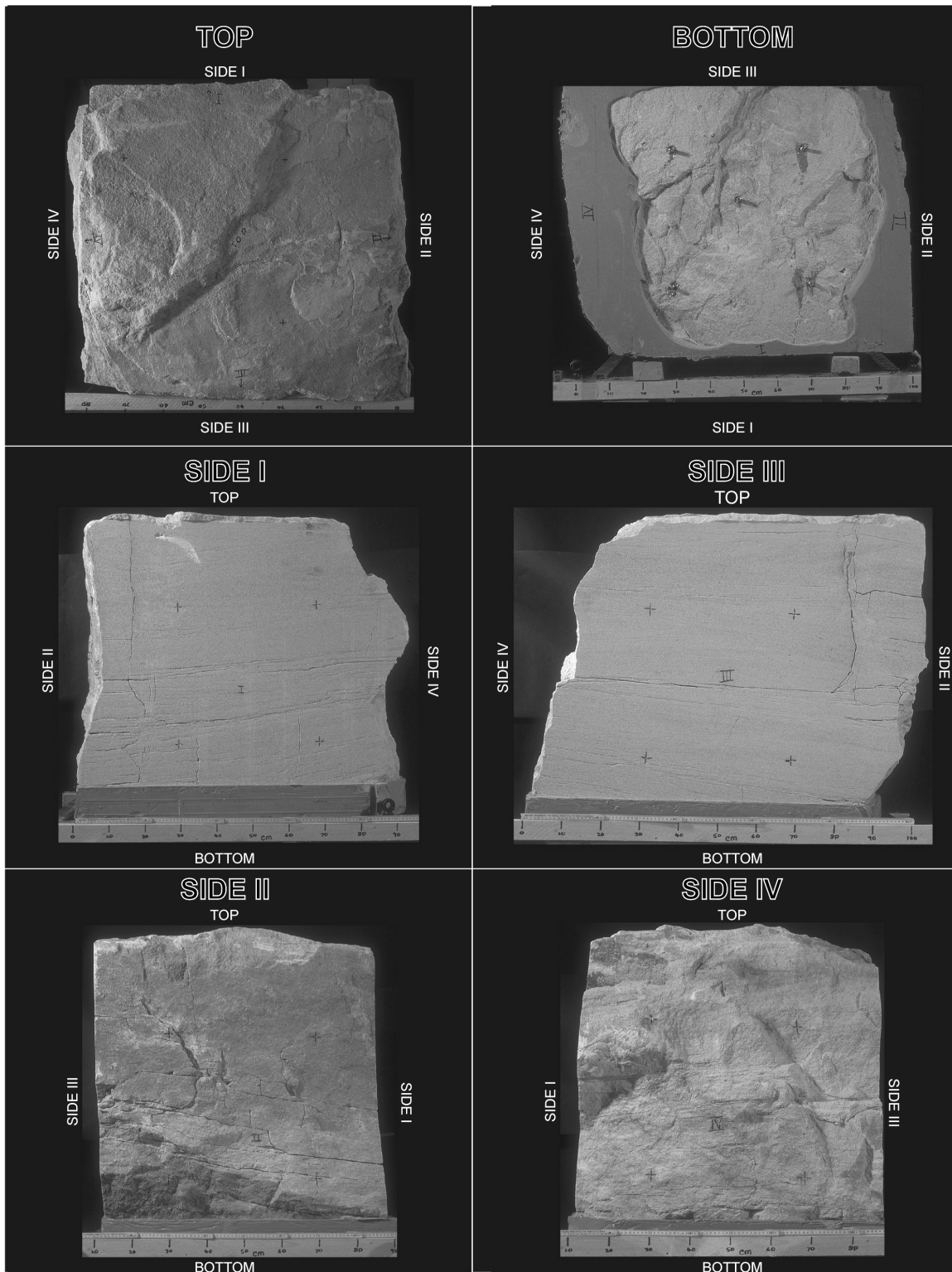
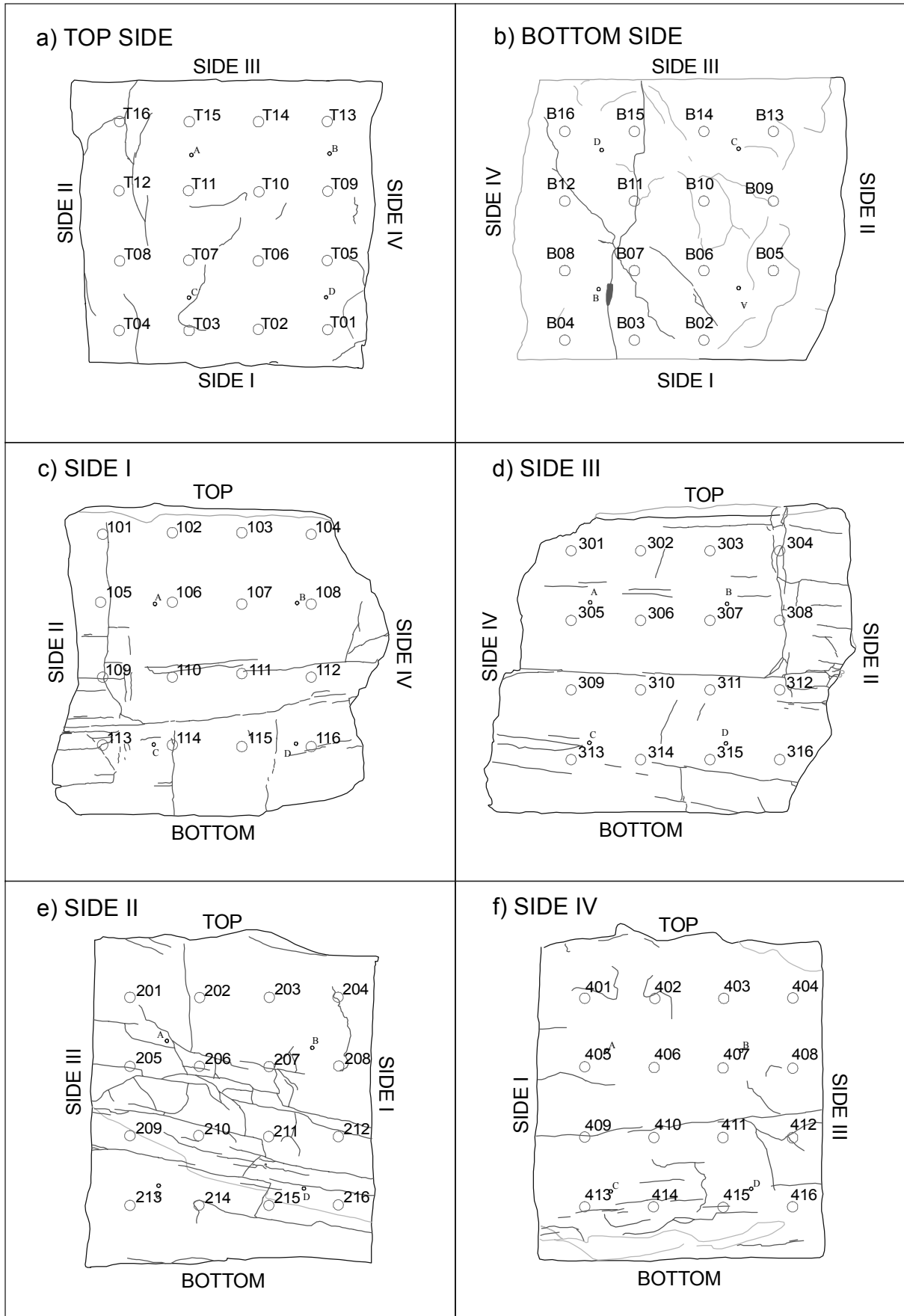


Figure A-1: Photograph of the fractured sandstone block (photographs taken from *McDermott* [1999]).

Figure A-2. (next page) Surface profiles and port locations of the fractured sandstone block (modified after *McDermott* [1999]).



0 0.5 [m]

○ Port, 30mm diameter
 ◦^A marker

▬ fractures
 ▬ bedding

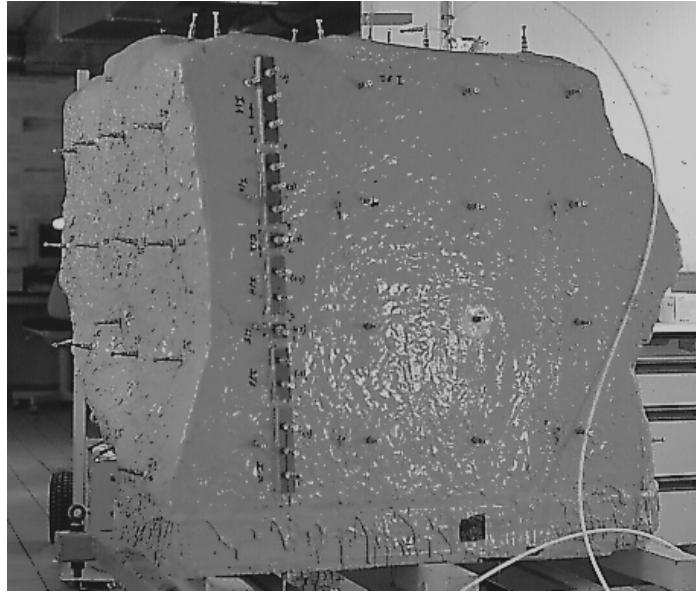
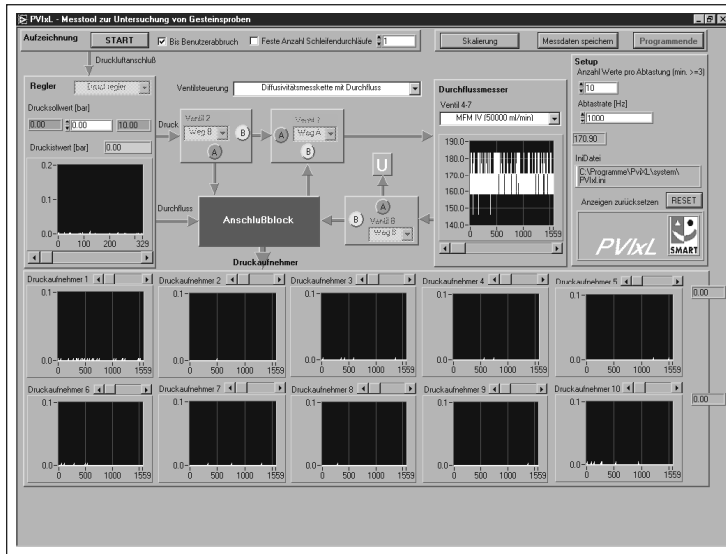


Figure A-3. The fractured sandstone block with resin coating and ports.

USER INTERFACE



PRESSURE SUPPLY

INPUT / OUTPUT

DATA TRANSMISSION LINES
FOR PRESSURE TRANSDUCER

Figure A-4. Setup of the multipurpose measuring device and illustration of the LabVIEW® based user interface.

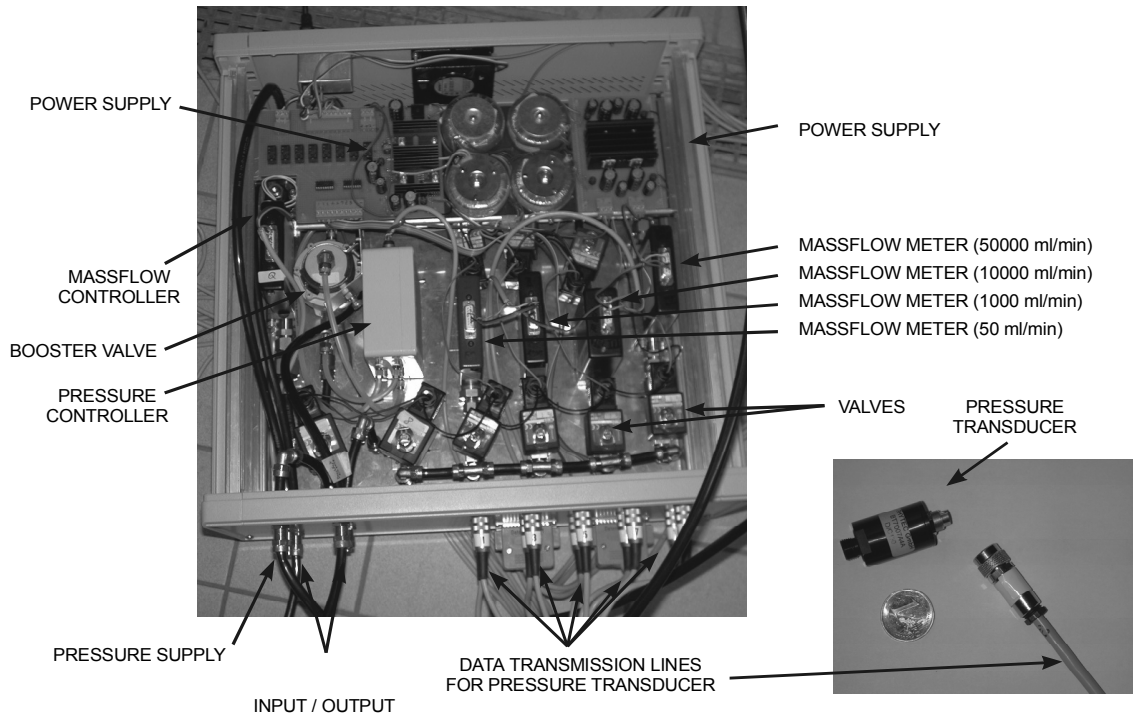


Figure A-5. Technical realization of the multi purpose measuring device.

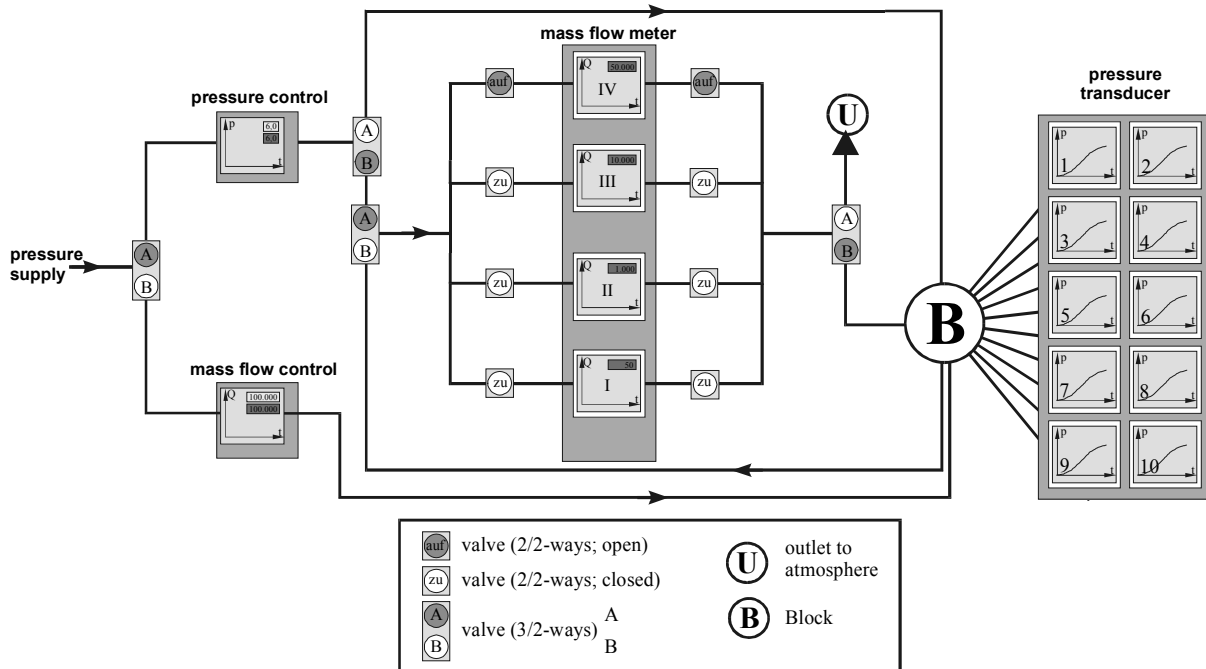


Figure A-6. Detailed diagram of the multi purpose measuring device.



In der Reihe C der Tübinger Geowissenschaftlichen Arbeiten (TGA) sind bisher erschienen:

- Nr. 1: Grathwohl, Peter (1989): Verteilung unpolarer organischer Verbindungen in der wasserungesättigten Bodenzone am Beispiel der leichtflüchtigen aliphatischen Chlorkohlenwasserstoffe. 102 S.
- Nr. 2: Eisele, Gerhard (1989): Labor- und Felduntersuchungen zur Ausbreitung und Verteilung leichtflüchtiger chlorierter Kohlenwasserstoffe (LCKW) im Übergangsbereich wasserungesättigte/wassergesättigte Zone. 84 S.
- Nr. 3: Ehmann, Michael (1989): Auswirkungen atmogener Stoffeinträge auf Boden- und Grundwasser sowie Stoffbilanzierungen in drei bewaldeten Einzugsgebieten im Oberen Buntsandstein (Nordschwarzwald). 134 S.
- Nr. 4: Irouschek, Thomas (1990): Hydrogeologie und Stoffumsatz im Buntsandstein des Nord-schwarzwaldes. 144 S.
- Nr. 5: Sanns, Matthias (1990): Experimentelle Untersuchungen zum Ausbreitungsverhalten von leichtflüchtigen Chlorkohlenwasserstoffen (LCKW) in der wassergesättigten Zone. 122 S. **Vergriffen!**
- Nr. 6: Seeger, Thomas (1990): Abfluß- und Stofffrachtseparation im Buntsandstein des Nord-schwarzwaldes. 154 S.
- Nr. 7: Einsele, Gerhard & Pfeffer, Karl-Heinz (Hrsg.) (1990): Untersuchungen über die Auswirkungen des Reaktorunfalls von Tschernobyl auf Böden, Klärschlamm und Sickerwasser im Raum von Oberschwaben und Tübingen. 151 S.
- Nr. 8: Douveas, Nikon G. (1990): Verwitterungstiefe und Untergrundabdichtung beim Talsperrenbau in dem verkarsteten Nord-Pindos-Flysch (Projekt Pigai-Aoos, NW-Griechenland). 165 S.
- Nr. 9: Schlöser, Heike (1991): Quantifizierung der Silikatverwitterung in karbonatfreien Deck-schichten des Mittleren Buntsandsteins im Nordschwarzwald. 93 S.
- Nr. 10: Köhler, Wulf-Rainer (1992): Beschaffenheit ausgewählter, nicht direkt anthropogen beeinflusster oberflächennaher und tiefer Grundwasservorkommen in Baden-Württemberg. 144 S.
- Nr. 11: Bundschuh, Jochen (1991): Der Aquifer als thermodynamisch offenes System. – Untersuchungen zum Wärmetransport in oberflächennahen Grundwasserleitern unter besonderer Berücksichtigung von Quellwassertemperaturen (Modellversuche und Geländebeispiele). 100 S. **Vergriffen!**
- Nr. 12: Herbert, Mike (1992): Sorptions- und Desorptionsverhalten von ausgewählten polyzyklischen aromatischen Kohlenwasserstoffen (PAK) im Grundwasserbereich. 111 S.
- Nr. 13: Sauter, Martin (1993): Quantification and forecasting of regional groundwater flow and transport in a karst aquifer (Gallusquelle, Malm, SW-Germany). 150 S.

- Nr. 14: Bauer, Michael (1993): Wasserhaushalt, aktueller und holozäner Lösungsabtrag im Wutachgebiet (Südschwarzwald). 130 S.
- Nr. 15: Einsele, Gerhard & Ricken, Werner (Hrsg.) (1993): Eintiefungsgeschichte und Stoffaustrag im Wutachgebiet (SW-Deutschland). 215 S.
- Nr. 16: Jordan, Ulrich (1993): Die holozänen Massenverlagerungen des Wutachgebietes (Südschwarzwald). 132 S.
- Nr. 17: Krejci, Dieter (1994): Grundwasserchemismus im Umfeld der Sonderabfalldeponie Billigheim und Strategie zur Erkennung eines Deponiesickerwassereinflusses. 121 S.
- Nr. 18: Hekel, Uwe (1994): Hydrogeologische Erkundung toniger Festgesteine am Beispiel des Opalinustons (Unteres Aalenium). 170 S. **(Vergriffen!)**
- Nr. 19: Schüth, Christoph (1994): Sorptionskinetik und Transportverhalten von polyzyklischen aromatischen Kohlenwasserstoffen (PAK) im Grundwasser - Laborversuche. 80 S.
- Nr. 20: Schlöser, Helmut (1994): Lösungsgleichgewichte im Mineralwasser des überdeckten Muschelkalks in Mittel-Württemberg. 76 S.
- Nr. 21: Pyka, Wilhelm (1994): Freisetzung von Teerinhaltstoffen aus residualer Teerphase in das Grundwasser: Laboruntersuchungen zur Lösungsrate und Lösungsvermittlung. 76 S.
- Nr. 22: Biehler, Daniel (1995): Kluftgrundwasser im kristallinen Grundgebirge des Schwarzwaldes – Ergebnisse von Untersuchungen in Stollen. 103 S.
- Nr. 23: Schmid, Thomas (1995): Wasserhaushalt und Stoffumsatz in Grünlandgebieten im württembergischen Allgäu. 145+ 92 S.
- Nr. 24: Kretzschmar, Thomas (1995): Hydrochemische, petrographische und thermodynamische Untersuchungen zur Genese tiefer Buntsandsteinwässer in Baden-Württemberg. 142 S. **(Vergriffen!)**
- Nr. 25: Hebestreit, Christoph (1995): Zur jungpleistozänen und holozänen Entwicklung der Wutach (SW-Deutschland). 88 S.
- Nr. 26: Hinderer, Matthias (1995): Simulation langfristiger Trends der Boden- und Grundwasser-versauerung im Buntsandstein-Schwarzwald auf der Grundlage langjähriger Stoffbilanzen. 175 S.
- Nr. 27: Körner, Johannes (1996): Abflußbildung, Interflow und Stoffbilanz im Schönbuch Waldgebiet. 206 S.
- Nr. 28: Gewalt, Thomas (1996): Der Einfluß der Desorptionskinetik bei der Freisetzung von Trichlorethen (TCE) aus verschiedenen Aquifersanden. 67 S.
- Nr. 29: Schanz, Ulrich (1996): Geophysikalische Untersuchungen im Nahbereich eines Karstsystems (westliche Schwäbische Alb). 114 S.
- Nr. 30: Renner, Sven (1996): Wärmetransport in Einzelklüften und Kluftaquiferen – Untersuchungen und Modellrechnungen am Beispiel eines Karstaquifers. 89 S.
- Nr. 31: Mohrlök, Ulf (1996): Parameter-Identifikation in Doppel-Kontinuum-Modellen am Beispiel von Karstaquiferen. 125 S.

- Nr. 32: Merkel, Peter (1996): Desorption and Release of Polycyclic Aromatic Hydrocarbons (PAHs) from Contaminated Aquifer Materials. 76 S.
- Nr. 33: Schiedek, Thomas (1996): Auftreten und Verhalten von ausgewählten Phthalaten in Wasser und Boden. 112 S.
- Nr. 34: Herbert, Mike & Teutsch, Georg (Hrsg.) (1997): Aquifersysteme Südwestdeutschlands - Eine Vorlesungsreihe an der Eberhard-Karls-Universität Tübingen. 162 S.
- Nr. 35: Schad, Hermann (1997): Variability of Hydraulic Parameters in Non-Uniform Porous Media: Experiments and Stochastic Modelling at Different Scales. 233 S.
- Nr. 36: Herbert, Mike & Kovar, Karel (Eds.) (1998): GROUNDWATER QUALITY 1998: Remediation and Protection - Posters -.- Proceedings of the GQ'98 conference, Tübingen, Sept. 21-25, 1998, Poster Papers. 146 S.
- Nr. 37: Klein, Rainer (1998): Mechanische Bodenbearbeitungsverfahren zur Verbesserung der Sanierungseffizienz bei In-situ-Maßnahmen. 106 S.
- Nr. 38: Schollenberger, Uli (1998): Beschaffenheit und Dynamik des Kiesgrundwassers im Neckartal bei Tübingen. 74 S.
- Nr. 39: Rügner, Hermann (1998): Einfluß der Aquiferlithologie des Neckartals auf die Sorption und Sorptionskinetik organischer Schadstoffe. 78 S.
- Nr. 40: Fechner, Thomas (1998): Seismische Tomographie zur Beschreibung heterogener Grundwasserleiter. 113 S.
- Nr. 41: Kleineidam, Sybille (1998): Der Einfluß von Sedimentologie und Sedimentpetrographie auf den Transport gelöster organischer Schadstoffe im Grundwasser. 82 S.
- Nr. 42: Hückinghaus, Dirk (1998): Simulation der Aquifergenese und des Wärmetransports in Karstaquiferen. 124 S.
- Nr. 43: Klingbeil, Ralf (1998): Outcrop Analogue Studies – Implications for Groundwater Flow and Contaminant Transport in Heterogeneous Glaciofluvial Quaternary Deposits. 111 S.
- Nr. 44: Loyek, Diana (1998): Die Löslichkeit und Lösungskinetik von polyzyklischen aromatischen Kohlenwasserstoffen (PAK) aus der Teerphase. 81 S.
- Nr. 45: Weiß, Hansjörg (1998): Säulenversuche zur Gefahrenbeurteilung für das Grundwasser an PAK-kontaminierten Standorten. 111 S.
- Nr. 46: Jianping Yan (1998): Numerical Modeling of Topographically-closed Lakes: Impact of Climate on Lake Level, Hydrochemistry and Chemical Sedimentation. 144 S.
- Nr. 47: Finkel, Michael (1999): Quantitative Beschreibung des Transports von polyzyklischen aromatischen Kohlenwasserstoffen (PAK) und Tensiden in porösen Medien. 98 S.
- Nr. 48: Jaritz, Renate (1999): Quantifizierung der Heterogenität einer Sandsteinmatrix (Mittlerer Keuper, Württemberg). 106 S.

- Nr. 49: Danzer, Jörg (1999): Surfactant Transport and Coupled Transport of Polycyclic Aromatic Hydrocarbons (PAHs) and Surfactants in Natural Aquifer Material - Laboratory Experiments. 75 S.
- Nr. 50: Dietrich, Peter (1999): Konzeption und Auswertung gleichstromgeoelektrischer Tracer-versuche unter Verwendung von Sensitivitätskoeffizienten. 130 S.
- Nr. 51: Baraka-Lokmane, Salima (1999): Determination of Hydraulic Conductivities from Discrete Geometrical Characterisation of Fractured Sandstone Cores. 119 S.
- Nr. 52: McDermott, Christopher I. (1999): New Experimental and Modelling Techniques to Investigate the Fractured System. 170 S.
- Nr. 53: Zamfirescu, Daniela (2000): Release and Fate of Specific Organic Contaminants at a Former Gasworks Site. 96 S.
- Nr. 54: Herfort, Martin (2000): Reactive Transport of Organic Compounds Within a Heterogeneous Porous Aquifer. 76 S.
- Nr. 55: Klenk, Ingo (2000): Transport of Volatile Organic Compounds (VOC's) From Soilgas to Groundwater. 70 S.
- Nr. 56: Martin, Holger (2000): Entwicklung von Passivsammlern zum zeitlich integrierenden Depositions- und Grundwassermonitoring: Adsorberkartuschen und Keramikdosimeter. 84 S.
- Nr. 57: Diallo, Mamadou Sanou (2000): Acoustic Waves Attenuation and Velocity Dispersion in Fluid-Filled Porous Media: Theoretical and Experimental Investigations. 101 S.
- Nr. 58: Lörcher, Gerhard (2000): Verarbeitung und Auswertung hyperspektraler Fernerkundungsdaten für die Charakterisierung hydrothermalen Systeme (Goldfield/Cuprite, Yellowstone National Park). 158 S.
- Nr. 59: Heinz, Jürgen (2001): Sedimentary Geology of Glacial and Periglacial Gravel Bodies (SW-Germany): Dynamic Stratigraphy and Aquifer Sedimentology. 102 S.
- Nr. 60: Birk, Steffen (2002): Characterisation of Karst Systems by Simulating Aquifer Genesis and Spring Responses: Model Development and Application to Gypsum Karst. 122 S.
- Nr. 61: Halm, Dietrich & Grathwohl, Peter (Eds.) (2002): Proceedings of the 1st International Workshop on Groundwater Risk Assessment at Contaminated Sites (GRACOS). 280 S.
- Nr. 62: Bauer, Sebastian (2002): Simulation of the genesis of karst aquifers in carbonate rocks. 143 S.
- Nr. 63: Rahman, Mokhlesur (2002): Sorption and Transport Behaviour of Hydrophobic Organic Compounds in Soils and Sediments of Bangladesh and their Impact on Groundwater Pollution – Laboratory Investigations and Model Simulations. 73 S.
- Nr. 64: Peter, Anita (2002): Assessing natural attenuation at field scale by stochastic reactive transport modelling. 101 S.
- Nr. 65: Leven, Carsten (2002): Effects of Heterogeneous Parameter Distributions on Hydraulic Tests - Analysis and Assessment. 88 S.